

AD-A060 913

NAVAL SURFACE WEAPONS CENTER DAHLGREN LAB VA
GLOBAL OCEAN TIDES. PART I. A DETAILED HYDRODYNAMICAL INTERPOLA--ETC(U)
SEP 78 E W SCHWIDERSKI

F/G 8/3

UNCLASSIFIED

NSWC/DL-TR-3866-PT-1

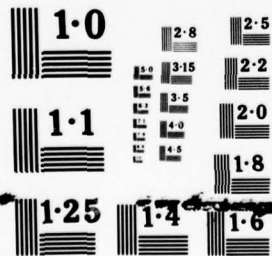
NL

1 OF 2
ADA
060913



ENCLOSURE
70
C000

1 OF 2
ADA
060913



NATIONAL BUREAU OF STANDARDS
MICROCOPY RESOLUTION TEST CHART

AD A060913

DDC FILE COPY

LEVEL II

UNCLASSIFIED

SECURITY CLASSIFICATION OF THIS PAGE (When Data Entered)

REPORT DOCUMENTATION PAGE		READ INSTRUCTIONS BEFORE COMPLETING FORM
1. REPORT NUMBER NSWC/DL-TR-3866-PT-1	2. GOVT ACCESSION NO.	3. RECIPIENT'S CATALOG NUMBER
4. TITLE (and Subtitle) GLOBAL OCEAN TIDES, PART I. A DETAILED HYDRODYNAMICAL INTERPOLATION MODEL.	5. TYPE OF REPORT & PERIOD COVERED Final rept.	6. PERFORMING ORG. REPORT NUMBER
7. AUTHOR(s) E. W. Schwiderski	8. CONTRACT OR GRANT NUMBER(s) ZR000001	9. PROGRAM ELEMENT, PROJECT, TASK AREA & WORK UNIT NUMBERS 61152N/ZR0000 1/ ZR000001/CK01AA
10. PERFORMING ORGANIZATION NAME AND ADDRESS Naval Surface Weapons Center, K05 Dahlgren, Virginia 22448	11. REPORT DATE September 1978	12. NUMBER OF PAGES
13. CONTROLLING OFFICE NAME AND ADDRESS Chief of Naval Material Department of the Navy Washington, DC 20360	14. MONITORING AGENCY NAME & ADDRESS (if different from Controlling Office) 96p.	15. SECURITY CLASS. (of this report) UNCLASSIFIED
15a. DECLASSIFICATION/DOWNGRADING SCHEDULE		
16. DISTRIBUTION STATEMENT (of this Report) Approved for public release: Distribution Unlimited.		
17. DISTRIBUTION STATEMENT (of the abstract entered in Block 20, if different from Report)		
18. SUPPLEMENTARY NOTES		
19. KEY WORDS (Continue on reverse side if necessary and identify by block number) Ocean Tides and Currents Numerical Modeling Tidal Charts		
20. ABSTRACT (Continue on reverse side if necessary and identify by block number) A new hydrodynamical interpolation technique has been developed and tested to construct a model of global ocean tides with the support of empirical tidal constants collected around the world. The discrete tide model features a 1° by 1° graded grid system in connection with a hydrodynamically defined bathymetry. The Laplace tidal equations are augmented by turbulent friction terms with novel mesh-area (latitude and depth) dependent eddy-viscosity and bottom-friction coefficients. The well-known astronomical tide-generating forces are modified by (see back)		

DD FORM 1473

1 JAN 73

EDITION OF 1 NOV 65 IS OBSOLETE

S/N 0102-LF-014-6601

UNCLASSIFIED

SECURITY CLASSIFICATION OF THIS PAGE (When Data Entered)

391 598

78

11 01 020

Liu

UNCLASSIFIED

SECURITY CLASSIFICATION OF THIS PAGE (When Data Entered)

(20)

Cont' effects due to solid earth tides and ocean-tidal loading. New averaged finite differences in time are used to enhance stability characteristics and to facilitate the hydrodynamical interpolation of empirical data. This unique interpolation is accomplished by a controlled adjustment of the bottom-friction coefficient and by redefining a more physical shoreline.

Extensive computer experiments were conducted to study the characteristics of the novel friction laws and hydrodynamical interpolation methods. The computed M_2 tide data along with all (specially labeled) empirical constants are tabulated in map form for four typical 30° by 50° ocean areas. A complete tabulation and discussion of the computed M_2 tide will be published in Part II of this report. It is estimated that the tabulated tidal charts permit a prediction of the M_2 -tide elevation of the ocean surface over the geoidal level with an accuracy of better than 5 cm anywhere in the open ocean and with somewhat less accuracy near rough shorelines. With the forthcoming construction of the lesser S_2 , N_2 , and K_2 ; K_1 , O_1 , P_1 , and Q_1 ; and M_4 , M_m , and S_{sa} tidal constituents, the total tide-prediction error can be kept below the 10-cm bound posed by applied researchers of today.

UNCLASSIFIED

SECURITY CLASSIFICATION OF THIS PAGE (When Data Entered)

FOREWORD

This report gives a comprehensive account of a five-year research effort devoted to developing a global ocean-tide model that permits a prediction of the tidal disturbances of the geoidal sea surface with an accuracy of better than 10 cm anytime and anywhere in the world oceans. This extraordinary accuracy is required in many military and civilian applications to geodesy, geophysics, oceanography, meteorology, astronomy, and space and missile technology. In particular, in the combined NASA-DoD mission to map the geoid at sea by satellite altimetry up to 10-cm accuracy, altimeter measurements of the geoidal ocean surface must be corrected for tidal disturbances of equivalent accuracy. After numerous and elaborate computer experiments, it is concluded that the tide model arrived at meets those requirements.

It is the author's most pleasant obligation to acknowledge the sustained and generous support of the Head of the center's Strategic Systems Department, Mr. R. A. Niemann. This research work would have been impossible without the continued sponsorship of the Head of the Department's Astronautics and Geodesy Division, Mr. R. J. Anderle, and his Assistant, Dr. C. Oesterwinter, who placed the challenging problem before the author and followed its slowly progressing solution with patience and confidence.

In the current year, the ongoing project on ocean tides and currents is supported by the center's Independent Research Fund and by a grant from the National Geodetic Survey of the Department of Commerce/NOAA/NOS.* The author wishes to take this special opportunity to thank his colleagues, Dr. C. J. Cohen and Dr. B. Zondek, for many critical, stimulating, and beneficial discussions and suggestions. Grateful acknowledgment must be extended to the author's programmer, Mr. L. Szeto, for his competent and effective preparation of the involved computer programs and his untiring cooperation in carrying out numerous and sometimes extensive program changes, many of which could not be described in this report.

The date of completion was June 15, 1978.

Released by

Ralph A. Niemann

RALPH A. NIEMANN, Head
Strategic Systems Department

ACCESSION for		
DTIC	White Section	<input checked="" type="checkbox"/>
DDC	Grey Section	<input type="checkbox"/>
UNANNOUNCED		<input type="checkbox"/>
JUSTIFICATION		
BY.....		
DISTRIBUTION/AVAILABILITY CODES		
Dist.	AVAIL.	and/w SPECIAL
A		

*National Oceanographic and Atmospheric Administration (NOAA)
National Ocean Survey (NOS)

ABSTRACT

A new hydrodynamical interpolation technique is developed and tested to construct a model of global ocean tides with the support of empirical tidal constants collected around the world. The discrete tide model features a 1° by 1° spherically graded grid system in connection with a hydrodynamically defined bathymetry recognizing barrier effects of large boundary and bottom anomalies. The Laplace tidal equations are augmented by turbulent friction terms with novel mesh-area (latitude and depth) dependent eddy-viscosity and bottom-friction coefficients. The well-known astronomical tide-generating forces are modified by simplified versions of secondary effects due to solid earth tides and ocean-tidal loading. Central staggered finite differences in space and new averaged finite differences in time are used to enhance decay, dispersion, and stability characteristics and to facilitate the hydrodynamical interpolation of empirical data. This unique interpolation is accomplished by a controlled adjustment of the bottom-friction coefficient and by redefining a more physical shoreline through a monitored in- or out-flow allowed across the artificial mathematical coastline.

Extensive computer experiments were conducted to study the characteristics of the novel friction laws and hydrodynamical interpolation methods and to determine by trial-and-error optimum friction, interpolation, and finite-differencing parameters. The computed M_2 -tide data along with all (specially labeled) empirical constants are tabulated in geographical map form for four typical 30° by 50° ocean areas. A complete tabulation and discussion of the computed M_2 tide will be published in Part II of this report. It is estimated that the tabulated tidal charts permit a prediction of the M_2 -tide elevation of the ocean surface over the geoidal rest level with an accuracy of better than 5 cm anywhere in the open ocean and with somewhat less accuracy near rough shorelines. With the forthcoming construction of the lesser S_2 , N_2 , and K_2 ; K_1 , O_1 , P_1 , and Q_1 ; and M_f , M_m , and S_{sa} tidal constituents, the total tide-prediction error can be kept below the 10-cm bound posed by applied researchers of today.

TABLE OF CONTENTS

	Page
FOREWORD	i
ABSTRACT	iii
LIST OF TABLES	vi
LIST OF FIGURES	vi
1. INTRODUCTION	1
2. REVIEW AND PREVIEW	5
3. THE CONTINUOUS OCEAN TIDAL EQUATIONS (COTEs)	17
A. THE NAVIER-STOKES EQUATIONS OF AVERAGED TURBULENT FLOW	17
B. BOTTOM AND SURFACE BOUNDARY CONDITIONS	18
C. REYNOLDS STRESSES AND EDDY DISSIPATION	20
D. THE TOTAL TIDE-GENERATING POTENTIAL	21
E. SIMPLIFYING ASSUMPTIONS	23
F. DERIVATION OF CONTINUOUS OCEAN TIDAL EQUATIONS	25
4. SECOND-ORDER ARCTIC TIDES	29
5. THE DISCRETE OCEAN-TIDE EQUATIONS (DOTEs)	35
A. THE 1° BY 1° GRADED GRID SYSTEM	35
B. HYDRODYNAMICAL OCEAN BATHYMETRY	36
C. EMPIRICAL TIDE DATA	37
D. DERIVATION OF DISCRETE OCEAN-TIDE EQUATIONS	41
E. LATERAL-BOUNDARY, INITIAL, AND FINAL DATA	49
F. HYDRODYNAMICAL INTERPOLATION OF EMPIRICAL TIDE DATA	52
G. STABILITY ANALYSIS	57
6. DISCUSSION OF THE TIDE MODEL	63
A. DISCRETE VERSUS CONTINUOUS OCEAN-TIDE EQUATIONS	63
B. QUALITY OF THE OCEAN-TIDE MODEL	67
C. CONCLUSIONS	80
REFERENCES	81
DISTRIBUTION	

LIST OF TABLES

Table	Page
1 Constants of Major Tidal Modes	3
2 Empirical M_2 -Tide Differences	38
3 Bermuda M_2 -Tide Observations	39
4a Deep-Sea M_2 -Tide Data for the Gulf of Mexico and Caribbean Sea	39
4b Deep-Sea M_2 -Tide Data for the Pacific and Atlantic Oceans	40
5a M_2 Tidal Amplitudes of the Northwestern Atlantic Ocean	70
5b M_2 Tidal Phases of the Northwestern Atlantic Ocean	71
6a M_2 Tidal Amplitudes of the Northeastern Pacific Ocean	74
6b M_2 Tidal Phases of the Northeastern Pacific Ocean	75
7a M_2 Tidal Amplitudes of the North-Central Pacific Ocean	76
7b M_2 Tidal Phases of the North-Central Pacific Ocean	77
8a M_2 Tidal Amplitudes of the Central Pacific Ocean	78
8b M_2 Tidal Phases of the Central Pacific Ocean	79

LIST OF FIGURES

Figure	Page
1 Boundary Cell In- and Out-Flow Illustration	11
2 Finite-Difference Schemes in Space	14
3 Finite-Difference Schemes in Time	15
4 Earth-Ocean Tidal Interaction	19
5 Illustration of Eigenvalues d_0 , d_1 , and $d_2 = \bar{d}_1$ in Circle $ d - d_c \leq d_r$	62
6a Illustration of Average Velocity	64
6b Illustration of Mean Normal Stress	66
7 Illustration of "Rejected" (Protruding) Empirical Tidal Amplitude or Phase Value	67

1. INTRODUCTION

The restless sea with its surfing waves, swirling currents, and swelling tides has fascinated, worried, and frightened mankind from the beginning. The mighty erosive and devastating power of ocean tides flooding shorelands and seaports always troubled land developers, harbor engineers, and seamen. The observed periodic feature of tides very early led laymen tidalists to record, analyze, and predict high and low tides in coastal waters and to warn and prepare people to take appropriate precautions. Indeed, quite satisfactory tide tables were constructed by simple rules of thumb. Nowadays, in seashore areas, newspapers, radio and television broadcasts, and special bulletins publish daily, monthly, and longer-range tide predictions of interest to many users.

Up to recent years, practical interest in ocean tides was essentially confined to coastal waters. With the advancement of science and technology, the need for extremely accurate tide predictions in all the world oceans has become an urgent problem. In fact, ocean tides represent fluctuating loads on the solid earth, which cause tilting of the crust and disturbances of the earth's stress and gravity fields. The precise knowledge of these loads permits researchers to determine important hydrodynamical parameters of the oceans and elastic parameters of the solid earth. Similarly, interactions between ocean tides and atmosphere, celestial bodies, and artificial satellites and missiles can be studied with high accuracy.

Recently, the National Aeronautics and Space Administration (NASA) and the Department of Defense (DoD) joined in the common mission to map the geoid at sea by satellite altimetry up to about 10-cm accuracy. However, the geoidal (rest) sea level is hydrodynamically disturbed by ocean tides and other currents due to pelagic density variations and atmospheric surface forces. Such hydrodynamical undulations of the sea surface topography reach amplitudes of more than 100 cm in open oceans and 200 cm in coastal waters. Thus, ocean tides and currents need to be determined with an accuracy compatible with the desired geoid accuracy in order to provide effective corrections for altimeter measurements.

In brief, contemporary researchers of today in geophysics, geodesy, oceanography, meteorology, astronomy, and space technology all pose the same challenging question:

We need to know, for any given time and place of the world oceans, the tidal elevation of the sea surface over its geoidal level within 10-cm accuracy.

In the past two decades, ocean tidalists have devoted a considerable effort to answer this extraordinary question by:

- a. Empirical methods; that is, by means of vast numbers of tidal recordings taken at continental, island, and deep-sea stations around the world.
- b. Theoretical methods; i.e., by tapping the wealth of novel mathematical tools designed by computer-oriented numerical analysts for the integration of appropriate hydrodynamical equations governing tidal currents with theoretical and/or empirical boundary and initial conditions.

Considerable progress in the qualitative mapping of ocean tides has indeed been made. Many realistic features of oceanic tides have been discovered and interpreted. This rich and extensive work will be briefly discussed in Section 2, Reviews and Previews. However, in spite of the massive empirical and theoretical effort, the satisfactory answer to the question posed above remained elusive. The constructed tidal charts vary over large ocean areas from investigator to investigator, and tide predictions fall considerably short of the desired accuracy. Nevertheless, the

published tidal maps, for instance, those by Pekeris and Accad (1969),* Zahel (1970, 1973, 1975), and Estes (1975, 1977), do suggest that the desired mapping of ocean tides might succeed with somewhat more refined models. A similar situation was recognized (Döös et al., 1974; and Reid et al., 1975) by numerical oceanographers and meteorologists modeling even more involved general ocean currents and atmospheric circulations. Obviously, the successful study of such turbulent fluid motions depends most of all on the realistic representation of the dissipative forces acting in the fluid interior and along its boundary. The special field of ocean tides, which are distinguished by their simplifying periodic property and by their widely observed boundary values, may be considered a proving ground for other models of turbulent fluid motions.

In the following treatise, a new combined hydrodynamical and empirical technique will be introduced and tested to construct, at first, the principal semidiurnal moon (M_2) tide. This procedure represents a modified version of the well-known hydrodynamical numerical method developed and tested by Hansen (1966) and his coworkers Friedrich (1966), Brettschneider (1967), Trepka (1967), and Zahel (1970, 1973, 1975), as well as by Estes (1975, 1977). Among other modifications, the most significant improvements of the results were attributed to:

a. A unique "hydrodynamical interpolation" of more than 2 000 empirical tidal data into the original purely hydrodynamical tide model. This interpolation is accomplished by a controlled local adjustment of the bottom-friction coefficient and by allowing a monitored in- or out-flow across the mathematical ocean boundary and, thus, redefining implicitly a more physical boundary.

b. A graded 1° by 1° grid system, in connection with a hydrodynamically defined bathymetry recognizing the important barrier effects of narrow ocean ridges.

c. New averaged finite differences in time enhancing decay, dispersion, and stability characteristics and facilitating the implicit hydrodynamical interpolation of empirical data (a).

d. A novel mesh-area (mesh-size and depth) dependent eddy viscosity specifying a more realistic eddy dissipation.

The complete results for the constructed M_2 tide will be published in table and map form in Part II of this report (Schwiderski, 1978 b). Similar charts for the S_2 , N_2 , and K_2 ; K_1 , O_1 , P_1 , and Q_1 ; and, possibly, M_f , M_m , and S_{sa} tides (Table 1) will be constructed and published as additional parts of this report. A separate tabulation (Schwiderski, 1978 a) of the new hydrodynamically defined ocean bathymetry is in preparation. All tidal and bathymetry data will be available in tape form at NSWC, Dahlgren, Virginia.

*A list of references is included at the end of this report.

Table 1. Constants of Major Tidal Modes

Tidal Mode	K^a (m)	σ^b (10^{-4} /sec)	χ^c (deg)
Semidiurnal Species			
M_2 = Principal Lunar	0.242 334	1.405 19	$2h_0^d - 2s_0$
S_2 = Principal Solar	0.113 033	1.454 44	0
N_2 = Elliptical Lunar	0.046 398	1.378 80	$2h_0 - 3s_0 + p_0$
K_2 = Declination Luni-Solar	0.030 704	1.458 42	$2h_0$
Diurnal Species			
K_1 = Declination Luni-Solar	0.141 565	0.729 21	$h_0 + 90$
O_1 = Principal Lunar	0.100 514	0.675 98	$h_0 - 2s_0 - 90$
P_1 = Principal Solar	0.046 843	0.725 23	$-h_0 - 90$
Q_1 = Elliptical Lunar	0.019 256	0.649 59	$h_0 - 3s_0 + p_0 - 90$
Long-Period Species			
Mf = Fortnightly Lunar	0.041 742	0.053 234	$2s_0$
Mm = Monthly Lunar	0.022 026	0.026 392	$s_0 - p_0$
Ssa = Semiannual Solar	0.019 446	0.003 982	$2h_0$

$^a K$ = amplitude of the partial tide.

$^b \sigma$ = frequency of the partial tide.

$^c \chi$ = astronomical argument of the partial tide.

$^d (h_0, s_0, p_0)$ = mean longitudes of sun, moon, and lunar perigee at Greenwich midnight;

$$h_0 = 279.696\ 68 + 36\ 000.768\ 930\ 485\ T + 3.03 \cdot 10^{-4} T^2,$$

$$s_0 = 270.434\ 358 + 481\ 267.883\ 141\ 37T - 0.001\ 133T^2 + 1.9 \cdot 10^{-6} T^3,$$

$$p_0 = 334.329\ 653 + 4\ 069.034\ 032\ 957\ 5T - 0.010\ 325T^2 - 1.2 \cdot 10^{-5} T^3,$$

where

$$T = [27\ 392.500\ 528 + 1.000\ 000\ 035\ 6D]/36\ 525,$$

$$D = d + 365(y - 1975) + \text{Int} [(y - 1975)/4],$$

d = day number of year ($d = 1$ for January 1),

$y \geq 1975$ = year number,

and

$\text{Int} [x]$ = integral part of x .

2. REVIEW AND PREVIEW

Very early, scientists linked the periodic phenomenon of ocean tides to the apparent motions of the moon and sun. The first physical explanation of tides was given by Newton (1687), who applied his newly discovered theory of gravitation and introduced the still important "equilibrium theory" of tides (Sect. 3.D): under the attraction of the moon and the sun, the sea surface is assumed to attain instantaneously the shape of a level surface in hydrostatic equilibrium. This theory was perfected after Newton in 1738 (Cantor, 1901) in a contest conducted by the Paris Academy of Sciences. Among the leading contestants for the best mathematical and physical description of ocean tides were such distinguished scientists as D. Bernoulli, Euler, and Maclaurin. The hydrostatic equilibrium theory explained in fact the periodicity and some other observed simple features of ocean tides, but failed entirely to describe all hydrodynamical properties that were clearly observed.

Although Newton recognized the distinct hydrodynamical nature of ocean tides, it was Laplace (1775) who formulated the first hydrodynamical equations of oceanic tidal motions (Sect. 3.F). The Laplace tidal equations (LTEs) consider an inviscid and incompressible fluid subject to kinetic, potential, and Coriolis forces generated by the primary astronomical tide-producing potential, which is directly proportional to the equilibrium tide. Numerous solutions of these equations were constructed by analytic and semi-analytic methods for idealized ocean basins, estuaries, and channels. Realistic results were sought by many well-known researchers, such as Laplace (1775), Airy (1842), Ferrel (1874), Thomson (Lord Kelvin, 1879), Hough (1897), Poincaré (1910), Lamb (1915), Proudman (1915), Proudman and Doodson (1927), Platzman (1971; 1972 a, b; 1974), and Miles (1974).

Most of this rich and elucidating work has been collected and analyzed in books and reviews (see References). The conclusions clarified many realistic properties of ocean tides including the existence of so-called amphidromic points around which oceanic tidal waves rotate with amazing wave speeds (Sec. 6.B). Nevertheless, the accurate and detailed prediction of ocean tides remained unsolved. More realistic physical and geometrical models and advanced mathematical techniques were obviously needed to compute the desired ocean tides.

The theoretical models as well as the empirical predictions of ocean tides were greatly aided by Thomson (Lord Kelvin, 1868), who, following an earlier suggestion by Laplace, introduced the method of harmonic analysis into tidal studies. The astronomical tide-generating potential (equilibrium tide) is expanded into an almost periodic (with a nonharmonic frequency spectrum) series of harmonic tidal components (Sect. 3.D). Later, G. H. Darwin (1883) improved the decomposition up to 39 terms, and Doodson (1921) carried it on to 400 frequency modes by introducing his ingenious Doodson numbers. A novel nonharmonic and, subsequently, harmonic decomposition of the equilibrium tide was derived by Cartwright and Taylor (1970).

The harmonic expansion of the tide-generating potential is evidently of fundamental significance for the mathematical analysis and prediction of ocean tides. If one assumes that ocean tides are governed by linear or almost linear equations of motion (e.g., LTEs, Sect. 3.F), then the oceanic tide is also representable as a linear superposition of harmonic modes. Every harmonic component of the equilibrium tide generates, through the ocean's response, a similar component of the oceanic tide of identical frequency differing only in two time-independent constants: the amplitudes and phases. Once these harmonic constants are determined for a given geographical location either by observation or by theoretical computations, then the time-dependent tide can be predicted by simple linear superposition. Moreover, every oceanic tidal mode is hydrodynamically independent of all others and can be constructed without any knowledge of the others.

However, some nonlinear oceanic responses in coastal areas, where the sea surface varies rapidly, may be necessary in a realistic tide model (Sect. 5.F). There, one must remember that any nonlinearity generates higher harmonic frequencies and causes involved interactions between different tidal modes and also other ocean currents. In this connection, one may compare the introductory remarks to the British Admiralty (1977) tide tables.

Over many years, massive tidal records (some longer than half a century with more than 10 million hourly readings) have been made with about 10 000 tide gauges placed around the world at continental and island stations. Most of these data have been harmonically analyzed for many ocean tide components. The extracted harmonic constants have been tabulated and are now available at, for instance, the National Ocean Survey (1942), the International Hydrographic Bureau (1966), and the British Admiralty (1977).

In recent years, Eyrie (1968), Filloux (1968), and Snodgrass (1968) developed sensitive deep-sea tide (pressure) gauges that can be placed almost anywhere on the ocean floor to record tidal variations for up to one year. Munk and Cartwright (1966) introduced the so-called "ocean response method" in order to analyze relatively short-time records with sufficient accuracy. Though this method is basically nonharmonic, it too yields as its end product the most desired harmonic constants. The local time series of the ocean tide is considered as a convolution of the tide-generating potential and a transfer function (complex response weights) which is, a priori, not known and, hence, must be determined in an optimum sense (Cartwright, 1968, 1969; and Cartwright et al., 1969). By using analyzed coastal reference stations, satisfactory results are being claimed for rather short recording times of two weeks and even one week. Deep-sea measurements have been published, for instance, by Munk et al. (1970), Irish et al. (1971), Nowroozi (1972), Mofjeld (1975), Pearson (1975 a, b), and Zettler et al. (1975).

By simple inspection of numerous observed ocean-tide data and experienced intuition, cotidal (equi-phase) and some corange (equi-amplitude) maps have been constructed for marginal seas and partial or worldwide oceans by Whewell (1833, 1848), Berghaus (1845), Harris (1904), Sterneck (1920, 1921), Prüfer (1939), Dietrich (1944 a, b), Villain (1952), Bogdanov (1961 a, b), Luther and Wunsch (1974), and others. All of these maps give a qualitative overview of the phenomena of ocean tides.

A more systematic empirical method to map large-scale ocean tides was proposed and demonstrated by Kuo et al. (1970 a, b), Jachens and Kuo (1973), and Kuo and Jachens (1977). In their inversion method, modern optimization techniques are utilized to fit low-degree polynomials simultaneously to observed ocean-tide data and to measured oceanic tidal disturbances of the solid-earth gravity, which are correlated through well-known interaction equations. While this approach is definitely more reliable than purely intuitive attempts, it appears to be constrained by rather low-degree polynomials which can hardly accommodate the various tidal undulations known from observations (Sect. 6.B). The method also offers no physical insight into the tidal phenomena and yields no information on tidal currents, which is needed in certain applications. Aside from those shortcomings, the method seems to yield promising results in limited ocean regions.

With the advent of electronic computers, hydrodynamical numerical methods dominated the theoretical scene to map worldwide ocean tides. The modern, large-scale numerical investigation of ocean tides was pioneered by Hansen (1948, 1949, 1966), who realized that the complexity of natural ocean basins renders any analytic treatment intractable. Hansen was soon followed by a long line of researchers, such as Gohin (1961), Accad and Pekeris (1963), Ueno (1963, 1964), Bogdanov et al. (1964), Bogdanov and Magarek (1967, 1969), Brettschneider (1967), Tiron (1967), Trepka (1967), Pekeris and Accad (1969), Marchuk et al. (1969), Zahel (1970, 1973, 1975), Hendershott (1972, 1975), Gordeyev et al. (1973), Marchuk et al. (1973), and Estes (1975, 1977). Their probing computer experiments of steadily increasing sophistication were paralleled and supported by an even longer list of numerical analysts modeling other fluid motions, in particular closely related general ocean currents and atmospheric circulations. Among the many investigators, only very few may be named in this connection because of their important contributions with direct relevance to ocean tides: Bryan (1963), Smagorinsky (1963), Friedrich (1966, 1970), Crowley (1968, 1970), Leith (1968), Cox (1970), O'Brien (1971), and Holland and Hirschman (1972), as well as Döös et al. (1974), and Reid et al. (1975).

Hansen (1948, 1949) began his large-scale hydrodynamical numerical investigations of ocean tides with the classical LTEs (Sect. 3.F). These equations are derived from the Euler-Lagrange equations of inviscid and incompressible fluid motions by integration over the ocean depth, invoking the hydrostatic-pressure assumption and neglecting all nonlinear effects and any motion in depth (Sect. 3.E). Most of those simplifying conditions could be justified by long-wave theory. The basic LTEs are the starting point for all ocean tide investigators. The quality of their work depends essentially on their more or less realistic modeling of the following hydrodynamical and mathematical components characterizing true tidal motions.

(a) Lateral Eddy Dissipation. To improve his results, Hansen (1966) recognized the fundamentally turbulent nature of tidal currents and augmented the LTEs by lateral eddy-dissipation terms (Sect. 3.C). Such interior friction forces were first introduced into fluid mechanics by Boussinesq (1877), who replaced the unknown turbulent Reynolds stress tensor by the known laminar stress tensor with a constant eddy viscosity at one's disposal. In oceanography, this simple concept was brought into practice by Ekman (1902) and was later effectively used, for instance, by Munk (1950) and Bryan (1963).

Ignoring the successes of Boussinesq's unique substitution, which serves to control the supercritical instability of turbulent flow in place of the Reynolds stresses, many researchers still regard this approximation as controversial, artificial, fictitious, and phony. Apparently, this difficulty originates from the observation that the "constant" eddy viscosity varies enormously in form and magnitude from investigator to investigator. While the kinematic molecular viscosity of water is of the order 10^{-2} cm²/sec, oceanic eddy viscosities of the order 10^0 to 10^{11} cm²/sec have been quoted (Cox, 1970; Zahel, 1970). Nevertheless, the huge variation of the eddy viscosity is physically plausible, and some empirical evidence for the lower value has been discussed by Munk (1966).

As was first realized by Prandtl (1925), the eddy viscosity is a characteristic quantity of the turbulent motion under investigation and not just a fluid constant such as the molecular viscosity. In fact, a prescribed eddy viscosity actually specifies the "macroscopical" (averaged) features of the "microscopically undefined" turbulent flow. Consequently, the quality of the modeling of any turbulent motion is directly linked to the investigator's realistic choice of the eddy viscosity.

The physically sound meaning of Boussinesq's approximation of the Reynolds stresses was first illustrated by Prandtl's (1925) celebrated "momentum Austausch (exchange, mixing) theory" of turbulent flow. With the help of constant "mixing-length parameters" (see, e.g., Schlichting, 1968), the eddy viscosity (momentum Austausch coefficient) is found to be dependent on the averaged flow velocity; i.e., the eddy dissipation appears as a quadratic phenomenon. In meteorology and oceanography, velocity-dependent eddy viscosities were derived on physical grounds by Smagorinsky (1963), Leith (1968), Crowley (1968, 1970), O'Brien (1971), and others.

Considering the complexity of the world oceans, it is attractive to retain the simplifying linearity of the tidal equations. Since averaged tidal velocities can be expected to be generally slow, it appears more consistent with the overall Stokes slow-motion assumption underlying the basic LTEs to employ a velocity-independent eddy viscosity (compare bottom friction below). Also, the refined studies of Zahel (1970, 1973, 1975), Marchuk et al. (1973), and Estes (1975, 1977) do not exhibit any need for nonlinear eddy-dissipation terms. However, the author's frustrating early experiments with a worldwide, constant eddy viscosity in an ocean of depths varying from 10 to 7 000 m (Sect. 5.B) clearly indicated that the lateral eddy viscosity must depend linearly on the ocean depth (Sect. 3.C). Eddy viscosities depending on $1/2$ and $3/2$ powers of the depth were also tried, but they failed to yield equally good results.

A renewed look at the phenomenon of turbulent motion led to the introduction of a lateral eddy viscosity that depends linearly on a horizontal (cell or mesh size) and a vertical (cell size or depth) mixing length (Eq. 6).

This physically plausible law explains the enormous variations of eddy viscosities mentioned above. The fact that the eddy viscosity must depend in some way on the mesh size (resolution) in discrete models of ocean currents was earlier noticed by Cox (1970), Friedrich (1970), Holland and Hirschman (1972), and Zahel (1975). It may be mentioned, that the author's extensive computer experiments with the novel law of eddy dissipation resulted in rather drastic improvements of the ocean-tide model.

(b) Bottom-Friction Law. In addition to eddy dissipation, Hansen (1966) supplemented the LTEs also by quadratic bottom-friction terms. In fluid mechanics, the physical significance of the quadratic law of wall friction was first pointed out by Boussinesq (1896). Later, G. I. Taylor (1918) applied it advantageously in his study of tidal currents in the Irish Sea.

In order to retain the linearity of the tidal equations for their adopted time-independent numerical procedure, Pekeris and Accad (1969) used the linear law of bottom friction with a coefficient depending inversely on the ocean depth. These authors also called attention to the earlier work by Grace (1931), who applied both the quadratic and the linear laws of bottom friction to the problem of tides in the Gulf of Suez. Grace experienced a slight preference for the linear law. Similarly to eddy dissipation (see above), it appears that the linear law of bottom friction is more consistent with all other assumed linearizations of the equations of slow (Stokes-like) averaged tidal motion (see, e.g., Schlichting (1968)). Furthermore, the convergence characteristics of the time-stepping computations carried out and displayed by Estes (1975) with the quadratic law of bottom friction fail to exhibit any nonlinear symptoms.

Other bottom-friction laws were considered by Johns (1966) and McGregor (1972), as well as by Kagan (1971 a, b). In Section 3.B, the linear law of bottom friction will be selected as preferable to the quadratic law at least over all open-ocean areas. In contrast to Pekeris and Accad (1969), the bottom-friction coefficient was found more realistic without any dependence on the ocean depth, which varies in the present model from 10 to 7 000 m. Analogous to the eddy viscosity (see (a)), the bottom-friction coefficient (as a vertical eddy viscosity) is assumed on physical arguments to depend on the bottom cell area; that is, on the two horizontal mesh sizes of the discrete tidal model considered (Eq. 4). Certain nonlinear bottom-friction effects will be introduced indirectly along coastal boundaries by the novel technique of hydrodynamical interpolation of empirical tide data described below and in Section 5.F.

(c) Primary and Secondary Tide-Generating Forces. Most numerical tidalists use only the moon's or sun's tide-generating potential as the primary driving force of ocean tides. For obvious mathematical advantages (see above), only one harmonic (mostly the largest M_2) component is investigated (Sect. 3.D). Recently recognized significant interactions between the solid earth and ocean tides motivated Farrell (1972 a, b; 1973) to suggest that accurate models of ocean tides should include tidal deformations of the solid earth, tidal loading of the ocean, and their associated perturbations of the primary tide-generating potential. Farrell went on to derive the mathematical expressions of those secondary tide-modifying forces, which should be incorporated in the forcing terms of the tidal equations.

Because of the elastic properties of the solid earth, it is sufficient for ocean-tide models to include only second-order Love number approximations (Sect. 3.D) of the terrestrial tide and its associated gravity disturbance. This simple static approximation sets both solid-earth tidal effects directly proportional to the equilibrium tide. Hence, any linear (or almost linear) ocean-tide model with homogeneous boundary data but without those secondary driving forces can be corrected, a posteriori, by applying a uniform factor to all amplitudes. No correction of the phases is required.

In order to express the responses of the solid earth and of the gravitational field to the ocean's tidal load, Farrell derived a Green's function expanded in spherical harmonics. This representation changes the character of

the equations of oceanic tidal motion from its differential form to a much more involved integro-differential form, which must be solved by some iteration process. Farrell's suggestion was picked up by Hendershott (1972, 1975), who attributed rather drastic effects to oceanic tidal loading although his numerical iteration procedure failed to converge. The same secondary forcing functions were also used by Estes (1977) in connection with Hansen's hydrodynamical numerical technique (see (g) and Sect. 5.D) without detecting any divergence difficulties. Estes' results did not confirm the drastic effects of oceanic tidal loading as claimed by Hendershott. The computed effects on amplitudes and phases are in magnitude considerably below those modifications that are needed and that could be achieved by varying eddy-dissipation and bottom-friction parameters (Sect's. 3.B and 3.C). Nevertheless, Estes' important computations definitely supported Farrell's original contention that an accurate description of ocean tides should include ocean loading effects.

In a critical discussion of Farrell's representation of oceanic tidal loading effects, Pekeris (in a presentation given in 1977 at the Office of Naval Research) noticed that the series expansion of the Green's function is only conditionally (not absolutely) convergent and possesses only a generalized derivative of Dirac's δ -function type. To avoid all complications of this representation, Pekeris suggested a simple static treatment of all effects due to oceanic tidal loading. Analogous to Newton's equilibrium theory and to the static approximation of the solid-earth tidal effects (see above), the solid earth and the gravity field are assumed to respond instantaneously to the ocean's tidal load; i.e., the responses are directly proportional to the ocean tide.

In Section 3.D, Pekeris' straightforward solution of the rather involved problem will be incorporated in the present model. The consistent, approximate treatment of both effects due to the solid-earth tide and to the ocean's tidal load can be considered as quite satisfactory, particularly for the present ocean tide model, which will be supported by numerous empirical tide data that naturally include all solid-earth and ocean responses. In agreement with Estes' results, the present computations displayed no startling changes traceable to oceanic tidal loading.

(d) Boundary and Initial Values. In order to specify a unique integral of the LTEs, Hansen (1948, 1949) supported his tide model with empirical tide data as boundary values known around the ocean basin considered. This boundary condition is easily implemented numerically by combining all equations of oceanic tidal motion into a single elliptic, second-order differential equation for the complex tidal amplitude, provided a linear law of bottom friction and no eddy-dissipation terms are considered. Although this attractive elliptic boundary-value problem has been studied by several investigators, it must be emphasized that it leaves the fluid flow across the ocean boundaries without any control. Such an unchecked violation of the stiff condition of conservation of mass is obviously somewhat hazardous. For example, it is clearly one major cause of the divergence problems encountered by Hendershott (1975; compare also Farrell, 1972 b).

Instead of empirical tidal data, Accad and Pekeris (1963) and other authors used the purely mathematical boundary condition of no-flow across the ocean shorelines. When higher-order eddy-dissipation terms are included, two sets of boundary data are required to specify a solution. Hansen (1966), Zahel (1970, 1972, 1975), Estes (1975, 1977), and others used the mathematical boundary conditions of no-flow across and free-slip along the ocean boundaries. Some authors (e.g., Marchuk et al., 1969) replaced the free-slip condition by the no-slip condition, which is appropriately used to specify laminar flows. However, in turbulent flows with very thin boundary layers and large eddy viscosities, the free-slip condition is preferred. Moreover, this condition is consistent with the single-layer-ocean assumption of almost depth-independent horizontal velocities. The author's computer experiments with both the free-slip and the no-slip conditions exhibited a slight preference for the first one.

Some authors used a mixture of either empirical or mathematical boundary values. For example, Tiron (1967) used observed tidal elevations wherever available and the condition of no-flow across the coastline everywhere else. In any case, whenever empirical tide boundary values were incorporated, all eddy-dissipation terms had to be neglected and the condition of conservation of mass had to be violated without any possible control.

In the present tide model (Sect. 5.E), the mathematical condition of no-flow across and free-slip along the ocean boundaries will be strictly maintained wherever no empirical tide data are known (mainly at the coast of Antarctica and the Arctic Sea). To improve the quality of the tide model, known empirical tidal elevations will be incorporated at some 2 000 shore points by a unique "hydrodynamical interpolation" technique without neglecting important eddy-dissipation terms and permitting only a "monitored small" break of the no-flow boundary condition.

First attempts to use the empirical tide data in place of any mass-conserving condition failed to produce realistic velocity distributions; i.e., unacceptably large periodic mass flows in and out of the oceans were encountered. A second attempt to keep the empirical tide data, while enforcing strictly the no-flow boundary condition, by adjusting the bottom-friction coefficient (see (b) and Sect. 5.F) point-wise near the shore to modify the velocity components, also failed to yield realistic results.

After some evaluation of this disappointing situation, it was felt that quite satisfactory results could be obtained by a certain measured compromise. The pointwise adjustment of the bottom-friction coefficient and the resulting modification of the velocity field had to be controlled by two uniform parameters (Sect. 5.F), which remained to be determined by trial-and-error computations to yield the best results while satisfying the mass-conservation condition as closely as possible. The remaining smaller violations of the no-flow boundary condition could then be explained, for instance, by the relatively large geometric inaccuracies of the shoreline of the model (e.g., shape, size, and depth of boundary mesh cells (see (f), Sect. 5.F, and Figure 1)). Naturally, only monitored strictly periodic in- and out-flows could be permitted over any boundary segment, so that the total water mass of the ocean remains conserved. The novel technique thus developed was found to bring about the most spectacular improvements of the tide model desired.

When the complete time-dependent problem is considered, its integration must be started from some meaningful, initial oceanic state, say, at rest. The computational process can be interrupted at any time for qualitative inspection and then restarted with or without parameter changes. The integration can be stopped when the time-periodic state imposed by the harmonic forcing function is reached with satisfactory accuracy. It may be pointed out that the time-dependent integration procedure was chosen in Section 5.D as preferable because its stability analysis reveals important dispersion, decay, and stability characteristics that determine the quality of the tide model. Moreover, the experience gained with tidal time-periodic currents can be directly utilized for the modeling of more involved general ocean currents and atmospheric circulations.

(e) *Polar Singularities and Ice Caps.* In spherical coordinates, the equations of oceanic tidal motion (COTEs, Sect. 3.F) become singular at the North Pole. Most authors avoid this difficulty by terminating the ocean basin at some fictitious northern boundary. In order to check his numerical method against an analytic solution in a circular arctic ocean basin, Zahel (1970) derived an analytic integral of the equations of motion without eddy-dissipation terms. In Section 4, a unique second-order analytic solution of the complete equations of tidal motion will be constructed. This special integral will be matched with the numerical solution which starts at 4° colatitude. It may be pointed out that the use of the analytic North Pole solution allows for a more uniform grading (see (f) and Sect. 5.A) of the 1° by 1° grid system needed for the definition of the finite difference analog. As will be shown, a less uniform grid system requires considerably more computer time.

In all tide models, it is tacitly assumed that the polar ice covers have very little effect on oceanic tidal currents. This assumption is probably justified within the desired accuracy. It is certainly true at least near the North Pole, where, according to the analytic solution (Sect. 4), all semidiurnal and diurnal tides vanish with the second or first power of the distance from the Pole. Furthermore, the present tide model is aided by numerous empirical tide data collected at coastal stations of the Arctic Ocean and by some data obtained at Antarctica, which naturally contain ice-cap effects.

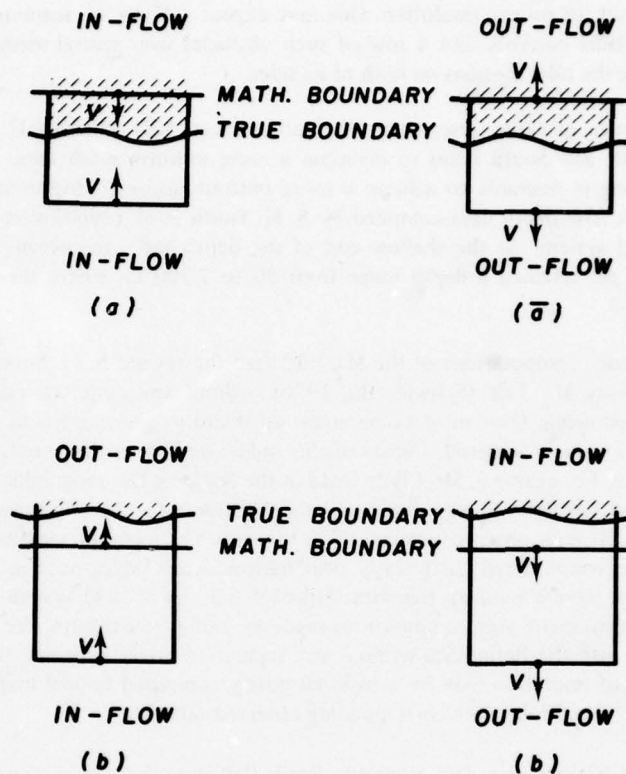


Figure 1. Boundary Cell In- and Out-Flow Illustration:
 (a) and (a), also (b) and (b) Are Half-Periods Apart
 (Shaded region is land area.)

(f) *The Gridded Ocean Basin and Bathymetry.* The definition of a finite-difference analog in place of the equations of oceanic tidal motion requires a mesh discretization of the ocean area under investigation. While one would like to utilize a grid system as finely detailed as possible to achieve a high resolution of the tidal currents, one is, of course, quite limited by the memory capacity of the computer facility available and by the known bathymetric charts of the ocean basins. For the worldwide oceans, essentially 1° by 1° averaged depth data were compiled by Dishon (1964), Dishon and Heezen (1968), and, independently, S. M. Smith et al. (1966). The latter collection has been somewhat revised by Gates and Nelson (1975), and both sets are available in tape form.

In spite of the specially collected depth data, all investigators prepared their own bathymetric charts corresponding to the ocean grid system chosen. All data are quite drastically curtailed by artificial limits on both the

shallow and deep ends of the depth range. Moreover, most computations were carried out on rather coarse grids of 2° by 2° to 6° by 6° . Obviously, in such an ocean geometry, much of the absolutely necessary resolution of, for example, narrow ocean ridges and continental shelves is lost. In fact, all published numerically constructed tidal maps suffer from such a lack of proper resolution. One may expect a 1° by 1° seamount or island to have little effect on the surrounding tidal currents, but a row of such obstacles over several mesh cells represents a hydrodynamical barrier separating the tidal motions on both of its sides.

Based on the experience of earlier researchers, the author (Sect. 5.B) utilizes a 1° by 1° grid system that is "graded" toward the North and South Poles to maintain a more uniform mesh area. As was demonstrated by Zahel (1970), such a grading is desirable to achieve a more uniform accuracy, higher stability, larger time steps, and shorter computer times. The depth data compiled by S. M. Smith et al. (1966) were revised and linearly interpolated to fit the new grid system. At the shallow end of the depth scale, the oceans were cut off at the 50-m depth level. The new data set retained a depth range from 50 to 7 700 m, where the upper limit remained untouched.

The author's exploratory computations of the M_2 tide used the revised S. M. Smith et al. (1966) depth data and constructed a Preliminary M_2 Tide (Schwiderski, 1976) without any empirical tidal elevations. The overall accuracy attained was encouraging. Over most ocean areas, satisfactory agreement with numerous observations at island and continental stations was achieved. Copies of this model have been requested by many research institutions for various applications. For example, Mr. Clyde Goad at the National Oceanographic and Atmospheric Administration's (NOAA) National Geodetic Survey computed the M_2 -tide effects on the moon's orbit and found, for the first time, good agreement with observations and other theories. Yet, a considerable lack of accuracy, especially in the phase constants, was encountered particularly over narrow ocean ridges, such as the Aleutian, Caribbean, Marianas, and Sunda Ridges, paralleling deep trenches. Although a 1° by 1° grid system was employed, the results showed no satisfactory improvement over computations made by earlier researchers. For example, the Pacific tide was found sweeping freely into the Bering Sea without any separation effect expected from the dividing Aleutian Ridge. This striking failure of resolution may be seen in all purely computed cotidal maps, such as the well-scaled map of Zahel (1970), which also displays the corresponding observed values.

A reinspection of the bathymetric data revealed clearly that even a 1° by 1° grid scheme falls far short in representing a narrow ocean ridge in a hydrodynamically proper fashion. The defect is particularly compounded when the narrow ridge parallels a deep trench. The reason for this deficiency is obviously the purely "hydrostatic" character of the averaging principle employed by S. M. Smith et al. (1966) in order to assign a depth value at the center of a mesh cell that is supposed to be representative for the entire cell. For instance, if the area of a mesh cell is (by subjective sight) more than half land, then it is called a "land cell" and the cell is given (for the present purpose) the depth value "zero." In the alternative case, the cell is declared "oceanic" and a depth value is assigned that conserves the estimated actual water mass. Because of this "hydrostatic" principle, cells were found that contained elongated islands crossing even several cells, but every cell was declared oceanic. Moreover, an oceanic trench portion of the cell with some 7 000-m true depth produced an average depth of more than 3 500 m. Clearly, for ocean current models the entire cell represents an impassable wall and the depth value should be "zero" instead of 3 500 m.

In order to eliminate the shortcomings of the bathymetric tables compiled by S. M. Smith et al. (1966) and to implement the necessary "hydrodynamical" averaging principle recognized above (Sect. 5.B), a renewed worldwide revision of the depth data was undertaken. More than 3 000 depth data belonging to continental, island, and submerged-ridge cells were modified. In addition, the minimum and maximum cutoff-depth values were set at 10 and 7 000 m, respectively. The maximum limit affected only few isolated holes with unnecessarily adverse consequences on the stability (Sect. 5.G) of the tide model. Exploratory computations with the new ocean-bottom relief im-

mediately reflected the improved resolution. The improvement of the results was even more spectacular when empirical tidal elevations (see (d) and Sect. 5.F) were hydrodynamically interpolated.

Naturally, it must be kept in mind that the decision to declare a boundary mesh cell as oceanic and the subsequent assignment of an averaged depth value is (even with an empirically founded judgment) entirely subjective and, hence, subject to some error. While isolated inaccuracies of this sort were generally found ineffective to alter the overall quality of the tide description, errors in a series could not be tolerated in a satisfactory tide model. Serious consequences of this uncertainty are greatly reduced in the present model, which is supported by numerous tide data observed at boundary stations. In fact, in the hydrodynamical interpolation procedure (see (d) and Sect. 5.F), it was established necessary to allow some monitored periodic in- and out-flow across the mathematically fixed land side of a boundary cell. The unknown, geographically true shoreline may be farther outside or inside the mathematical cell and, thus, really require some small, periodic out- or in-flow (see Figure 1), respectively. Evidently, the permissible in- or out-flow is enhanced at river estuaries and at narrow entrances of border seas (e.g., the Mediterranean Sea), which are excluded from consideration as meshwise disconnected from the main oceanic body. The selected (Sect. 5.C) and incorporated empirical tide data, however, do reflect the true situation more closely.

(g) *The Finite-Difference Analog.* On the gridded ocean basin (see (f) and Sect. 5.A), the differential equations of oceanic tidal motions can be converted into a discrete, finite-difference analog for a computerized solution. Since the beginning of the computer age, numerous finite-differencing schemes with various characteristics have been developed and tested by numerical analysts working in applied mathematics, fluid mechanics, oceanography, meteorology, etc. The application of those techniques with or without possible variations to the present ocean-tide problem depends essentially on the numerical tidalist's empirically founded modeling skill and imagination, limited only by the available computer capacity. Since the forcing function (see (c) and Sect. 3.D) of the basic tide model is time-periodic, the integration at hand may be accomplished as a boundary-value problem (BVP) or as an initial-value problem (IVP).

In the chosen BVP approach, one removes the complex time-periodic factor from all three dependent variables; i.e., tidal elevation and east and north velocity components, provided the basic tide model is strictly* linear (see (a), (b), and Sect. 4). In the remaining complex (time-independent) differential equations for the complex amplitudes of the independent variables, all spacial derivatives may then be replaced by central finite differences corresponding to the grid system. As was first pointed out by Richardson (1922), the differencing scheme may be chosen "regular," "semistaggered," or (fully) "staggered;" that is, the three dependent variables may be tabulated (computed) at collocated, semidislocated, or fully dislocated points, respectively, as shown in Figure 2.

The resulting three difference equations may be combined into two equations for the complex velocity amplitudes by eliminating the complex tidal amplitude, which is directly computable from the velocity via the continuity equation. With sufficient velocity boundary conditions (no-flow and, if necessary, free-slip or no-slip; see (d)), one winds up with an implicit, complex system of linear equations that can be solved by modern computerized methods. If higher-order, eddy-dissipation terms are included in the basic tide model, the linear system to be solved becomes quite involved. Such a system has not yet been tried. However, if eddy dissipation is completely neglected (see (a) and Sect. 3.C), the linear system to be solved is considerably simpler and has been successfully inverted by Accad and Pekeris (1963) and Pekeris and Accad (1969).

The same three complex-difference equations derived above for the three dependent variables can also be combined into a single difference equation for the complex tidal amplitude, provided all eddy-dissipation terms are

*If nonlinear properties (e.g., square law of bottom friction) are modeled, infinite Fourier series could, in principle, be used, but those lead to an involved infinite system of equations.

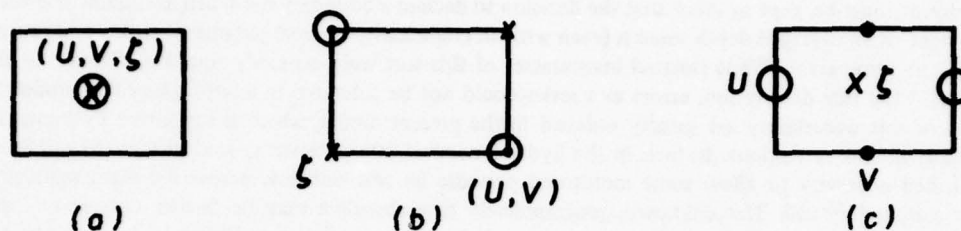


Figure 2. Finite-Difference Schemes in Space: (a) Regular, (b) Semi-staggered, (c) (Fully) Staggered (o U -Point, • V -Point, x ζ -Point)

neglected. This alternative approach to the linear BVP is obviously advantageous whenever empirical tidal-boundary values are introduced in place of the purely mathematical velocity-boundary conditions imposed in the first approach. Of course, the obtained simpler-difference analog must still be integrated by standard computer programs. This oversimplified model attracted the attention of several investigators, such as Hansen (1948, 1949), Bogdanov and Magarek (1967, 1969), and Hendershott (1972).

Since the basic tide model is time-dependent, it may be integrated as an IVP starting from some specified initial state. In addition to the advantages already pointed out under (d) above, this most natural approach leaves unrestricted room for full-scale, realistic modeling of oceanic tidal currents, including linear or nonlinear eddy dissipation (a) and bottom friction (b) as well as mathematical boundary data together with hydrodynamically interpolated empirical tidal data (d). In fact, in Section 6.A it will be argued that it is the discrete, time-dependent, finite-difference analog that reflects the physically realistic properties of oceanic tidal currents much more perfectly and ponderably than the continuous differential model. The differential equations can be used advantageously to define various finite-difference formulations, but it is neither possible nor desirable to seek convergence of the discrete solution to the continuous integral as is the objective in laminar-flow problems.

The finite-difference scheme of the BVP discussed above remains the same for the IVB in space variables. In the differential equations of oceanic tidal motion, derivatives in space variables may be replaced by central finite differences employing a Richardson regular, semistaggered, or (fully) staggered scheme. The resulting equations contain first-order derivatives in time, which can be inverted by integration over one or two time steps along the degenerated characteristic* of the system, i.e., parallel to the t -axis. The remaining (not explicitly integrable) integrals are then replaced by some average integration rule (e.g., one-point tangential, two-point trapezoidal, three-point Simpson). Depending on the chosen time-integration formula, the obtained finite-difference analog must be solved by a computer applying either an explicit or implicit time-stepping procedure that starts from an initial state and incorporates mathematical (no-flow, free-slip, or no-slip) and empirical boundary data (see (d)).

*It may be suggested here that an integration along the ruled lines of the characteristic cone of the system might be preferable; but this alternative, or some mean of both possibilities, has never been tried in the modeling of ocean currents.

As was recognized by Richardson (1922), the time integration may utilize a "regular," a "step-over" ("leap-frog"), or an "intermediary" ("alternating") time-stepping scheme. In the "regular" scheme, all three (real) dependent variables (east and north velocity components and tidal height) are computed and tabulated at the same time points (Figure 3a). In Richardson's "step-over" (now often called "leap-frog") method, both velocity components are co-timed, but tidal elevations are computed and tabulated at intermediate points (Figure 3b). In the "intermediary" (or alternating) procedure, all three dependent variables are computed and tabulated coincidentally, but both velocity components use computationally auxiliary intermediate time points in an alternating fashion (Figure 3c).

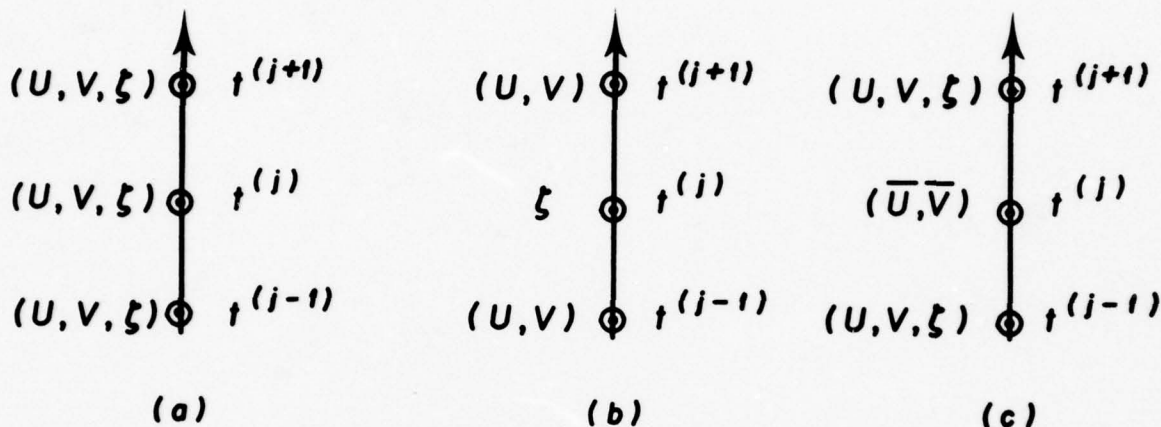


Figure 3. Finite-Difference Schemes in Time: (a) Regular, (b) Step-Over (Leap-Frog), (c) Intermediary (Alternating); (U, V, ζ) Computed and Tabulated, (\bar{U}, \bar{V}) Computed Not Tabulated

Although the step-over scheme is widely used in general ocean-current and atmospheric circulation studies, the regular and intermediary schemes seem to have been preferred in tidal models. The intermediary method has been applied in a rather involved explicit-implicit form by Marchuk et al. (1969), Gordeyev et al. (1973), and Marchuk et al. (1973) to tidal computations in border seas and in a global ocean model. In the now well-known hydrodynamical numerical method of Hansen (1966), the staggered scheme in space is combined with the regular scheme in time in an explicit and convenient fashion. The method was successfully applied by Zahel (1970, 1973, 1975) and Estes (1975, 1977) to the tides in global oceans on 4° , 3° , 2° , and 1° square-grid systems.

The principles of the Hansen technique have been selected as most appropriate for the present investigation because of their simplicity and versatility. As will be shown in Section 5.E; the staggered scheme in space permits a very easy work-in of no-flow and free-slip (or no-slip) boundary data. The integration rule over one time step used by Hansen will be improved in Section 5.D by using mixed averages without losing the important explicit property of the finite-difference scheme. This modification resulted in an enhanced stability of the system. Moreover, it facilitated the implicit hydrodynamical interpolation of empirical tide data.

3. THE CONTINUOUS OCEAN TIDAL EQUATIONS (COTES)

A. THE NAVIER-STOKES EQUATIONS OF AVERAGED TURBULENT FLOW

Because of the enormous dimensions of the world oceans, their hydrodynamical tidal motion, generated by the attraction of the moon and/or sun, must be considered entirely turbulent. Accordingly, any comprehensive modeling of oceanic tidal currents should begin with the complete Navier-Stokes equations of averaged turbulent motions of a viscous, incompressible fluid including all unknown Reynolds stresses (see, e.g., Schlichting, 1968), which must provide the major friction stress to keep the intrinsic supercritical instability of the flow under control. In rotating spherical polar coordinates (λ , ϕ , r), these equations may be written in the form (see, e.g., Whitaker, 1968)

$$u_t + \frac{u}{r \cos \phi} u_\lambda + \frac{v}{r} u_\phi + w u_r - \frac{uv}{r} - \frac{uv}{r} \tan \phi + \frac{uw}{r} = \frac{1}{r \cos \phi} \left(q - \frac{p}{\rho} \right)_\lambda + 2\Omega (v \sin \phi - w \cos \phi) + f^\lambda, \quad (1a)$$

$$v_t + \frac{u}{r \cos \phi} v_\lambda + \frac{v}{r} v_\phi + w v_r + \frac{u^2}{r} \tan \phi + \frac{vw}{r} = \frac{1}{r} \left(q - \frac{p}{\rho} \right)_\phi - 2\Omega u \sin \phi - \frac{1}{2} \Omega^2 r \sin 2\phi + f^\phi, \quad (1b)$$

$$w_t + \frac{u}{r \cos \phi} w_\lambda + \frac{v}{r} w_\phi + w w_r - \frac{1}{r} (u^2 + v^2) = - \left(G + \frac{1}{\rho} P_r \right) + 2\Omega u \cos \phi + \Omega^2 r \cos^2 \phi + f^r, \quad (1c)$$

$$\frac{1}{r \cos \phi} [u_\lambda + (v \cos \phi)_\phi] + \frac{1}{r^2} (r^2 w)_r = 0, \quad (2)$$

$$\rho f^\lambda = \frac{1}{r \cos \phi} \tau_\lambda^{\lambda\lambda} + \frac{1}{r} \tau_\phi^{\lambda\phi} + \tau_r^{\lambda r} + \frac{3}{r} \tau^{\lambda r} - \frac{2}{r} \tau^{\lambda\phi} \tan \phi, \quad (3a)$$

$$\rho f^\phi = \frac{1}{r \cos \phi} [\tau_\lambda^{\lambda\phi} + (\tau^{\phi\phi} \cos \phi)_\phi] + \tau_r^{\phi r} + \frac{3}{r} \tau^{\phi r} + \frac{1}{r} \tau^{\lambda\lambda} \tan \phi, \quad (3b)$$

$$\rho f^r = \frac{1}{r \cos \phi} [\tau_\lambda^{\lambda r} + (\tau^{\phi r} \cos \phi)_\phi] + \tau_r^{rr} + \frac{1}{r} (2\tau^{rr} - \tau^{\phi\phi} - \tau^{\lambda\lambda}). \quad (3c)$$

In these equations, all subscripts denote indicated partial derivatives, while all superscripts denote indicated components of the turbulent dissipation vector f or the Reynolds stress tensor τ . Furthermore, the following notations are used:

t	= universal time in sec
λ	= east longitude
ϕ	= $\frac{\pi}{2} - \theta$ = north latitude (θ = colatitude)
r	= polar radius in m

- (u, v, w) = east, north, and radial velocities, respectively, in m/sec (averaged)
 p = pressure (averaged)
 q = total tide-generating potential
 f = dissipation vector
 τ = Reynolds stress tensor (to be specified)
 Ω = $0.72722 \times 10^{-4} \text{ sec}^{-1}$ = earth angular velocity
 ρ $\approx 10^3 \text{ kg/m}^3$ = density of sea water
 G = 9.81 m/sec^2 = gravity acceleration

The equations of turbulent "mean" motion are obtained by a formal time-averaging procedure applied to the Navier-Stokes equations of viscous laminar flow that leads to the concepts of "averaged" velocities and pressure, as well as to the unknown Reynolds stress tensor, τ , containing the filtered out, fluctuating velocity residuals in quadratic form (see, e.g., Schlichting, 1968). A discussion of the physical meaning of these and following turbulence notions may be postponed to Section 6.A. The momentum equations (Eq's. 1) maintain the momentum balance between the familiar kinetic (inertial acceleration) forces on the left side and the forces of potential (tide, gravity, and pressure), Coriolis, centrifugal acceleration, and dissipation of the right. The continuity equation (Eq. 2) expresses the condition of conservation of mass. The Reynolds stress tensor, τ , and the total tide-generating potential, q , will be specified in Sections 3.C and 3.D.

B. BOTTOM AND SURFACE BOUNDARY CONDITIONS

The global oceans at hydrostatic rest may be described by

- (α) $r = R = 0.637 \times 10^7 \text{ m}$ = spherical (geoidal rest) sea surface (all geoidal undulations are neglected without any significant loss of accuracy),
 (β) $r = R - H(\lambda, \phi)$ = sea-bottom relief, where
 (γ) $H = H(\lambda, \phi)$ = realistic ocean depth in m ($H(\lambda, \phi) = 0$ for land points, see Sect. 5.B), and
 (δ) $p = P - G\rho z$ = hydrostatic sea-pressure distribution with constant (arbitrary) sea-surface pressure P , where
 (ϵ) $z = r - R$ = new depth variable, so that $z = 0$ denotes $r = R$ (see Figure 4).

Due to the time-dependent, tide-generating potential, q , acting on the ocean and solid earth, the hydrostatic conditions $(\alpha) - (\epsilon)$ are altered to the following hydrodynamical boundary conditions of the sea surface and bottom (see Figure 4):

- (a) $z^s = \zeta^s = \zeta^s(\lambda, \phi, t)$ = total sea surface tidal elevation over geoid $z = 0$;
 (b) $z^b = \zeta^b(\lambda, \phi, t) - H(\lambda, \phi)$ = sea-bottom tidal relief, where
 (c) $\zeta^b = \zeta^b(\lambda, \phi, t)$ = total bottom tidal elevation over rest relief $z = -H(\lambda, \phi)$;
 (d) $\zeta = \zeta(\lambda, \phi, t) = \zeta^s - \zeta^b$ = ocean tidal elevation (measured by bottom tidal pressure gauges) to be modeled;
 (e) $\zeta^e = \zeta^e(\lambda, \phi, t)$ = earth tidal elevation to be specified (Sect. 3.D, Eq's. 9);
 (f) $\zeta^{eo} = \zeta^{eo}(\lambda, \phi, t) = \zeta^e - \zeta^b$ = earth dip-response to oceanic tidal load, ζ (Eq. 10);
 (g) $p^s = P$ = constant surface pressure (no atmospheric pressure considered);
 (h) $w^s = \zeta_t^s$ = surface radial velocity;
 (i) $\tau^s = 0$ = no surface stress (free-slip, no wind force considered);
 (j) $(u^b, v^b, w^b) \cdot \nabla(H + z) \approx \zeta_t^b$ = no flow across ocean bottom (∇ = gradient vector);
 (k) $\tau^b = \rho B(u^b, v^b)$ = bottom stress vector specified by invoking the linear law of bottom friction (Sect. 2(b)) with the coefficient

$$B = b\mu \cos \phi = \bar{b}l^2 \mu \cos \phi \quad (4a)$$

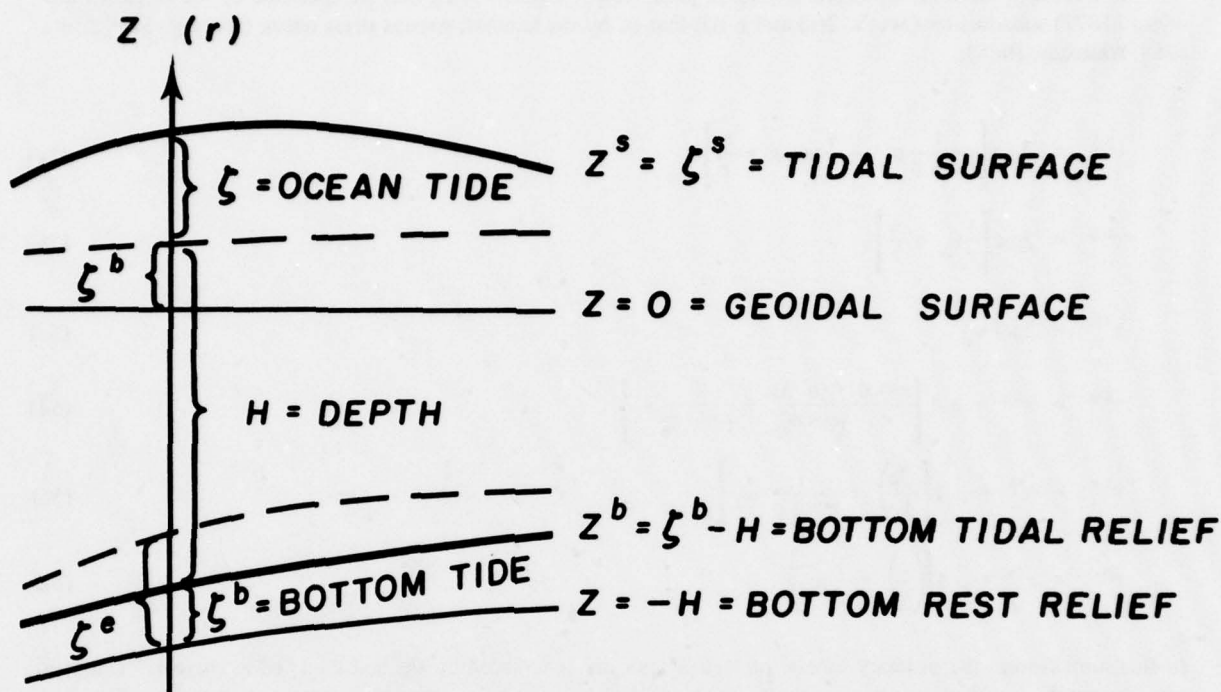


Figure 4. Earth-Ocean Tidal Interaction: ζ = Ocean Tide, ζ^e = Earth Tide, ζ^s = Surface Tide, ζ^b = Bottom Tide, $\zeta^{eo} = \zeta^e - \zeta^b$ = Earth Dip-Response to Ocean Tide, and H = Ocean Depth

depending on the cell bottom area $L^2 \mu \cos \phi$ (Sect. 6.A), where

(l) L = chosen equatorial mesh size (Sect. 5.A),

(m) μ = mesh "grading" parameter (Sect. 5.A), and

(n) $b = \bar{b} L^2$ = uniform bottom friction parameter, which must be determined by trial-and-error computations for best results. The M_2 tide (Sect. 6.B and Part II) was computed with

$$b = 0.01 \text{ m/sec}, \quad (4b)$$

which is considerably below the value used by Pekeris and Accad (1969). Some implicit local adjustments of b will be allowed in Section 5.F to better accommodate observed tidal data.

(o) Lateral boundary values will be specified in Section 5.E.

C. REYNOLDS STRESSES AND EDDY DISSIPATION

The formally derived, unknown Reynolds stress tensor, τ (Sect. 3.A), may be specified by the original Bousinesq (1877) substitution (Sect's. 2(a) and 6.A); that is, by the laminar, viscous stress tensor (see, e.g., Schlichting, 1968; Whitaker, 1968):

$$\tau^{\lambda\lambda} = 2\rho A \left[\frac{1}{r \cos \phi} u_{\lambda} - \frac{v}{r} \tan \phi + \frac{w}{r} \right], \quad (5a)$$

$$\tau^{\phi\phi} = 2\rho A \left[\frac{1}{r} v_{\phi} + \frac{w}{r} \right], \quad (5b)$$

$$\tau^{rr} = 2\rho A w_r, \quad (5c)$$

$$\tau^{\lambda\phi} = \tau^{\phi\lambda} = \rho A \left[\frac{\cos \phi}{r} \left(\frac{u}{\cos \phi} \right)_{\phi} + \frac{1}{r \cos \phi} v_{\lambda} \right], \quad (5d)$$

$$\tau^{\lambda r} = \tau^{r\lambda} = \rho A \left[r \left(\frac{u}{r} \right)_r + \frac{1}{r \cos \phi} w_{\lambda} \right], \quad (5e)$$

$$\tau^{\phi r} = \tau^{r\phi} = \rho A \left[\left(\frac{v}{r} \right)_r + \frac{1}{r} w_{\phi} \right]. \quad (5f)$$

In this substitution, the ordinary kinetic molecular viscosity is replaced by the so-called "eddy viscosity" (momentum Austausch — exchange, mixing — coefficient), which remains to be modeled to represent the true turbulent flow characteristics at hand as closely as possible.

In order to achieve a greater modeling flexibility, it is customary to divide the eddy viscosity into a "vertical" eddy viscosity associated with vertical shear and into a "horizontal" (lateral) eddy viscosity* associated with horizontal shear. In single-layer ocean models like the present one (Sect. 3.E), the separate treatment of the vertical eddy viscosity needs no explicit specification, because (Eq's. 28) the viscosity becomes an important part of the bottom-friction coefficient, B , defined by Equations 4a and 4b.

Based on the author's extensive computer experiments and on the physical arguments elaborated in Sections 2(a), 5.G, and 6.A the (horizontal) eddy viscosity, A , may now be specified by

$$A = \frac{a}{2} L H (\lambda, \phi) (1 + \mu \cos \phi). \quad (6a)$$

In this definition, L and μ denote the mesh size and grading parameters introduced in Section 3.B(1) and (m). Accordingly, the novel eddy viscosity depends on the mean lateral cross-section area $H \times L(1 + \mu \cos \phi)/2$ of the flow cell of depth H and average northeast mesh size $L(1 + \mu \cos \phi)/2$. The remaining reduced eddy-dissipation coefficient, a (in sec), must be subjected to trial-and-error computations in order to achieve best results uniformly** over

*Since east and north dimensions are usually nearly equal, no need for two lateral eddy viscosities has ever been encountered.

**Different a -values for the Pacific, North and South Atlantic, and Indian Oceans were also tested without significant effects.

all oceans. It may be recalled from Section 2(a) that some dependence of A on the mesh size L was noticed by several earlier researchers. Clearly, the strong variations of L and the depth H explain the huge magnitude differences of the "constant" eddy viscosity used by analysts in different problems. In the present case with H varying from 10 to 7 000 m (Eq's. 50, 51, 71, 103, and 123), the eddy viscosity varied between

$$1.3 \cdot 10^3 \frac{\text{m}^2}{\text{sec}} < A < 1.3 \cdot 10^6 \frac{\text{m}^2}{\text{sec}}, \quad (6b)$$

which fits the customary range very well. It is perhaps fortuitous yet interesting to note that for a cubic cell of about 1-in. (2.54-cm.) mesh size the eddy viscosity, A (Eq's. 6a, b), reduces to the value of the molecular viscosity of water.

D. THE TOTAL TIDE-GENERATING POTENTIAL

The total tide-producing potential, q (Sect. 3.A), may be expressed in the form

$$q = G(\eta + \eta'), \quad (7)$$

where $G\eta$ is the "primary" astronomical potential directly proportional to Newton's equilibrium tide η (see Sect. 2). The remaining "secondary" potential $G\eta'$ can be expanded into its three major parts

$$G\eta' = G(\eta^o + \eta^e - \eta^{eo}), \quad (8)$$

which reveal their corresponding origins (Figure 4, Sect. 3.B(d), (e), (f), respectively);

$G\eta^o$ = gravity potential perturbation due to the ocean tide ξ

$G\eta^e$ = gravity potential perturbation due to the earth tide ξ^e

$G\eta^{eo}$ = gravity potential perturbation due to the earth dip-response ξ^{eo} caused by the ocean load (tide) ξ

Attention to the significance of the earth-ocean tidal interactions manifested in the five quantities ξ^e , η^e , ξ^{eo} , η^{eo} , and η^o was called for by Farrell (1972 a, b; 1973). As was argued in Section 2(c), it is sufficient in ocean-tide models to use the following approximate relations:

$$\xi^e \approx 0.61\eta, \quad \eta^e \approx 0.30\eta, \quad (9a)$$

$$\xi^e - \eta^e \approx 0.31\eta, \quad (9b)$$

and

$$\xi^{eo} - \eta^{eo} + \eta^o \approx 0.10\xi. \quad (10)$$

The first relations (Eq's. 9) used by Hendershott (1972, 1975), Zahel (1975), Estes (1977), and others, can be justified by second-order Love number approximations. The second relation (Eq. 10) has been suggested by Pekeris (see Sect. 2(c)), who also recommended the factor 0.10 after evaluating the Green's function representation of the three oceanic tidal load effects (ξ^{eo} , η^{eo} , η^o) derived by Farrell. Apparently, the suggestion by Pekeris (Eq. 10) is physically just as plausible as the accepted approximation (Eq's. 9). In Equations 9a and 9b, it is assumed that the solid-earth tide, ξ^e , and its subsequent gravity perturbation, $G\eta^e$, are essentially instantaneous responses to the tide-generating potential, q . Analogously, in Equation 10 it is assumed that the solid-earth dip, ξ^{eo} , and the gravity perturbations, η^{eo} and η^o , are almost instantaneous responses to the ocean's tidal load, ξ . It may be mentioned that the author conducted extensive computer experiments using the factors 0.00, 0.08, and 0.12 instead

of 0.10 in Equation 10. The last two factors produced no noteworthy alterations of the results. The first factor (0.00) obviously deletes all oceanic tidal-load effects to which critically large significance has been attached by Hendershott (1972, 1975). The author's computations supported the marginal effects of oceanic tidal loading found by Estes (1977).

Following Thomson (Lord Kelvin, 1868), G. H. Darwin (1883), Doodson (1921), and Cartwright and Tayler (1970), the primary astronomical tide-generating potential, G_2 , or, equivalently, the equilibrium tide, η , may be expanded into a series (see, e.g., Dietrich, 1963) of "harmonic components" (constituents), η_ν , with a nonharmonic frequency spectrum

$$\eta = \sum_{\nu=0} \eta_\nu(\lambda, \phi, t). \quad (11)$$

In the final analysis of ocean tides, the following three major species will have to be considered:

(a) Semidiurnal Equilibrium Tides

$$\nu = 2: \eta_2 = K \cos^2 \phi \cos(\sigma t + 2\lambda + \chi) \quad (12)$$

(b) Diurnal Equilibrium Tides

$$\nu = 1: \eta_1 = K \sin 2\phi \cos(\sigma t + \lambda + \chi) \quad (13)$$

(c) Long-Period Equilibrium Tides

$$\nu = 0: \eta_0 = \frac{K}{2}(1 - 3\cos^2 \phi) \cos(\sigma t + \chi) \quad (14)$$

In Equations 12-14, the constants (K, σ, χ) denote

K = amplitude of equilibrium tide (in m)

σ = frequency of equilibrium tide (in sec^{-1})

χ = astronomical argument of equilibrium tide (in rad)

In Table 1, these constants are listed for the major tidal modes with amplitudes larger than 4 percent of the leading semidiurnal moon (M_2) tide. The daily astronomical argument, χ , can be neglected in the following construction of the oceanic tidal modes

$$\zeta = \xi(\lambda, \phi) \cos(\sigma t + \chi - \delta(\lambda, \phi)) \quad (15a)$$

corresponding to the considered mode of the equilibrium tide, $\eta = \eta_\nu$. According to Equation 15a, only the "harmonic constants"

$$\xi = \xi(\lambda, \phi) = \text{tidal amplitude (in m)}$$

and

$$\delta = \delta(\lambda, \phi) = \text{Greenwich phase (in rad)}$$

} (15b)

need to be found, provided the tide model is linear or almost linear (Sect. 2(g)).

E. SIMPLIFYING ASSUMPTIONS

In addition to the simplifying assumptions made concerning bottom friction (Sect. 3.B(k)-(n)), eddy dissipation (Sect. 3.C), and total tide-generating potential (Sect. 3.D), the following simplifications may be invoked:

(a) Hydrostatic pressure assumption in Equations 1; i.e.,

(α) Neglect all quadratic inertial accelerations (Stokes slow-motion assumption consistent with linear eddy dissipation and bottom friction (see, e.g., Schlichting, 1968))

(β) Neglect all centrifugal accelerations

(γ) Neglect vertical Coriolis force

(δ) Neglect vertical dissipation

(ϵ) Neglect vertical motion

(b) Single-layer ocean assumption in Equations 1 and 2; i.e.,

(α) $r = R + z \approx R$, but $\partial r = \partial z$

(β) $\zeta(\lambda, \phi, t) \ll H(\lambda, \phi)$

$\zeta^b(\lambda, \phi, t) \ll H(\lambda, \phi)$

(γ) $u(\lambda, \phi, z, t) \approx u(\lambda, \phi, t)$

$v(\lambda, \phi, z, t) \approx v(\lambda, \phi, t)$

It may be pointed out that all assumptions of (a) and (b) are well justified over most flow areas. In particular, the strong assumptions (b, γ) are realistic because the tide-generating potential is a body force. Moreover, the motion is fully turbulent and, hence, the averaged velocity profile exhibits only a very thin boundary layer and laminar sublayer (see, e.g., Schlichting, 1968). It may be mentioned that for the same reason the condition of free-slip at a boundary wall (Sect's. 2(d) and 5.E) seems more appropriate than the no-slip condition used in laminar-flow situations. The assumption (b, γ) is, of course, much less realistic in general ocean currents, which are driven by surface pressure and wind forces and/or by density variations confined to the upper ocean layers.

By applying assumption (a) to Equation 1c, one finds the hydrostatic pressure

$$p_z = -G\rho,$$

i.e.,

$$p - p^s = \int_z^{\zeta^s} G\rho dz = G\rho(\zeta^s - z),$$

or, with (Sect. 3.B (a) - (g))

$$\begin{aligned} p^s &= P, \\ \zeta^s &= \zeta + \zeta^b = \zeta + \zeta^e - \zeta^{eo}, \\ p &= G\rho (\zeta + \zeta^e - \zeta^{eo} - z) + P. \end{aligned} \quad (16)$$

With Equations 7-10 and 16, one has

$$\begin{aligned} q - \frac{p}{\rho} &= G [\eta - (\zeta^e - \eta^e) - \zeta + (\zeta^{eo} - \eta^{eo} + \eta^o)] - P/\rho, \\ \text{i.e.,} \\ q - \frac{p}{\rho} &= G (\alpha\eta - \beta\zeta) - P/\rho. \end{aligned} \quad (17a)$$

Where,

$$\begin{aligned} \alpha &= 0.69, \\ \beta &= 0.90. \end{aligned} \quad (17b)$$

In the following equations, it is convenient to introduce the notations

$$\bar{H}_\lambda = H_\lambda/H, \quad \bar{H}_{\lambda\lambda} = H_{\lambda\lambda}/H, \quad (18)$$

$$\bar{H}_\phi = H_\phi/H, \quad \bar{H}_{\phi\phi} = H_{\phi\phi}/H, \quad (19)$$

and

$$\tilde{H}_\phi = \bar{H}_\phi - \mu \sin \phi / (1 + \mu \cos \phi) \quad (20)$$

so that (Eq. 6a)

$$A_\lambda = A \bar{H}_\lambda, \quad A_\phi = A \tilde{H}_\phi. \quad (21)$$

Using the simplifications (a) and (b) and Equations 17-21 in Equations 1 and 2, one arrives at the reduced equations of motion:

$$u_t = \frac{G}{R \cos \phi} (\alpha\eta - \beta\zeta)_\lambda + 2\Omega v \sin \phi + f^\lambda, \quad (22a)$$

$$v_t = \frac{G}{R} (\alpha\eta - \beta\zeta)_\phi - 2\Omega u \sin \phi + f^\phi, \quad (22b)$$

and

$$u_{\lambda} + (v \cos \phi)_{\phi} + R \cos \phi w_z = 0, \quad (23)$$

where (Eq's. 3a, b; 5a-f; and 21)

$$\begin{aligned} f^{\lambda} = & \frac{A}{R^2 \cos^2 \phi} [u_{\lambda\lambda} + 2\bar{H}_{\lambda} u_{\lambda} - u] + A u_{zz} \\ & + \frac{A}{R^2} [u_{\phi\phi} + (\tilde{H}_{\phi} - \tan \phi) u_{\phi} + \tilde{H}_{\phi} u \tan \phi] \\ & + \frac{A}{R^2 \cos \phi} [(\tilde{H}_{\phi} - 2 \tan \phi) v_{\lambda} - 2\bar{H}_{\lambda} v \tan \phi], \end{aligned} \quad (24a)$$

$$\begin{aligned} f^{\phi} = & \frac{A}{R^2 \cos^2 \phi} [v_{\lambda\lambda} + \bar{H}_{\lambda} v_{\lambda} - v] + A v_{zz} \\ & + \frac{A}{R^2} [v_{\phi\phi} + (2\tilde{H}_{\phi} - \tan \phi) v_{\phi}] \\ & + \frac{A}{R^2 \cos \phi} [(2u_{\lambda} + \bar{H}_{\lambda} u) \tan \phi + \bar{H}_{\lambda} u_{\phi}]. \end{aligned} \quad (24b)$$

F. DERIVATION OF CONTINUOUS OCEAN TIDAL EQUATIONS

Under the single-layer ocean assumptions made in Section 3.E(b), the reduced Equations 22 and 23 may be integrated over the instantaneous ocean depth ($z^s - z^b = H + \xi$) while observing the surface- and bottom-boundary data specified in Section 3.B. For that purpose, it is useful to introduce the "integrated" velocity components:

$$U(\lambda, \phi, t) = \int_{z^b}^{z^s} u dz \approx uH = (\text{integrated}) \text{ east velocity} \quad (25a)$$

and

$$V(\lambda, \phi, t) = \int_{z^b}^{z^s} v dz \approx vH = (\text{integrated}) \text{ north velocity}, \quad (25b)$$

where the term "integrated" may be omitted when no confusion appears possible.

Using the simplifications and notations of Section 3.E, one finds the helpful approximations with the corresponding replacements ($u \leftrightarrow v$, $U \leftrightarrow V$, $\lambda \leftrightarrow \phi$):

$$\int_{z^b}^{z^s} u_t dz = U_t - u^s z_t^s + u^b z_t^b \approx U_t, \quad (26a)$$

$$\int_{z^b}^{z^s} u_{\lambda} dz = U_{\lambda} - u^s z_{\lambda}^s + u^b z_{\lambda}^b \approx U_{\lambda} - \bar{H}_{\lambda} U, \quad (26b)$$

and

$$\int_{zb}^{zs} u_{\lambda\lambda} dz \approx U_{\lambda\lambda} - \bar{H}_\lambda U_\lambda + (\bar{H}_\lambda^2 - \bar{H}_{\lambda\lambda})U - H_\lambda u_\lambda^b. \quad (26c)$$

The bottom-boundary conditions imposed in Section 3.B(j) and (k) assume the following approximate forms:

$$\zeta_t^b = \frac{H_\lambda}{R \cos \phi} u^b + \frac{H_\phi}{R} v^b + w^b, \quad (27)$$

$$\frac{1}{\rho} \tau^{b\lambda} = \frac{B}{H} U \approx A \left(\frac{H_\lambda u_\lambda^b}{R^2 \cos^2 \phi} + \frac{H_\phi u_\phi^b}{R^2} + u_z^b \right), \quad (28a)$$

and

$$\frac{1}{\rho} \tau^{b\phi} = \frac{B}{H} V \approx A \left(\frac{H_\lambda v_\lambda^b}{R^2 \cos^2 \phi} + \frac{H_\phi v_\phi^b}{R^2} + v_z^b \right). \quad (28b)$$

With Equations 25-28 and the surface-boundary conditions in Section 3.B(h) and (i), the proposed integration of Equations 22 and 23 is easily carried out and yields the following "continuous ocean tidal equations" (COTEs with $\theta = \pi/2 - \phi = \text{colatitude}$):

$$\begin{aligned} U_t = & \frac{GH}{R \sin \theta} (\alpha\eta - \beta\zeta)_\lambda - U \left(\frac{B}{H} + \frac{A}{R^2} H^\lambda \right) \\ & + \frac{A}{R^2} \left[\frac{U_{\lambda\lambda} + \bar{H}_\lambda U_\lambda}{\sin^2 \theta} + U_{\theta\theta} + (\cot \theta - \bar{H}_\theta + \tilde{H}_\theta) U_\theta \right] \\ & + \frac{A}{R^2 \sin \theta} [\bar{H}_\lambda \tilde{H}_\theta V - (2 \cot \theta + \tilde{H}_\theta) V_\lambda] + 2\Omega V \cos \theta, \end{aligned} \quad (29a)$$

$$\begin{aligned} V_t = & \frac{GH}{R} (\beta\zeta - \alpha\eta)_\theta - V \left(\frac{B}{H} + \frac{A}{R^2} H^\theta \right) \\ & + \frac{A}{R^2} \left[\frac{V_{\lambda\lambda}}{\sin^2 \theta} + V_{\theta\theta} + (\cot \theta - \bar{H}_\theta + 2\tilde{H}_\theta) V_\theta \right] \\ & + \frac{A}{R^2 \sin \theta} [2 \cot \theta U_\lambda - \bar{H}_\lambda U_\theta - (\cot \theta - \bar{H}_\theta) \bar{H}_\lambda U] - 2\Omega U \cos \theta, \end{aligned} \quad (29b)$$

and

$$R \sin \theta \zeta_t + U_\lambda - (V \sin \theta)_\theta = 0, \quad (30)$$

where $\alpha = 0.69$, $\beta = 0.10$, and

$$H^\lambda = \frac{\bar{H}_{\lambda\lambda} + 1 + H_\lambda^2}{\sin^2 \theta} + \bar{H}_{\theta\theta} - \bar{H}_\theta (\bar{H}_\theta - \tilde{H}_\theta) + (\bar{H}_\theta + \tilde{H}_\theta) \cot \theta, \quad (31a)$$

$$H^\theta = \frac{\bar{H}_{\lambda\lambda} + 1}{\sin^2 \theta} + \bar{H}_{\theta\theta} + \bar{H}_\theta (\cot \theta - \bar{H}_\theta + 2\tilde{H}_\theta), \quad (31b)$$

$$\bar{H}_\theta = H_\theta/H, \quad \bar{H}_{\theta\theta} = H_{\theta\theta}/H,$$

$$\tilde{H}_\theta = \bar{H}_\theta + \mu \cos \theta / (1 + \mu \sin \theta), \quad (32)$$

and

$$A = \frac{a}{2} LH(\lambda, \theta) (1 + \mu \sin \theta), \quad B = b \mu \sin \theta. \quad (33)$$

It may be mentioned that for $\alpha = \beta = 1$ and $A = B = 0$ the ocean-tide equations (Eq's. 29 and 30) reduce to the considerably simpler classical Laplace tidal equations. Evidently, the complete COTEs require second derivatives ($H_{\lambda\lambda}$, $H_{\theta\theta}$) of the bottom topography, which can be assumed to exist without placing major restrictions on the realistic features of the bathymetry. It is interesting to note that those second derivatives in H^λ and H^θ act as modifying bottom-friction terms. A ridge-like ocean floor (say, $H_{\lambda\lambda} > 0$) always adds to the bottom-friction terms (U, V) B/H , while a valley ($H_{\lambda\lambda} < 0$) always diminishes bottom friction.

4. SECOND-ORDER ARCTIC TIDES

As was mentioned in Section 2(e), the COTEs (Eq's. 29 and 30) become singular at the North Pole. For the intended numerical procedure it is therefore advantageous to seek an approximate analytic solution around this singularity that can be matched together with the numerical solution at some appropriate colatitude. In fact, a unique "second-order arctic tide" solution can be determined for all three species of tide-generating potentials listed as Equations 12, 13, and 14, provided the ocean depth around the North Pole is assumed constant.

The COTEs (Eq's. 29 and 30) for constant depth, $H = H_0$, constant eddy viscosity, $A = A_0$, and constant bottom-friction coefficient, $B = B_0$, assume the simpler form

$$U_t = \frac{GH_0}{R \sin \theta} (\alpha \eta - \beta \zeta)_\lambda + 2\Omega V \cos \theta - \frac{B_0}{H_0} U + \frac{A_0}{R^2 \sin^2 \theta} [U_{\lambda\lambda} - U + \sin \theta (\sin \theta U_\theta)_\theta - 2 \cos \theta V_\lambda], \quad (34a)$$

$$V_t = \frac{GH_0}{R} (\beta \zeta - \alpha \eta)_\theta - 2\Omega U \cos \theta - \frac{B_0}{H_0} V + \frac{A_0}{R^2 \sin^2 \theta} [V_{\lambda\lambda} - V + \sin \theta (\sin \theta V_\theta)_\theta + 2 \cos \theta U_\lambda], \quad (34b)$$

and

$$\zeta_t + \frac{1}{R \sin \theta} [U_\lambda - (V \sin \theta)_\theta] = 0. \quad (35)$$

The forcing equilibrium tides, η (Eq's 12, 13, and 14), may be written in the unified complex form

$$\eta = \bar{\eta}(\lambda, \theta) e^{i\sigma t}, \quad (36)$$

where

$$\bar{\eta} = \bar{\eta}_\nu(\lambda, \theta) = \begin{cases} K \sin^2 \theta e^{2i\lambda}, & (\nu = 2) \\ K \sin 2\theta e^{i\lambda}, & (\nu = 1) \\ \frac{K}{2} (1 - 3 \sin^2 \theta), & (\nu = 0). \end{cases} \quad (37a)$$

$$(37b)$$

$$(37c)$$

With the substitution

$$(\eta, \zeta, U, V) = (\bar{\eta}, \bar{\zeta}, \bar{U}, i\bar{V}) e^{i\sigma t} \quad (38)$$

one arrives at the following three complex differential equations in (λ, θ) :

$$\sigma \bar{U} = \frac{iGH_0}{R \sin \theta} (\beta \bar{\xi} - \alpha \bar{\eta})_\lambda + 2\bar{\Omega} \bar{V} \cos \theta + i \frac{B_0}{H_0} \bar{U} - \frac{iA_0}{R^2 \sin^2 \theta} [\bar{U}_{\lambda\lambda} - \bar{U} + \sin \theta (\sin \theta \bar{U}_\theta)_\theta - 2i \cos \theta \bar{V}_\lambda], \quad (39a)$$

$$\sigma \bar{V} = \frac{GH_0}{R} (\alpha \bar{\eta} - \beta \bar{\xi})_\theta + 2\bar{\Omega} \bar{U} \cos \theta + i \frac{\bar{B}}{H_0} \bar{V} - \frac{iA_0}{R^2 \sin^2 \theta} [\bar{V}_{\lambda\lambda} - \bar{V} + \sin \theta (\sin \theta \bar{V}_\theta)_\theta - 2i \cos \theta \bar{U}_\lambda], \quad (39b)$$

and

$$\sigma \bar{\xi} = \frac{1}{R \sin \theta} [i \bar{U}_\lambda + (\bar{V} \sin \theta)_\theta]. \quad (40)$$

The reduced Equations 39 and 40 may be solved for regular solutions by power series in $\sin \theta$ (essentially polar distance) of the form:

For $\nu = 2$ and $\nu = 0$,

$$\left. \begin{aligned} \bar{\xi} &= \xi_0(\lambda) + \xi_1(\lambda) \sin \theta + \xi_2(\lambda) \sin^2 \theta + \dots, \\ \bar{U} &= U_0(\lambda) + U_1(\lambda) \sin \theta + U_2(\lambda) \sin^2 \theta + \dots, \end{aligned} \right\} \quad (41)$$

and

$$\bar{V} = \cos \theta [V_0(\lambda) + V_1(\lambda) \sin \theta + V_2(\lambda) \sin^2 \theta + \dots];$$

and for $\nu = 1$,

$$\left. \begin{aligned} \bar{\xi} &= \cos \theta [\xi_0(\lambda) + \xi_1(\lambda) \sin \theta + \xi_2(\lambda) \sin^2 \theta + \dots], \\ \bar{U} &= \cos \theta [U_0(\lambda) + U_1(\lambda) \sin \theta + U_2(\lambda) \sin^2 \theta + \dots], \end{aligned} \right\} \quad (42)$$

and

$$\bar{V} = V_0(\lambda) + V_1(\lambda) \sin \theta + V_2(\lambda) \sin^2 \theta + \dots$$

By truncating the series expansions (Eq's. 41 and 42) after the second order in $\sin \theta$ and substituting these truncations into Equations 39 and 40 up to the same quadratic power, one arrives after some lengthy but simple algebra at the following unique "second-order arctic tidal approximations."

For semidiurnal tides ($\nu = 2$),

$$\left. \begin{aligned} \eta &= K \sin^2 \theta e^{i(2\lambda + \sigma t)}, \\ \zeta &= 6\bar{K} \sin^2 \theta e^{i(2\lambda + \sigma t)}, \\ U &= -2\bar{K} \sigma R \sin \theta e^{i(2\lambda + \sigma t)}, \end{aligned} \right\} \quad (43)$$

and

$$V = -i\bar{K} \sigma R \sin \theta e^{i(2\lambda + \sigma t)},$$

where

$$\bar{K} = \alpha G H_0 K / [6\beta G H_0 + \sigma R^2 (2\Omega - \sigma) + i\sigma (6A_0 + B_0 R^2 / H_0)]; \quad (43a)$$

and for diurnal tides ($\nu = 1$),

$$\left. \begin{aligned} \eta &= K \sin 2\theta e^{i(\lambda + \sigma t)}, \\ \zeta &= 3\bar{K}_1 \sin 2\theta e^{i(\lambda + \sigma t)}, \\ U &= (\bar{K}_2 + 6\bar{K}_3 \sin^2 \theta) \cos \theta e^{i(\lambda + \sigma t)}, \end{aligned} \right\} \quad (44)$$

and

$$V = i [\bar{K}_2 + 2(\bar{K}_3 + \bar{K}_1 \sigma R) \sin^2 \theta] e^{i(\lambda + \sigma t)},$$

where

$$\left. \begin{aligned} \bar{K}_3 &= \frac{K_{31} K_{33} (K_{22} - K_{12})}{K_{22} (K_{13} K_{31} - K_{11} K_{32}) - K_{12} (K_{31} K_{23} - K_{21} K_{32})}, \\ \bar{K}_2 &= \frac{1}{K_{12}} [K_{33} - \bar{K}_3 (K_{13} - K_{11} K_{32} / K_{31})], \\ \bar{K}_1 &= -\bar{K}_3 K_{32} / K_{31}; \end{aligned} \right\} \quad (44a)$$

and

$$\begin{aligned}
 K_{11} &= (6\beta GH_0 - \sigma^2 R^2) + i\sigma(6A_0 + B_0 R^2/H_0), \\
 K_{12} &= -\Omega R, \\
 K_{13} &= R(6\Omega - \sigma) + \frac{i}{R}(12A_0 + B_0 R^2/H_0), \\
 K_{21} &= 6\beta GH_0 + 4i\alpha A_0, \\
 K_{22} &= R(\sigma - 2\Omega) - \frac{i}{R}(2A_0 + B_0 R^2/H_0), \\
 K_{23} &= 16iA_0/R, \\
 K_{31} &= 2\sigma\Omega R^2, \\
 K_{32} &= R(2\Omega - 3\sigma) + 3\frac{i}{R}(12A_0 + B_0 R^2/H_0), \\
 K_{33} &= 2\alpha GH_0 K.
 \end{aligned}
 \tag{44b}$$

For long-period tides ($\nu = 0$),

$$\begin{aligned}
 \eta &= \frac{K}{2} (1 - 3 \sin^2 \theta) e^{i\sigma t}, \\
 \zeta &= 2\tilde{K}_1 (2 - 3 \sin^2 \theta) e^{i\sigma t}, \\
 U &= \tilde{K}_2 \sin \theta e^{i\sigma t},
 \end{aligned}
 \tag{45}$$

and

$$V = i\tilde{K}_1 \sigma R \sin 2\theta e^{i\sigma t},$$

where

$$\begin{aligned}
 \tilde{K}_3 &= 4\sigma\Omega R^3 / [\sigma R^2 - i(2A_0 + B_0 R^2/H_0)], \\
 \tilde{K}_2 &= \tilde{K}_1 \tilde{K}_3, \\
 \tilde{K}_1 &= 3\alpha GH_0 K / 2 [(6\beta GH_0 - \sigma^2 R^2 + \Omega R \tilde{K}_3) + i\sigma(6A_0 + B_0 R^2/H_0)].
 \end{aligned}
 \tag{45a}$$

It is important to note that the surprising uniqueness is achieved by requiring a regular integral at the North Pole (Eq's. 41 or 42) and by truncating the series of the solution and the differential equations after the second power of $\sin \theta$. Of course, without the second-order truncation, uniqueness can no longer exist. Undetermined coefficients become available to satisfy prescribed boundary data, say, at distant continental shorelines.

In the present global-tide model, the arctic tides (Eq's. 43, 44, and 45) will be considered valid up to 1° colatitude (the first land occurs at colatitude 7° ; see Bathymetric Tables in Schwiderski (1978a)). For colatitudes 2° and 3° , a linear interpolation will be used to match the polar solution with the numerical solution computed south of 3° colatitude.

It is interesting to observe that if the Coriolis force and eddy dissipation are neglected ($\Omega = 0, A_0 = 0$), then the second-order arctic tides (Eq's. 43, 44, and 45) become exact global tides with the constants

$$\bar{K} = \alpha G H_0 K / [(6\beta G H_0 - \sigma^2 R^2) + i\sigma B_0 R^2 / H_0],$$

$$\bar{K}_1 = 2\bar{K}, \quad \bar{K}_2 = -2\sigma R \bar{K}, \quad \bar{K}_3 = 0,$$

$$\tilde{K}_1 = \frac{3}{2}\bar{K}, \quad \tilde{K}_2 = 0, \quad \tilde{K}_3 = 0.$$

From Equations 43, 44, and 45, one concludes that all second-order arctic tides, ζ , vanish at the North Pole with the same order as their corresponding driving equilibrium tides η . Hence, only long-period tides exist at the North Pole.

5. THE DISCRETE OCEAN-TIDE EQUATIONS (DOTES)

A. THE 1° BY 1° GRADED GRID SYSTEM

With the exception of Antarctica (south of colatitude $\theta = 168^\circ$), the entire (ocean and land) area of the globe is covered by a 1° by 1° grid system that is "graded" toward the poles. Each spherically rectangular mesh cell $S_{m,n}$ is bounded on the east and west by longitudes $\lambda_m = m^\circ$ and $\lambda_{m-\mu} = (m - \mu)^\circ$, respectively, and to the south and north by colatitudes $\theta_n = n^\circ$ and $\theta_{n-1} = (n - 1)^\circ$, respectively, so that

$$S_{m,n} = \left\{ \begin{matrix} (m - \mu)^\circ & (n - 1)^\circ \\ & n^\circ \end{matrix} \right\} m^\circ, \quad (46)$$

where

$$\begin{aligned} m &= \mu, 2\mu, \dots, (360 \rightarrow 0) \\ \text{and} \\ n &= 1, 2, \dots, 168. \end{aligned} \quad (47)$$

The "grading" parameter $\mu = \mu_n$ is defined by

$$\begin{aligned} \mu &= 1 \text{ for } n = 30 \text{ to } 150 \\ \mu &= 2 \text{ for } n = 15 \text{ to } 29 \text{ and } n = 151 \text{ to } 168 \\ \mu &= 4 \text{ for } n = 8 \text{ to } 14 \\ \mu &= 8 \text{ for } n = 1 \text{ to } 7 \end{aligned} \quad (48)$$

As was mentioned in Section 2(f), the grading of the network toward the poles is necessary, in order to maintain a more uniform mesh area for higher accuracy and stability (Sect. 5.G) of the discrete tide model. In fact, the grading equations (Eq's. 48) have been chosen in such a way that

$$\mu \sin n^\circ \geq \frac{1}{2} \text{ for } n = 4, 8, 15, 30, 150, 165; \quad (49)$$

i.e., the southern mesh size remains larger than half the equator mesh size. This important condition is violated for $n = 1^\circ, 2^\circ, 3^\circ$ and $n = 166^\circ, 167^\circ, 168^\circ$. However, in Section 4 it was pointed out that the numerically discrete tide model begins at colatitude $\theta = 4^\circ$. For colatitudes $\theta = 3^\circ$ and 2° , the numerical solution will be matched by linear interpolation to the second-order arctic-tide approximations derived in Section 4, which are assumed to be useful up to colatitude $\theta = 1^\circ$. As will be shown in Section 5.G, the slight violation of the condition in Equation 49 at the three southern colatitudes is not so severe as to affect the stability characteristics of the model. In any case, no need was apparent to justify an additional grading step, which is accompanied by an unnecessary, extra computational effort (Sect. 5.D).

In the global network defined above, land and ocean mesh cells are distinguished by zero or nonzero depth data which will be assigned to each cell (Sect. 5.B). The "mathematical" boundaries of the oceans follow in an obviously zigzagging fashion the mesh lines of boundary cells. However, empirical tide data known at continental and island stations will be utilized to specify indirectly more physically true boundaries (Sect's. 2(f) and 5.F).

B. HYDRODYNAMICAL OCEAN BATHYMETRY

The ocean-depth data collected by S. M. Smith et al. (1966) were rearranged and linearly interpolated to fit the new 1° by 1° graded grid system described in Section 5.A. The original data bank had to be corrected for obvious errors in continental and oceanic labeling, ocean and land signs, shorelines, and some exponents. All land elevations were set to zero including all depth data less than 50 m. Furthermore, the following meshwise-disconnected border seas were excluded from consideration by assigning zero-depth values to their corresponding mesh cells: the Baltic, Kattegat, Irish, Mediterranean, Red, Japan, Sulu, and Ceram Seas; the Hudson and Korean Bays; and the Chihlian, Persian, and Californian Gulfs.

After some negative computational experience, the depth data, which were originally defined by applying a "hydrostatic" averaging principle (see Sect. 2(f)), were revised using the following "hydrodynamical" principles:

(a) Boundary cells at or near continental shorelines consisting of more than half oceanic areas of depths larger than 5 m were designated ocean cells, and the average oceanic depth values were assigned as the "hydrodynamically" averaged depths of the entire cells. The new depth value is preferable to the "hydrostatically" averaged depth, which preserves the actual water mass but ascribes artificially a shallow shelf character to the cell.

(b) Island cells were declared terrestrial cells with depths zero if either the island areas were larger than half the mesh areas or the (elongated) island lengths exceeded the mesh diameters.

(c) Island cells that remained oceanic cells were assigned depth values less than the hydrostatically averaged values. In this case and in situations of submerged seamounts or narrow ocean ridges (e.g., Aleutian, Marianas, and Caribbean), the hydrodynamical depths depended on the assessed "barrier" effects of the current obstacles: the longer and/or higher the barrier, the lesser the depth.

(d) The assigned minimum depth was

$$H_m = \min H(\lambda, \theta) = 20 \text{ m}, \quad (50)$$

which is lowered to 10 m by the averaging equations (Eq's. 71). The maximum depth was set at

$$H_M = \max H(\lambda, \theta) = 7\,000 \text{ m}, \quad (51)$$

which eliminated a few isolated deeper values that unnecessarily lessened the stability of the tide model (Sect. 5.G). The averaged North Pole depth was found to be

$$H_0 = 3\,600 \text{ m}, \quad (52)$$

which is needed to compute second-order arctic tides (Sect. 4) for colatitude line $n = 1$.

(e) All depth data $H_{m,n}$ are considered representative for the center of the cell $S_{m,n}$; i.e., for $m = \mu, 2\mu, \dots, 360$ and $n = 1, 2, \dots, 168$,

$$H_{m,n} = H(\lambda_m, \theta_n), \quad (53)$$

where $\lambda_m = (m - \mu/2)^\circ$ and $\theta_n = (n - 1/2)^\circ$.

As was already pointed out in Section 2(f), the hydrodynamically justified principles discussed above in (a)–(e) are, naturally, quite subjective and by no means free of any error. Nevertheless, some computational experiments indicated only very minor effects of isolated depth data changes. More than 3 000 depth values were changed but only very few of those required additional readjustments in order to keep some limitation on the first and second derivatives of $H(\lambda, \theta)$; i.e., on the relative differences given by Equations 71. Furthermore, the hydrodynamical interpolation of empirical tidal data (Sect. 5.F) known at continental and island stations greatly diminishes the need for precise boundary-depth data. The revised depth data bank used in the present tidal computations will be published in Schwiderski (1978 a).

C. EMPIRICAL TIDE DATA

The present tide model incorporates, by a unique hydrodynamical interpolation procedure (Sect. 5.F), empirical tidal data observed and harmonically analyzed at numerous continental and island stations. These data were taken from publications by the National Ocean Survey (1942), the International Hydrographic Bureau (1966), the British Admiralty (1977), and by Pekeris and Accad (1969), Zahel (1970, 1973), Cartwright (1971), and Luther and Wunsch (1974). Unfortunately, the most recent publication by the British Admiralty (1977) lists harmonic constants only for the four major tide components M_2 , S_2 , K_1 , and O_1 and excludes the European waters completely.

The voluminous data banks had to be screened in order to eliminate observations that are meaningless or unreliable for the present ocean-tide investigations. For example, tidal constants were excluded that were listed for stations deep inside estuaries or narrow bays (e.g., Hudson River, Bay of Fundy), at the mouth of large rivers (e.g., Amazon), between sheltering islands (e.g., Alexander Archipelago, Solomon Islands), and inside sheltering reefs (e.g., Great Barrier Reef).

About 2 500 stations were selected for further examination of their data concerning locally restricted distortions. For instance, some data taken over short distances along a coastline displayed rather drastically alternating times of high water, which are obviously meaningless for oceanic tidal studies. At many stations, different tables gave different tidal constants. Some of those discrepancies at island stations are shown for the M_2 tide in Table 2. Similarly, for some mesh cells, several different station data were available, and only one representative average had to be chosen. This situation is illustrated in Table 3 for the M_2 tide around Bermuda. Many of those differences can probably be explained as simple errors in printing or computing. For instance, the phase difference of about 1 hr at Port Galets on La Reunion Island (Table 2) seems to be due to some error in observing the correct reference time, which varies from listing to listing. Most differences, such as those shown for Bermuda stations in Table 3, are definitely true local variations. In this connection, the important tidal measurements by Gallagher et al. (1971) at Fanning Atoll in the Central Pacific may be mentioned. Tides outside and inside the small atoll's lagoon differed by about 50% (20 cm) in amplitude and by a phase lag of about 50° (1 hr, 40 min.).

In general, the most recent listings in the British Admiralty Tide Tables (1977) were chosen over older tabulations as most reliable. The selection of the data was further aided by the earlier and subsequent tidal computations. Altogether, some 1 700 M_2 -tide data were selected and assigned to the centers of their respective mesh cells. Using linear interpolation and tidal computations, the total number of prescribed tide data used in the M_2 -tide construction was increased to more than 2 000. Essentially all continental boundary cells carry empirically supported tide data. The empirical coverage is only marginal at Arctic and Antarctic shorelines. Most empirical tide data known at island stations are also included in the tide model. All empirical tide data will be distinguished from computed values by underlining in the printed tide tables, which will be published (see Tables 5-8) as supplemental parts of this report (Schwiderski, 1978 b).

Table 2. Empirical M_2 -Tide Differences

Station Latitude, Longitude	B.A.T. (77) ^a		N.O.S. (42) ^d		Others Initialed	
	ξ^b (m)	δ^c (°)	ξ (m)	δ (°)	ξ (m)	δ (°)
Tenerife, Canary Island (A) 28°29'N 16°14'W	0.67	18			0.69	30 Z ^e
Port Praia, Cape Verde Island (A) 14°55'N 23°31'W	0.42	244			0.43	220 Z ^e
Ascension Island (A) 7°55'S 14°25'W	0.33	177			0.51	174 P, Z
St. Helena Island (A) 15°55'S 5°42'W	0.32	81			0.34	87 P, Z
Fristan da Cunha Island (A) 37°02'S 12°18'W	0.23	12			0.34	354 P, Z
Agalega Island (I) 10°26'S 56°40'E	0.29	350			0.29	290 Z
Port Galets, La Reunion Isla. (I) 20°55'S 55°17'E	0.16	302	0.14	328	0.14	328 Z
Mawson, Antarctica (I) 67°36'S 62°53'E	0.04	232			0.04	155 Z
Wilkes Station, Antarctica (I) 66°15'S 110°31'E	0.28	162			0.38	140 Z
Welles Harbor, Midway Island (P) 28°12'N 117°22'W	0.11	82			0.11	91 P, Z
Eniwetok Atoll, Marshall Is. (P) 11°21'N 162°21'E	-0.36	127	0.36	137		
Iles Wallis, Fiji Island (P) 13°22'S 176°11'W	0.53	178	0.52	154		
Suva Harbor, Viti Levu, Fiji I. (P) 18°09'S 178°26'E	0.56	195	0.50	212		

^aB.A.T. (77) = British Admiralty Tables (1977).^b ξ = tidal amplitude.^c δ = tidal phase relative to Greenwich.^dN.O.S. (42) = National Ocean Survey (1942).^eZ = Zahel (1970).^fP = Pekeris and Accad (1969).

Table 3. Bermuda M_2 -Tide Observations

Station Latitude, Longitude	ξ^a (cm)	$\delta^b(^{\circ})$	Reference
St. George's Island 32.55N, 64.70W	36	359	British Admiralty (1977)
St. David's Island 32.37N, 64.65W	34	355	British Admiralty (1977)
Great Sound 32.32N, 64.83W	38	6	British Admiralty (1977)
St. George's Island 32.37N, 64.70W	35	0	U.S. Nat. Ocean Survey (1942)
St. George's Island 32.40N, 64.70W	37	0	Pekeris & Accad (1969)
St. George's Island 32.37N, 64.70W	36	359	Zahel (1970)
St. George's Island 32.40N, 64.70W	36	358	Zettler et al. (1975)
Deep Sea (GOBI IV) 32.29N, 64.50W	38	11	J. T. Kuo Letter (1977)

^a ξ = tidal amplitude.^b δ = tidal phase relative to Greenwich.Table 4a. Deep-Sea M_2 -Tide Data for the Gulf of Mexico and Caribbean Sea

Station Latitude, Longitude	Observed		Model		Error	
	ξ^a (cm)	$\delta^b(^{\circ})$	ξ (cm)	$\delta(^{\circ})$	$\Delta\xi$ (cm)	$\Delta\delta(^{\circ})$
W Florida Shelf St 26.71N, 84.25W	7	97	7	92	0	-5
Deep Gulf St 24.77N, 89.65W	1.3	226	1.6	225	+0.3	-1
Misteriosa Bank 18.88N, 83.81W	8	84	9	89	+1	+5
Rosalind Bank 16.61N, 80.34W	7	107	8	102	+1	-5
East Carib. St. (6-month) 16.54N, 64.88W	0.5	156	1.6	151	+1	-5
East Carib. St. (1-month) 16.52N, 64.91W	0.6	153	1.5	148	0.9	-5

^a ξ = tidal amplitude.^b δ = tidal phase relative to Greenwich.

Table 4b. Deep-Sea M_2 -Tide Data for the Pacific and Atlantic Oceans

Station Latitude, Longitude	Observed		Model		Error	
	ξ^a (cm)	δ^b (°)	ξ (cm)	δ (°)	$\Delta\xi$ (cm)	$\Delta\delta$ (°)
Pacific St. 1 (Middleton) 58.76N, 145.71W	110	284	included			
Pacific St. 3 (Tofino) 48.97N, 127.29W	99	239	included			
Pacific St. (San Francisco) 38.16N, 124.91W	54	227	included			
Pacific St. (Josie II) 34.00N, 144.99W	27	267	27	273	0	+6
Pacific St. (Flicki) 32.24N, 120.86W	43	149	included			
Pacific St. (Josie I) 31.03N, 119.80W	43	142	included			
Pacific St. (Kathy) 27.75N, 124.37W	29	128	27	130	-2	+2
Pacific St. (Filloux) 24.78N, 129.02W	19	107	18	105	-1	-2
Atlantic St. 1 (N.Y. Bight) 39.32N, 64.36W	44	350	included			
Atlantic St. (N.C. St. 1) 32.69N, 75.62W	48	356	46	358	-2	+2
Atlantic St. (Savannah B) 31.95N, 80.68W	88	15	included			
Atlantic St. (Scope) 30.43N, 76.42W	45	358	46	3	+2	+5
Atlantic St. (AOML 1) 28.14N, 69.75W	34	1	35	6	+1	+5
Atlantic St. (AOML 3) 28.24N, 67.54W	34	359	34	4	0	+5
Atlantic St. (MERT) 27.99N, 69.67W	34	360	34	6	0	+6
Atlantic St. (REIKO) 27.97N, 69.67W	35	1	34	6	-1	+5
Atlantic St. (EDIE-May) 26.46N, 69.33W	32	3	32	7	0	+4
Atlantic St. (EDIE-March) 26.45N, 69.32W	31	1	32	7	+1	+6

^a ξ = tidal amplitude.^b δ = tidal phase relative to Greenwich.

Naturally, it must be remembered that the selection of representative empirical tidal data (compare depth data, Sect. 5.B) is not at all free of subjective judgment and may be somewhat erratic. Obviously, only future additional tidal measurements can improve this model in this respect. Nevertheless, according to the instruction notes accompanying the British Admiralty Tide Tables (1977), it can probably be assumed that almost all important tide data selected carry an accuracy that is at least as high as the desired 10 cm specified in Section 1. In any case, computational experiments showed that isolated reasonable variations of the boundary-tide data do not affect significantly the adjacent oceanic tides. It was also found insignificant to the overall quality of the tide model whether the empirical data were assigned to the centers or to the shore boundaries of the respective cells (see Part II).

Attempts were made to incorporate also recent deep-sea tidal measurements (Sect. 2) into the present model. Since the hydrodynamical interpolation of empirical data is essentially based on bottom and boundary irregularities (see Sect. 5.F(a)-(d), (ā)), no physically valid justification was found to include distant offshore deep-sea measurements into the model. However, some deep-sea measurements near rough shore and bottom areas were included. Fortunately, without exception, all excluded offshore deep-sea measurements known to the author agree very well with the computed M_2 -tide data (see Table 4).

D. DERIVATION OF DISCRETE OCEAN-TIDE EQUATIONS

Following essentially the hydrodynamical numerical method of Hansen (1966) and Zahel (1970), the COTEs (Eq's. 29 and 30) may now be converted to an explicit finite-difference analog called "discrete ocean-tide equations" (DOTEs). In a first step, all spacial derivatives will be replaced by divided central finite differences using the Richardson (1922) staggered scheme (Sect. 2(g)) illustrated in Figure 2c. In agreement with the graded grid system defined in Section 5.A, it is convenient to introduce the following notations:

$$\Delta \theta = \pi/360 = 1/2^\circ \text{ mesh size,} \quad (54)$$

$$\Delta \lambda = \mu \Delta \theta, \quad L = 2R \Delta \theta, \quad (55)$$

$$\Delta t = \text{time step to be specified;}$$

and for a fixed, oceanic mesh cell $S_{m,n}$ (Eq's. 46, 47, 48) at u -points (Figure 2c)

$$\left. \begin{aligned} \lambda_m(u) &= 2(m - \mu) \Delta \lambda, \\ \theta_n(u) &= (2n - 1) \Delta \theta, \\ U_{m,n}(t) &= U(\lambda_m(u), \theta_n(u), t), \\ \eta_{m,n}(t, u) &= \eta(\lambda_m(u), \theta_n(u), t), \\ \Gamma_n(u) &= 1/\mu \sin \theta_n(u); \end{aligned} \right\} \quad (56)$$

at v-points (Figure 2c)

$$\begin{aligned}
 \lambda_m(v) &= (2m - \mu) \Delta \lambda, \\
 \theta_n(v) &= 2n \Delta \theta, \\
 V_{m,n}(t) &= V(\lambda_m(v), \theta_n(v), t), \\
 \eta(t; v) &= \eta(\lambda_m(v), \theta_n(v), t), \\
 \Gamma_n(v) &= 1/\mu \sin \theta_n(v);
 \end{aligned}
 \tag{57}$$

and at ζ -points (Figure 2c)

$$\begin{aligned}
 \lambda_m(\zeta) &= \lambda_m(v), \\
 \theta_n(\zeta) &= \theta_n(u), \\
 \xi_{m,n}(t) &= \zeta(\lambda_m(v), \theta_n(u), t)
 \end{aligned}
 \tag{58}$$

For the first COTE (Eq. 29a) at u -points one has the following differential-difference replacements:

$$\begin{aligned}
 4\Delta\lambda \frac{U(t)}{\lambda, m, n} &\rightarrow \frac{U(t)}{m+\mu, n} - \frac{U(t)}{m-\mu, n}, \\
 4\Delta\lambda^2 \frac{U(t)}{\lambda\lambda, m, n} &\rightarrow \frac{U(t)}{m+\mu, n} - 2\frac{U(t)}{m, n} + \frac{U(t)}{m-\mu, n}, \\
 4\Delta\theta \frac{U(t)}{\theta, m, n} &\rightarrow \frac{U(t)}{m, n+1} - \frac{U(t)}{m, n-1}, \\
 4\Delta\theta^2 \frac{U(t)}{\theta\theta, m, n} &\rightarrow \frac{U(t)}{m, n+1} - 2\frac{U(t)}{m, n} + \frac{U(t)}{m, n-1}, \\
 4V(t; u)_{m, n} &\rightarrow \left[\frac{V(t)}{m, n} + \frac{V(t)}{m, n-1} \right] + \left[\frac{V(t)}{m-\mu, n} + \frac{V(t)}{m-\mu, n-1} \right], \\
 4\Delta\lambda V(t; u)_{\lambda, m, n} &\rightarrow \left[\frac{V(t)}{m, n} + \frac{V(t)}{m, n-1} \right] - \left[\frac{V(t)}{m-\mu, n} + \frac{V(t)}{m-\mu, n-1} \right], \\
 \text{and} \\
 2\Delta\lambda \xi(t; u)_{\lambda, m, n} &\rightarrow \frac{\xi(t)}{m, n} - \frac{\xi(t)}{m-\mu, n}.
 \end{aligned}
 \tag{59}$$

For the second COTE (Eq. 29b) at v-points one has the analogous differential-difference substitutions

$$\begin{aligned}
 4\Delta\lambda^2 V(t)_{\lambda\lambda, m, n} &\rightarrow V(t)_{m+\mu, n} - 2V(t)_{m, n} + V(t)_{m-\mu, n}, \\
 4\Delta\theta V(t)_{\theta, m, n} &\rightarrow V(t)_{m, n+1} - V(t)_{m, n-1}, \\
 4\Delta\theta^2 V(t)_{\theta\theta, m, n} &\rightarrow V(t)_{m, n+1} - 2V(t)_{m, n} + V(t)_{m, n-1}, \\
 4U(t; v)_{m, n} &\rightarrow [U(t)_{m+\mu, n+1} + U(t)_{m, n}] + [U(t)_{m+\mu, n} + U(t)_{m, n+1}], \\
 4\Delta\lambda U(t; v)_{\lambda, m, n} &\rightarrow [U(t)_{m+\mu, n+1} - U(t)_{m, n}] + [U(t)_{m+\mu, n} - U(t)_{m, n+1}], \\
 4\Delta\theta U(t; v)_{\theta, m, n} &\rightarrow [U(t)_{m+\mu, n+1} - U(t)_{m, n}] - [U(t)_{m+\mu, n} - U(t)_{m, n+1}],
 \end{aligned} \tag{60}$$

and

$$2\Delta\theta\zeta(t; v)_{\theta, m, n} \rightarrow \zeta(t)_{m, n+1} - \zeta(t)_{m, n}.$$

The third COTE (Eq. 30) at ζ -points becomes directly

$$R \sin \theta_n(u) \zeta(t)_{t, m, n} = \frac{1}{2\Delta\lambda} [U(t)_{m, n} - U(t)_{m+\mu, n}] + \frac{1}{2\Delta\theta} [\sin \theta_n(v) V(t)_{m, n} - \sin \theta_{n-1}(v) V(t)_{m, n-1}]. \tag{61}$$

It may be noted that in Equations 59 and 60 $V(t; u)$ at u -points and $U(t; v)$ at v -points, are defined as linear averages of adjacent $V(t)$ at v -points and $U(t)$ at u -points, respectively. After defining obvious analogous substitutions for the depth function, $H(\lambda, \theta)$ (given at ζ -points, Sect. 5.B), and its first and second partial derivatives at u - and v -points, one arrives at the following spacially differenced equations:

$$\begin{aligned}
 \Delta t U(t)_{t, m, n} &= \alpha \Delta t \frac{GH(u)_{m, n}}{R \sin \theta_n(u)} \eta(t, u)_{\lambda, m, n} + A^{(3)}_{m, n} [\zeta(t)_{m-\mu, n} - \zeta(t)_{m, n}] - A^4_{m, n} U(t)_{m, n} \\
 &+ A^5_{m, n} U(t)_{m+\mu, n} + A^6_{m, n} U(t)_{m-\mu, n} + A^7_{m, n} U(t)_{m, n+1} + A^8_{m, n} U(t)_{m, n-1} \\
 &+ A^9_{m, n} [(V(t)_{m, n} + V(t)_{m, n-1}) - (V(t)_{m-\mu, n} + V(t)_{m-\mu, n-1})] \\
 &+ A^{10}_{m, n} [(V(t)_{m, n} + V(t)_{m, n-1}) + (V(t)_{m-\mu, n} + V(t)_{m-\mu, n-1})],
 \end{aligned} \tag{62a}$$

$$\begin{aligned}
\Delta t V(t)_{t,m,n} = & \alpha \Delta t \frac{GH(v)_{m,n}}{R} \eta(t,v)_{\theta,m,n} + B^3_{m,n} [\zeta(t)_{m,n+1} - \zeta(t)_{m,n}] - B^4_{m,n} V(t)_{m,n} \\
& + B^5_{m,n} [V(t)_{m+\mu,n} + V(t)_{m-\mu,n}] + B^6_{m,n} V(t)_{m,n+1} + B^7_{m,n} V(t)_{m,n-1} \\
& + B^8_{m,n} [U(t)_{m+\mu,n+1} - U(t)_{m,n}] + B^9_{m,n} [U(t)_{m+\mu,n} - U(t)_{m,n+1}] \\
& + B^{10}_{m,n} [U(t)_{m+\mu,n+1} + U(t)_{m,n} + U(t)_{m+\mu,n} + U(t)_{m,n+1}], \quad (62b)
\end{aligned}$$

and

$$\Delta t \zeta(t)_{t,m,n} = C^1_n [U(t)_{m,n} - U(t)_{m+\mu,n}] + C^2_n V(t)_{m,n} - C^3_n V(t)_{m,n-1}, \quad (63)$$

where all A , B , C , and H 's are defined by Equations 69, 70, and 71.

In the second part of the differencing process, a regular, finite-difference scheme (Sect. 2(g), Figure 3a) in time is defined by integrating Equations 62 and 63 over a single time step, Δt , using an average integration rule of the form ($U \rightarrow V \rightarrow \zeta$)

$$\int_{t_j}^{t_{j+1}} U(t) dt = \Delta t \left[\kappa U^{j+1} + (1-\kappa) U^j \right], \quad (64)$$

where

$$\begin{aligned}
U^j &= U(t_j), \\
t_j &= (j-1)\Delta t, j = 1, 2, \dots, \quad (65)
\end{aligned}$$

and κ = some differencing parameters, which usually satisfy the restriction

$$0 \leq \kappa \leq 1. \quad (66)$$

As will be seen, the resulting discrete ocean-tide equations (DOTEs) are very sensitive to the choice of the differencing parameters, κ , and the time step, Δt . In fact, depending on the chosen values of κ and Δt , the DOTEs may be stable or unstable (Sect. 5.G) for any specified values of eddy viscosity, A , and bottom-friction coefficient, B . Moreover, different values of κ for Equations 62a, 62b, and 63 and for the various point values of U , V , and ζ can be chosen so that the resulting DOTEs may become explicit or implicit. Considering the complexity of the ocean basin and the large number of oceanic mesh cells, an explicit form for the DOTEs is here preferred.

After carrying out the integration of Equations 62 and 63 with the three (obvious) differencing parameters $\kappa = 0, \kappa$, and $\bar{\kappa}$, one arrives at the following explicit DOTEs:

$$\begin{aligned}
 [1 + \kappa A_{m,n}^4] U_{m,n}^{j+1} &= A_{m,n}^1 \sin \frac{\sigma \Delta t}{2} (2j - 1) + A_{m,n}^2 \cos \frac{\sigma \Delta t}{2} (2j - 1) \\
 &+ A_{m,n}^3 [\xi_{m-\mu,n}^j - \xi_{m,n}^j] + [1 - (1 - \kappa) A_{m,n}^4] U_{m,n}^j \\
 &+ A_{m,n}^5 U_{m+\mu,n}^j + A_{m,n}^6 U_{m-\mu,n}^j + A_{m,n}^7 U_{m,n+1}^j + A_{m,n}^8 U_{m,n-1}^j \\
 &+ A_{m,n}^9 [(V_{m,n}^j + V_{m,n-1}^j) - (V_{m-\mu,n}^j + V_{m-\mu,n-1}^j)] \\
 &+ A_{m,n}^{10} [(V_{m,n}^j + V_{m,n-1}^j) + (V_{m-\mu,n}^j + V_{m-\mu,n-1}^j)] , \tag{67a}
 \end{aligned}$$

$$\begin{aligned}
 [1 + \kappa B_{m,n}^4] V_{m,n}^{j+1} &= B_{m,n}^1 \cos \frac{\sigma \Delta t}{2} (2j - 1) + B_{m,n}^2 \sin \frac{\sigma \Delta t}{2} (2j - 1) \\
 &+ B_{m,n}^3 [\xi_{m,n+1}^j - \xi_{m,n}^j] + [1 - (1 - \kappa) B_{m,n}^4] V_{m,n}^j \\
 &+ B_{m,n}^5 [V_{m+\mu,n}^j + V_{m-\mu,n}^j] + B_{m,n}^6 V_{m,n+1}^j + B_{m,n}^7 V_{m,n-1}^j \\
 &+ B_{m,n}^8 [U_{m+\mu,n+1}^j - U_{m,n}^j] + B_{m,n}^9 [U_{m+\mu,n}^j - U_{m,n+1}^j] \\
 &+ B_{m,n}^{10} [U_{m+\mu,n+1}^j + U_{m,n}^j + U_{m+\mu,n}^j + U_{m,n+1}^j] , \tag{67b}
 \end{aligned}$$

and

$$\begin{aligned}
 \xi_{m,n}^{j+1} &= \xi_{m,n}^j + \bar{\kappa} [C_n^1 (U_{m,n}^{j+1} - U_{m+\mu,n}^{j+1}) + C_n^2 V_{m,n}^{j+1} - C_n^3 V_{m,n-1}^{j+1}] \\
 &+ (1 - \bar{\kappa}) [C_n^1 (U_{m,n}^j - U_{m+\mu,n}^j) + C_n^2 V_{m,n}^j - C_n^3 V_{m,n-1}^j] . \tag{68}
 \end{aligned}$$

The coefficients of the DOTEs (Eq's. 67 and 68) are

$$\begin{aligned}
 A_{m,n}^1 &= A_{m,n} \cos 2\nu (m - \mu) \Delta\theta, \\
 A_{m,n}^2 &= A_{m,n} \sin 2\nu (n - \mu) \Delta\theta, \\
 A_{m,n}^3 &= \beta \Delta t G H(u) \Gamma_n(u) / L, \\
 A_{m,n}^4 &= 2a \frac{\Delta t}{L} \psi_n(u) [\omega_n(u) H(u) - \tilde{H}(u)] + b \Delta t / \Gamma_n(u) H(u), \\
 A_{m,n}^5 &= a \frac{\Delta t}{L} \psi_n(u) \Gamma_n^2(u) H(u) [1 + \bar{H}(u)], \\
 A_{m,n}^6 &= a \frac{\Delta t}{L} \psi_n(u) \Gamma_n^2(u) H(u) [1 - \bar{H}(u)], \\
 A_{m,n}^7 &= a \frac{\Delta t}{L} H(u) [\psi_n(u) + \frac{\mu \Delta \theta}{2} (2 + \Gamma_n(u)) \cos (2n - 1) \Delta\theta], \\
 A_{m,n}^8 &= a \frac{\Delta t}{L} H(u) [\psi_n(u) - \frac{\mu \Delta \theta}{2} (2 + \Gamma_n(u)) \cos (2n - 1) \Delta\theta], \\
 A_{m,n}^9 &= a \frac{\Delta t}{L} \Gamma_n(u) H(u) [\psi_n(u) \hat{H}(u) - \frac{\mu \Delta \theta}{2} (3 + 2\Gamma_n(u)) \cos (2n - 1) \Delta\theta],
 \end{aligned} \tag{69a}$$

and

$$\begin{aligned}
 A_{m,n}^{10} &= -a \frac{\Delta t}{L} \Gamma_n(u) H(u) \bar{H}(u) [\psi_n(u) \hat{H}(u) - \frac{\mu \Delta \theta}{2} \cos (2n - 1) \Delta\theta] \\
 &\quad + \frac{\Delta t}{2} \Omega \cos (2n - 1) \Delta\theta,
 \end{aligned}$$

where

$$A_{m,n} = -4 \frac{\alpha G}{\sigma R} K H(u) \sin \frac{\sigma \Delta t}{2} \begin{cases} \sin (2n - 1) \Delta\theta, & \nu = 2 \\ \cos (2n - 1) \Delta\theta, & \nu = 1 \\ 0 & \nu = 0 \end{cases}$$

and

$$\psi_n(u) = \frac{1}{2} (1 + 1/\Gamma_n(u)), \quad \omega_n(u) = 1 + \Gamma_n^2(u); \tag{69a}$$

$$B_{m,n}^1 = B_{m,n} \cos \nu (2m - \mu) \Delta \theta,$$

$$B_{m,n}^2 = -B_{m,n} \sin \nu (2m - \mu) \Delta \theta,$$

$$B_{m,n}^3 = \beta \Delta t G H(v) / L,$$

$$B_{m,n}^4 = 2a \frac{\Delta t}{L} \psi_n(v) [\omega_n(v) H(v) - \tilde{H}(v)] + b \Delta t / \Gamma_n(v) H(v),$$

$$B_{m,n}^5 = a \frac{\Delta t}{L} \psi_n(v) \Gamma_n^2(v) H(v),$$

$$B_{m,n}^6 = a \frac{\Delta t}{L} H(v) [\psi_n(v) (1 - \hat{H}(v)) + \frac{\mu \Delta \theta}{4} (3 + 2\Gamma_n(v)) \cos 2n\Delta \theta],$$

$$B_{m,n}^7 = a \frac{\Delta t}{L} H(v) [\psi_n(v) (1 + \hat{H}(v)) - \frac{\mu \Delta \theta}{4} (3 + 2\Gamma_n(v)) \cos 2n\Delta \theta],$$

$$B_{m,n}^8 = a \frac{\Delta t}{L} \Gamma_n(v) \psi_n(v) H(v) [2\mu \Delta \theta \Gamma_n(v) \cos 2n\Delta \theta - \bar{H}(v)],$$

$$B_{m,n}^9 = a \frac{\Delta t}{L} \Gamma_n(v) \psi_n(v) H(v) [2\mu \Delta \theta \Gamma_n(v) \cos 2n\Delta \theta + \bar{H}(v)],$$

and

$$B_{m,n}^{10} = -a \frac{\Delta t}{L} \Gamma_n(v) \psi_n(v) H(v) \bar{H}(v) [\mu \Delta \theta \Gamma_n(v) \cos 2n\Delta \theta + \hat{H}(v)] - \frac{\Delta t}{2} \Omega \cos 2n\Delta \theta,$$

where

$$B_{m,n} = -4 \frac{\alpha G}{\sigma R} K H(v) \sin \frac{\sigma \Delta t}{2} \begin{cases} 2 \sin 4n\Delta \theta, & \nu = 2 \\ \cos 4n\Delta \theta, & \nu = 1 \\ -3 \sin 4n\Delta \theta, & \nu = 0 \end{cases}$$

and

$$\psi_n(v) = \frac{1}{2} (1 + 1/\Gamma_n(v)), \quad \omega_n(v) = 1 + \Gamma_n^2(v); \quad (69b)$$

$$C_n^{(1)} = \frac{\Delta r}{L} \Gamma_n(u),$$

$$C_n^{(2)} = \mu \frac{\Delta r}{L} \Gamma_n(u) \sin 2n\Delta\theta,$$

and

$$C_n^3 = \mu \frac{\Delta r}{L} \Gamma_n(u) \sin 2(n-1)\Delta\theta.$$

(70)

In these coefficients, the following depth functions were used at u -points:

$$H(u) = \frac{1}{2} [H_{m,n} + H_{m-\mu,n}],$$

$$\bar{H}(u) = \frac{1}{4H(u)} [H(u)_{m+\mu,n} - H(u)_{m-\mu,n}],$$

$$\hat{H}(u) = \frac{1}{4H(u)} [H(u)_{m,n-1} - H(u)_{m,n+1}],$$

$$\tilde{H}(u) = H(u)_{m,n} \left\{ \omega_n(u) - 2\Gamma_n^2(u) [\bar{H}^2(u) + (\mu\Delta\theta)^2] \right.$$

$$\left. + \mu\Delta\theta \psi_n(u) \cos(2n-1)\Delta\theta [(3 + 2\Gamma_n(u)) \hat{H}(u) - \mu\Delta\theta \Gamma_n(u) \cos(2n-1)\Delta\theta] \right\}$$

$$- \frac{1}{2} [\Gamma_n^2(u) (H(u)_{m+\mu,n} + H(u)_{m-\mu,n}) + (H(u)_{m,n+1} + H(u)_{m,n-1})];$$

(71a)

and at v -points

$$H(v) = \frac{1}{2} [H_{m,n} + H_{m,n+1}],$$

$$\bar{H}(v) = \frac{1}{4H(v)} [H(v)_{m+\mu,n} - H(v)_{m-\mu,n}],$$

$$\hat{H}(v) = \frac{1}{4H(v)} [H(v)_{m,n-1} - H(v)_{m,n+1}],$$

$$\tilde{H}(v) = H(v)_{m,n} \left\{ \omega_n(v) - 2[\hat{H}^2(v) + (\mu\Delta\theta)^2 \Gamma_n^2(v)] \right.$$

$$\left. + \mu\Delta\theta \psi_n(v) \hat{H}(v) [3 + \Gamma_n(v)] \cos 2n\Delta\theta \right\}$$

$$- \frac{1}{2} [\Gamma_n^2(v) (H(v)_{m+\mu,n} + H(v)_{m-\mu,n}) + (H(v)_{m,n+1} + H(v)_{m,n-1})].$$

(71b)

It may be mentioned that for $\kappa = 0$ and $\bar{\kappa} = 1$, the finite-difference scheme coincides with the technique used, e.g., by Hansen (1966), Zahel (1970, 1973, 1975), and Estes (1975, 1977). Extensive exploratory computations were carried out by the author with numerous κ and $\bar{\kappa}$ values within the ranges $0 \leq \kappa \leq 1.5$ and $0.5 \leq \bar{\kappa} \leq 1$. The computations produced no drastic differences, provided the eddy and bottom-friction coefficients a and b and the time step Δt were suitably chosen within their respective stability constraints (Sect. 5.G). Finally, it was decided to use the values

$$\kappa = \bar{\kappa} = 1 \quad (72)$$

because they yielded a preferable stability and seemingly best results. Moreover, this deviation from the Hansen-Zahel method became most significant for the hydrodynamical interpolation of empirical tidal data described in Section 5.F. Indeed, this novel technique uses the special property that for $\kappa = 1$ the bottom-friction coefficient, b , which enters only in A^4 and B^4 (Eq's. 69), becomes essentially a scaling multiplier of $U_{m,n}^{j+1}$ and $V_{m,n}^{j+1}$ in Equations 67a and 67b. Thus, together with $\bar{\kappa} = 1$ in Equation 68, the bottom-friction coefficient can easily be adjusted locally to match more closely prescribed tidal data.

With κ and $\bar{\kappa}$ specified by Equation 72, the DOTEs (Eq's. 67 and 68) still contain the parameters a , b , and Δt , which remain at one's disposal within their respective stability ranges (Sect. 5.G). They will be utilized to achieve best results by trial-and-error computations. The DOTEs (Eq's. 67a, b, and 68) can be applied to all oceanic mesh cells $S_{m,n}$ with $m = \mu, 2\mu, \dots, 360$ and $n = 4, 5, \dots, 168$ sweeping across the globe from $n = 4$ to $n = 168$. This procedure can be executed, provided suitable initial and lateral boundary data (Sect. 5.E) are prescribed. At colatitude line $n = 4$, the numerical solution is matched to the second-order arctic solution (Sect. 4) by the linear interpolation ($m = \mu, 2\mu, \dots, 360$)

$$\left. \begin{aligned} U_{m,3}^{j+1} &= \frac{1}{3} [2U_{m,4}^{j+1} + U_{m,1}^{j+1}], \\ U_{m,2}^{j+1} &= \frac{1}{3} [U_{m,4}^{j+1} + 2U_{m,1}^{j+1}], \end{aligned} \right\} (U \rightarrow V \rightarrow \xi) \quad (73)$$

where $U_{m,1}^{j+1}$, $V_{m,1}^{j+1}$, and $\xi_{m,1}^{j+1}$ are computed by Equations 43, 44, or 45. For colatitude lines $n = 7, 14, 29, 150$, spacially corresponding data (U, V, ξ) on $n = 8, 15, 30, 151$ (see Eq's. 46, 47, and 48) are defined by linear interpolation. Vice versa for $n = 8, 15, 30, 151$, spacially corresponding values (U, V, ξ) on $n = 7, 14, 29, 150$ are also defined by linear interpolation.

E. LATERAL-BOUNDARY, INITIAL, AND FINAL DATA

In order to complete the ocean-tide model, the DOTEs (Eq's. 67 and 68) must be supplemented by suitable lateral-boundary and initial values. As was explained in Section 2(d), in turbulent-flow situations, the mathematical boundary conditions usually preferred are (a) no-flow across the ocean shorelines and (b) free-slip along the ocean shorelines. It is clearly at this point that the great attractiveness of Richardson's (1922) staggered, finite-difference scheme (Sect's. 2(g) and 5.D) manifests itself in the practical simplicity with which the no-flow and free-slip (or no-slip) boundary conditions can be worked into the model. In fact, if $S_{m,n}$ is an oceanic boundary cell, then, by

definition (Sect. 5.A and Figure 2c), the zig-zagging mathematical boundary lines follow only mesh lines and pass only through velocity (u and/or v) points. The no-flow condition (a) is implemented by declaring at those points

$$U_{m,n}^{j+1} = 0 \text{ and/or } V_{m,n}^{j+1} = 0, \quad (74)$$

respectively. If, say, the v -point of $S_{m,n}$ is oceanic and the v -points of $S_{m-\mu,n}$ and/or $S_{m+\mu,n}$ are terrestrial, then the free-slip condition (b) is satisfied by reflectively setting*

$$V_{m-\mu,n}^{j+1} = +V_{m,n}^{j+1} \text{ and/or } V_{m+\mu,n}^{j+1} = +V_{m,n}^{j+1}, \quad (75)$$

respectively.

The mathematical boundary conditions (a) and (b) were applied by Hansen (1966), Zahel (1970, 1973, 1975), Estes (1975, 1977), and others. In the present model, these conditions are strictly enforced only at boundary points where no known empirical tidal data are available. However, at most oceanic boundary cells, empirical tidal constants are defined in Section 5.C. These data are worked into the present tide model by a unique hydrodynamical interpolation procedure (Sect. 5.F) that requires a controlled violation of the no-flow condition (a).

The construction of the M_2 tide was started at $j = 1$ ($t_1 = 0$) with an ocean completely at rest; i.e., with the initial values ($m = \mu, 2\mu, \dots, 360; n = 1, 2, \dots, 168$)

$$U_{m,n}^1 = V_{m,n}^1 = \xi_{m,n}^1 = 0. \quad (76)$$

The computations were carried over a prescribed number of time steps, $j = J$ (mostly a quarter period), and then printed for inspection of the results. With or without program and/or parameter changes, the computations were restarted using the latest or any earlier taped output instead of the initial values (Eq. 76). Occasionally, it was beneficial to speed up an unwanted slow decay of transient eigenmodes by "negatively" averaging the output data of half a period time difference; i.e., by setting

$$\bar{U}_{m,n}^J = \frac{1}{2} [U_{m,n}^J - U_{m,n}^{J-\bar{J}}], \quad U \rightarrow V \rightarrow \xi, \quad (77)$$

where $\sigma \Delta t \bar{J} = \pi$. This simple procedure diminishes all undesirable eigenmodes of lower frequency than the forced frequency, σ , and, similarly, most higher frequency modes. The negatively averaged data (Eq. 77) represent obviously improved initial data.

Two output tidal elevations $2\bar{J}$ -time steps apart (mostly a quarter-period apart),

$$\left. \begin{aligned} \xi_{m,n}^J &= \xi_{m,n} \cos [\sigma \Delta t J - \delta_{m,n}] \\ \text{and} \\ \xi_{m,n}^{J-2\bar{J}} &= \xi_{m,n} \cos [\sigma \Delta t (J - 2\bar{J}) - \delta_{m,n}], \end{aligned} \right\} \quad (78)$$

*If the no-slip condition is imposed, then the + signs in Equations 75 must be changed to - signs.

were used to compute the tidal "amplitudes"

$$\xi_{m,n} = [\xi_1^2 + \xi_2^2]^{1/2} \quad (79)$$

and "phases"

$$\delta_{m,n} = \arctan y/x \quad (= 0 \text{ for } x = y = 0), \quad (80)$$

where

$$\left. \begin{aligned} \xi_1 &= (\xi_{m,n}^{J-2J} + \xi_{m,n}^J)/2 \cos \sigma \Delta t J, \\ \xi_2 &= (\xi_{m,n}^{J-2J} - \xi_{m,n}^J)/2 \sin \sigma \Delta t J, \end{aligned} \right\} \quad (81)$$

$$\left. \begin{aligned} y &= \xi_1 \sin \sigma \Delta t (J - \bar{J}) - \xi_2 \cos \sigma \Delta t (J - \bar{J}), \\ x &= \xi_1 \cos \sigma \Delta t (J - \bar{J}) + \xi_2 \sin \sigma \Delta t (J - \bar{J}). \end{aligned} \right\} \quad (82)$$

In the finished product, i.e., when all (unforced) transient eigenmodes have satisfactorily decayed, the amplitudes (Eq. 79) and phases (Eq. 80) become essentially independent of time and undergo no further variation of significance after continued computations.

In the final M_2 -tide model presented in Part II, the convergence toward the steady state of the amplitudes and phases was found to be generally oscillating. So the integration process could safely be terminated when the amplitudes and phases over most ocean areas varied by less than 1 cm and 1° , respectively. This excellent convergence feature held true even at most coastal points. The convergence was slightly less complete only in some coastal cells where the tidal elevations are extremely large and vary rapidly from degree to degree. But even in those anomalous places (e.g., on the Patagonian Shelf; see the Tide Tables in Part II), the convergence error was well below the desired 10 cm specified in Section 1.

In order to follow the convergence of the computer program more closely, the squared tidal-amplitude sum

$$\xi_n^2 = \sum_{m=\mu}^{360} \xi_{m,n}^2 \quad (83)$$

was computed and printed for each fixed colatitude line $n = 4, 5, \dots, 168$. To compute the amplitudes $\xi_{m,n}$ in Equation 83, Equations 79 and 81 were used for $2J = 1$ and $J = j + 1$; i.e., for two consecutive time steps in connection with Equation 68. In this measure (Eq. 83), the convergence was carried to almost three significant figures for all n .

F. HYDRODYNAMICAL INTERPOLATION OF EMPIRICAL TIDE DATA

The discrete ocean-tide model developed so far is completely specified with the exception of the eddy and bottom-friction coefficients, a and b , and the time step, Δt (Eq's. 69 and 70). When those parameters are chosen uniformly for the entire ocean basin within certain stability limits (Sect. 5.G), then a unique solution can be computed, and any agreement or disagreement with observed tidal data must be accepted unless a compromising modification of the well-posed problem is feasible.

Preliminary computations carried out with this purely theoretical tide model produced results (Sect. 2(f)) that fulfilled the accuracy requirements posed in Section 1 over most ocean areas. Nevertheless, a brief glance at the many significant variations of ocean tides observed at continental and island stations (see, e.g., the underlined empirical M_2 -tide data in Tables 5-8, and Part II) leaves one convinced that such local tidal features could not be accommodated by a mathematical model that ignores local boundary details.

In order to enhance the quality of the purely hydrodynamical tide model described above, it appeared desirable to seek a physically acceptable way to incorporate the empirical tidal data themselves into the program. In a simple exploratory experiment, the arranged empirical tidal amplitudes, $\tilde{\xi}_{m,n}$, and phases, $\tilde{\delta}_{m,n}$ (Sect. 5.C), were introduced into the computer program and used (when available) in place of Equation 68 by setting

$$\tilde{\xi}_{m,n}^{j+1} = \tilde{\xi}_{m,n} \cos(\sigma \Delta t j - \tilde{\delta}_{m,n}). \quad (84)$$

The results represented a rather spectacular detailed improvement of the tidal model, very close to the final tide data presented in Tables 5-8 and Part II.

Unfortunately, the substitution of Equation 84 for the sensitive equation of conservation of mass (Eq. 68) constitutes a "continuity gap"

$$\Delta \xi_{m,n}^{j+1} = \tilde{\xi}_{m,n}^{j+1} - \xi_{m,n}^{j+1}, \quad (85)$$

which remained bounded but grew unrealistically large in some areas after continued integration in time. Also, the velocity field near such observed points became unacceptably distorted.

Of course, the continuity gap (Eq. 85) can be attributed to the following major causes which are physically plausible and have been briefly mentioned before:

(a) The bottom-friction coefficient, b (in A^4 and B^4 of Eq's. 69), which is most effective in boundary cells, depends on local shore features such as true cell size and bottom slope and roughness (Sect. 3.B(k)-(n)).

(b) The boundary cells are idealized by definition of strictly mathematical boundaries (see Sect's. 2(f) and 5.A, and Figure 1).

(c) The depth data of boundary cells are subjectively defined and, hence, faulty (Sect's. 2(f) and 5.B).

(d) The empirical tidal constants in Equation 84 are also faulty to some degree because of inaccurate measurements, harmonic analyses, and subjective selections and assignments to the centers of the boundary cells (Sect. 5.C).

(e) The discrete ocean-tide model is certainly not an exact description of the true oceanic tide; e.g., at boundaries, nonlinear inertial terms assume significance.

Obviously, the last two (hopefully minor) faults can be reduced only through continued future observations and modeling. However, the first two faults, (a) and (b), can be weakened by "hydrodynamically interpolating" the empirical tidal elevations (Eq. 84) into the tidal model and narrowing the continuity gap (Eq. 85) to an acceptable level as follows:

(a) Adjusting the velocity field by a locally controlled implicit variation of the bottom-friction coefficient, b , in Equations 69.

(b) Lifting the strict condition of no-flow across the mathematical ocean boundary and allowing for a monitored in- or out-flow by implicitly defining a more physical ocean boundary (Figure 1).

Since the finite-differencing parameters κ and $\bar{\kappa}$ in Equations 67 and 68 have been chosen by Equation 72, the bottom-friction coefficient, b , in A^4 and B^4 of Equations 69 can be considered "implicitly" varied by directly replacing the velocity components in Equation 68 as follows:

$$\left. \begin{aligned} U_{m,n}^{j+1} &\rightarrow U_{m,n}^{j+1} + \left| U_{m,n}^{j+1} \right| (wu_1 + \bar{w}\bar{u}_1), \\ U_{m+\mu,n}^{j+1} &\rightarrow U_{m+\mu,n}^{j+1} + \left| U_{m+\mu,n}^{j+1} \right| (wu_2 + \bar{w}\bar{u}_2), \\ V_{m,n}^{j+1} &\rightarrow V_{m,n}^{j+1} + \left| V_{m,n}^{j+1} \right| (wv_1 + \bar{w}\bar{v}_1), \end{aligned} \right\} \quad (86)$$

and

$$V_{m,n-1}^{j+1} \rightarrow V_{m,n-1}^{j+1} + \left| V_{m,n-1}^{j+1} \right| (wv_2 + \bar{w}\bar{v}_2),$$

provided $\tilde{\xi}_{m,n} \neq 0$; i.e., provided an empirical tidal amplitude is available for the considered mesh cell $S_{m,n}$. In Equations 86, the consistency and scale parameters (u, \bar{u}) and (v, \bar{v}) are defined by

$$\left\{ \begin{array}{ll} u_1 = 1, & \bar{u}_1 = 0 \\ u_1 = 0, & \bar{u}_1 = A_{m,n}^4 \\ u_1 = 0, & \bar{u}_1 = 0 \end{array} \right. \quad \begin{array}{l} \text{for } \Delta \xi_{m,n}^{j+1} \cdot U_{m,n}^{j+1} < 0, \\ \text{otherwise, but} \\ \text{if } \tilde{\xi}_{m-\mu,n} \neq 0; \end{array} \quad (87a)$$

$$\left\{ \begin{array}{ll} u_2 = 1, & \bar{u}_2 = 0 \\ u_2 = 0, & \bar{u}_2 = A_{m+\mu,n}^4 \end{array} \right. \quad \begin{array}{l} \text{for } \Delta \xi_{m,n}^{j+1} \cdot U_{m+\mu,n}^{j+1} > 0, \\ \text{otherwise;} \end{array} \quad (87b)$$

$$\left\{ \begin{array}{ll} v_1 = 1, & \bar{v}_1 = 0 \\ v_1 = 0, & \bar{v}_1 = B_{m,n}^4 \end{array} \right. \quad \begin{array}{l} \text{for } \Delta \xi_{m,n}^{j+1} \cdot V_{m,n}^{j+1} < 0, \\ \text{otherwise;} \end{array} \quad (87c)$$

and

$$\left\{ \begin{array}{ll} v_2 = 1, & \bar{v}_2 = 0 \\ v_2 = 0, & \bar{v}_2 = B_{m,n-1}^4 \\ v_2 = 0, & \bar{v}_2 = 0 \end{array} \right. \quad \begin{array}{l} \text{for } \Delta \xi_{m,n}^{j+1} \cdot V_{m,n-1}^{j+1} > 0, \\ \text{otherwise, but} \\ \text{if } \tilde{\xi}_{m,n-1} \neq 0. \end{array} \quad (87d)$$

The continuity gap (Eq. 85) will be narrowed when the "control parameters" w and \bar{w} are determined successively by

$$w = \begin{cases} \Delta \xi_{m,n}^{j+1} / \xi & \text{for } \xi \neq 0, \\ 0 & \text{for } \xi = 0 \end{cases} \quad (88a)$$

with the first "control limit"

$$|w| \leq k_1 \quad (88b)$$

and

$$\bar{w} = \begin{cases} [\Delta \xi_{m,n}^{j+1} - w\xi] / \bar{\xi} & \text{for } \bar{\xi} \neq 0, \\ 0 & \text{for } \bar{\xi} = 0 \end{cases} \quad (89a)$$

with the second control limit

$$|\bar{w}| \leq k_2, \quad (89b)$$

where (see Eq. 68)

$$\left. \begin{aligned} \xi &= C_n^1 [u_1 |U_{m,n}^{j+1}| + u_2 |U_{m+\mu,n}^{j+1}|] + v_1 C_n^2 |V_{m,n}^{j+1}| + v_2 C_n^3 |V_{m,n-1}^{j+1}| \\ \bar{\xi} &= C_n^1 [\bar{u}_1 |U_{m,n}^{j+1}| + \bar{u}_2 |U_{m+\mu,n}^{j+1}|] + \bar{v}_1 C_n^2 |V_{m,n}^{j+1}| + \bar{v}_1 C_n^3 |V_{m,n-1}^{j+1}| \end{aligned} \right\} \quad (90)$$

It is important to note that $u_i \cdot \bar{u}_i = 0$ and $v_i \cdot \bar{v}_i = 0$ for $i = 1, 2$. Accordingly, both control limits, k_1 and k_2 , which are at one's disposal, regulate the allowed decrease or, respectively, increase of the velocity components in Equations 86; i.e., the implicitly permitted corresponding increase or decrease of the local bottom-friction coefficients in Equations 67. Since the integration sweeps across the ocean from $m = \mu$ to 360 and $n = 4$ to 168, the special choice of $u_1 = \bar{u}_1 = 0$ and $v_2 = \bar{v}_2 = 0$ in Equations 87a and 87d excludes possible double adjustments of the velocity components. Also, if $u_1 \neq \bar{u}_1$ and/or $v_2 \neq \bar{v}_2$, backward adjustments of the tidal elevations via the corresponding Equation 68 must be made. This requires the replacements

$$\left. \begin{aligned} \xi_{m-\mu,n}^{j+1} &\rightarrow \xi_{m-\mu,n}^{j+1} - C_n^1 \left| U_{m,n}^{j+1} \right| (w u_1 + \bar{w} \bar{u}_1) \\ \text{and} \\ \xi_{m,n-1}^{j+1} &\rightarrow \xi_{m,n-1}^{j+1} - C_n^2 \left| V_{m,n-1}^{j+1} \right| (w v_2 + \bar{w} \bar{v}_2). \end{aligned} \right\} (91)$$

Analogous substitutions in the forward directions of m and n follow automatically in the integration process.

The velocity replacements in Equations 86 may be illustrated by the example

$$\begin{aligned} U_{m,n}^{j+1} &> 0, \quad U_{m+\mu,n}^{j+1} > 0, \quad V_{m,n}^{j+1} > 0, \quad V_{m,n-1}^{j+1} \geq 0, \\ \Delta \xi_{m,n}^{j+1} &> 0, \quad \tilde{\xi}_{m-\mu,n} &= 0, \quad \tilde{\xi}_{m,n-1} \neq 0. \end{aligned} \quad (92)$$

One finds $w > 0$, $\bar{w} \geq 0$, and

$$\left. \begin{aligned} U_{m,n}^{j+1} &\rightarrow U_{m,n}^{j+1} (1 + \bar{w} A_{m,n}^4), \\ U_{m+\mu,n}^{j+1} &\rightarrow U_{m+\mu,n}^{j+1} (1 - w), \\ V_{m,n}^{j+1} &\rightarrow V_{m,n}^{j+1} (1 + \bar{w} B_{m,n}^4), \end{aligned} \right\} (93)$$

and

$$\xi_{m-\mu,n}^{j+1} \rightarrow \xi_{m-\mu,n}^{j+1} - C_n^1 U_{m,n}^{j+1} \bar{w} A_{m,n}^4.$$

At this point, it must be mentioned that attempts were explored to lift the control limits prescribed by k_1 and k_2 in Equations 88b and 89b in an effort to close the continuity gap completely. However, since the bottom-friction coefficient, b , in A^4 and B^4 of Equations 69 is rather small (Eq. 4b), the control limits, k_1 and k_2 , had to be kept small to achieve best results. Computations conducted with large control limits k_1 (excessive bottom friction) seemed to close the continuity gap, but the tidal and velocity fields in the open oceans assumed unrealistically small values. Large control limits k_2 (insufficient bottom friction) produced strong instabilities as anticipated from the analysis in Section 5.G. To safely check the possible instability, the second control parameter \bar{w} (Eq's. 86, 87, and 93) was defined, respectively, in units of $\bar{u} = A^4$ and $\bar{v} = B^4$ in contrast to $u = 1$ and $v = 1$, used for the first control parameter w .

After some trial-and-error computations, the following control limits were chosen for the M_2 -tide model:

$$k_1 = .03, \quad k_2 = .06. \quad (94)$$

These moderate values reflect the well-known fact that the magnitude of bottom friction has a strong effect on the motions considered. Indeed, with some minor improvements of the tidal field, significant improvements of the continuity gap, velocity field, and convergence of the integration were achieved. This procedure was applied to all oceanic cells with known empirical tide data (Eq. 84), provided these cells bordered terrestrial cells or contained small islands or other bottom irregularities. No meaningful reason was seen to apply the same bottom-friction adjustment procedure to distant offshore oceanic cells with available deep-sea tide measurements. A comparison of computed tide data with those empirical deep-sea values is given in Table 4.

In order to implement the second step (b) of the hydrodynamical interpolation procedure, the following velocity replacements in oceanic mesh cells bordering terrestrial cells were defined:

$$\left. \begin{aligned} U_{m,n}^{j+1} &\rightarrow \tilde{w} \tilde{u}_1 U_{m+\mu,n}^{j+1}, \\ U_{m+\mu,n}^{j+1} &\rightarrow \tilde{w} \tilde{u}_2 U_{m,n}^{j+1}, \\ V_{m,n}^{j+1} &\rightarrow \tilde{w} \tilde{v}_1 V_{m,n-1}^{j+1} \end{aligned} \right\} \quad (95)$$

and

$$V_{m,n-1}^{j+1} \rightarrow \tilde{w} \tilde{v}_2 V_{m,n}^{j+1},$$

provided $\tilde{\xi}_{m,n} \neq 0$ in Equation 84. The parameters $(\tilde{u} \tilde{v})$ are mutually consistent by definition:

$$\left. \begin{aligned} \tilde{u}_1 &= 1 \quad \text{if } U_{m,n}^{j+1} = 0, \quad \text{otherwise } \tilde{u}_1 = 0, \\ \tilde{u}_2 &= 1 \quad \text{if } U_{m+\mu,n}^{j+1} = 0, \quad \text{otherwise } \tilde{u}_2 = 0, \\ \tilde{v}_1 &= 1 \quad \text{if } V_{m,n}^{j+1} = 0, \quad \text{otherwise } \tilde{v}_1 = 0, \end{aligned} \right\} \quad (96)$$

and

$$\tilde{v}_2 = 1 \quad \text{if } V_{m,n-1}^{j+1} = 0, \quad \text{otherwise } \tilde{v}_2 = 0.$$

The remaining continuity gap will be further narrowed when the control parameter \tilde{w} is determined to be in agreement with Equations 68, 85, 88, 89, and 90 by

$$\tilde{w} = \begin{cases} [\Delta \xi_{m,n}^{j+1} - w \xi - \bar{w} \bar{\xi}] / \tilde{\xi} & \text{for } \tilde{\xi} \neq 0 \\ 0 & \text{for } \tilde{\xi} = 0 \end{cases} \quad (97a)$$

with the third control limit

$$|\tilde{w}| \leq k_3, \quad (97b)$$

where

$$\tilde{\xi} = C_n^1 [\tilde{u}_1 U_{m+\mu,n}^{j+1} - \tilde{u}_2 U_{m,n}^{j+1}] + \tilde{V}_1 C_n^2 V_{m,n-1}^{j+1} - \tilde{V}_2 C_n^3 V_{m,n}^{j+1}. \quad (98)$$

Obviously, the substitutions (Eq's. 95) specify consistent in- or out-flows across the mathematical boundaries of oceanic coastal cells as illustrated in Figure 1 without explicitly fixing the physical boundary line. Again, no complete removal of the continuity gap was possible. The most satisfactory results for the M_2 tide (Part II) were achieved by setting the third control limit (Eq. 79b) at

$$k_3 = 0.5. \quad (99)$$

While the improvement of the tidal field was again moderate, the remaining continuity gaps and near-shore velocity distortions assumed uniformly satisfactory levels. These remaining small shortcomings of the model can easily be attributed to the boundary inaccuracies (c), (d) and (e) listed above, but for which no simple remedies were found.

It may be emphasized that the rather significant change in the near-shore velocity field permitted by the in- and out-flow specifications (Eq's. 95) affected the tidal field only in a minor fashion. This important phenomenon is in agreement with the well-known fact that the pressure distribution in a fluid motion is very insensitive to large but local velocity variations. For instance, it is perhaps the most important postulate in Prandtl's boundary-layer theory (see, e.g., Schlichting, 1968), and it is the basis of the hydrostatic-pressure assumption invoked here in Section 3.E for the present tidal model.

G. STABILITY ANALYSIS

A rigorous stability analysis of the homogeneous DOTEs (Eq's. 67 and 68) is, of course, not possible. However, under the assumption of constant coefficients A , B , and C , the simplified DOTEs possess Fourier-type eigen-solutions (Eq's. 109) that permit a local stability analysis of the difference system. As is well known (see, e.g., Richtmyer, 1957), such a local stability analysis produces stability limits that are usually sufficient for computational purposes. Indeed, computer experiments showed that the stability limits so derived below were scrupulously binding for the success of the integration. The following analysis is an expanded version of the investigation presented by Zahel (1970).

In detail, the following simplifications may be assumed:

- (a) $b = 0$; i.e., no bottom friction
- (b) $\Omega = 0$; i.e., no Coriolis force
- (c) For an arbitrary but fixed mesh cell (see Eq's. 56, 57, and 69a, b),

$$\begin{aligned}
& \Gamma = \Gamma_n(u) = \Gamma_n(v) = 1/\mu \sin \theta = \text{locally constant}, \\
& \psi = \psi_n(u) = \psi_n(v) = \frac{1}{2}(1 + 1/\Gamma), \\
& \omega = \omega_n(u) = \omega_n(v) = 1 + \Gamma^2; \\
& H = H_{m,n}(u) = H_{m,n}(v) = \text{locally constant}, \\
& \bar{H}_{m,n}(u) = \hat{H}_{m,n}(u) = \tilde{H}_{m,n}(u) = 0, (u \rightarrow v).
\end{aligned}
\tag{100}$$

and

It may be mentioned that the assumptions (a) and (b) have been made in order to display more clearly the most important stability characteristics of the DOTEs that are due to eddy dissipation and to the differencing parameters, κ and $\bar{\kappa}$. It is relatively easy to show that the bottom friction is always stabilizing, while the Coriolis force (in the present differencing scheme) is slightly destabilizing.

For the following derivations, it is helpful to introduce some specified reference values θ_r and H_r (consistent with Eq's. 100), Γ_r , ψ_r , and ω_r , and

$$a_r = \frac{1}{\psi_r} \left(\frac{G}{\omega_r H_r} \right)^{1/2}, \quad \Delta t_r = L/(\omega_r H_r G)^{1/2}. \tag{101}$$

Finally, the following relative quantities may be introduced:

$$\begin{aligned}
\bar{\psi} &= \psi/\psi_r, \quad \bar{\omega} = \omega/\omega_r, \quad h = H/H_r, \\
\tau &= \Delta t/\Delta t_r, \quad \epsilon = a/a_r.
\end{aligned}
\tag{102}$$

For example, in this notation the eddy viscosity, A (Eq. 6), assumes the form

$$A = \epsilon a_r \psi H L, \tag{103}$$

where ϵ is the "dimensionless eddy coefficient."

The M_2 -tide Tables 5-8 (and Part II) are computed with the reference values

$$\theta_r = 30^\circ, H_r = 7\,259.84 \text{ m}, \tag{104}$$

so that

$$\begin{aligned}
\psi_r &= 3/4, & a_r &= 0.021\,919\,2 \text{ sec}^{-1}, \\
\omega_r &= 5, & \Delta t_r &= 186.309 \text{ sec}, \\
180\sigma\Delta t_r/\pi &= 1.5^\circ, & J_p &= 360^\circ/1.5^\circ = 240,
\end{aligned}
\tag{105}$$

where J_p is the number of time steps required to integrate through one tidal period with $\Delta t = \Delta t_p$. Due to the grading of the grid system (Eq. 49), one has almost everywhere ($n \neq 1, 2, 3$, and 166, 167, 168)

$$1 \leq \bar{\psi} \leq \frac{4}{3}, \quad 1 \geq \bar{\omega} \geq \frac{2}{5}. \quad (106)$$

Similarly, due to the cutoff depth data (Eq's. 50, 51, 71), one has the limits

$$0.0013 < h < 1. \quad (107)$$

Several other reference values within the stability limits have been explored. Particularly extensive computations were carried out with $\Delta t_p = 248.412$ sec (so that $J_p = 180$), but the above reference values appeared to yield the best results.

With the simplifications and notations above, the coefficients (Eq's. 69 and 70) of the homogeneous DOTEs (Eq's. 67 and 68) become

$$\left. \begin{aligned} A^1 &= A^2 = B^1 = B^2 = 0, \\ A^3 &= \Gamma B^3 = \beta GH \Gamma \Delta t / L, \\ A^4 &= B^4 = 2h\epsilon\tau\bar{\psi}\bar{\omega}, \\ A^5 &= A^6 = B^5 = B^6 = h\epsilon\tau\bar{\psi}/\omega_r, \\ A^7 &= A^8 = B^7 = \Gamma^2 A^5, \\ A^9 &= A^{10} = B^8 = B^9 = B^{10} = 0, \\ C^1 &= \Gamma \Delta t / L, \quad C^2 = C^3 = \Delta t / L. \end{aligned} \right\} \quad (108)$$

The reduced DOTEs (with constant coefficients) yield the Fourier-type eigensolutions

$$\left. \begin{aligned} U_{m,n}^j &= U_0 d^j e^{i[\gamma_1(2m - 2\mu)\Delta\lambda + \gamma_2(2n - 1)\Delta\theta]}, \\ V_{m,n}^j &= V_0 d^j e^{i[\gamma_1(2m - \mu)\Delta\lambda + \gamma_2(2n - 1)\Delta\theta]}, \end{aligned} \right\} \quad (109)$$

and

$$\xi_{m,n}^j = \xi_0 d^j e^{i[\gamma_1(2m - \mu)\Delta\lambda + \gamma_2(2n - 1)\Delta\theta]}$$

with an arbitrary wave vector (γ_1, γ_2) and some nonzero amplitude vectors (U_0, V_0, ξ_0), provided the eigenvalue d satisfies the cubic characteristic equation

$$\begin{vmatrix} (A_{11} - dA_{10}) & 0 & A_{13} \\ 0 & (A_{22} - dA_{10}) & A_{23} \\ (1 - \bar{\kappa} + \bar{\kappa}d)A_{31} & (1 - \bar{\kappa} + \bar{\kappa}d)A_{32} & (1 - d) \end{vmatrix} = 0, \quad (110)$$

where (after some algebra)

$$\left. \begin{aligned} A_{10} &= 1 + \kappa A^4 = 1 + 2\kappa\epsilon\tau\bar{\psi}\bar{\omega}, \\ A_{11} &= A_{22} = A_{10} - 2A^4s^2, \\ \text{and} \quad A_{13}A_{31} + A_{32}A_{23} &= -4\beta h\bar{\omega}\tau^2s^2 \end{aligned} \right\} \quad (111a)$$

with

$$0 \leq s^2 \leq \frac{\Gamma^2 \sin^2 \gamma_1 \Delta \theta + \sin^2 \gamma_2 \Delta \theta}{\Gamma^2 + 1} \leq 1. \quad (111b)$$

The cubic characteristic in Equation 110 yields the three eigenvalues ($d_0, d = d_1, d_2$)

$$d_0 = 1 - 4\epsilon\tau\bar{\psi}\bar{\omega}s^2/A_{10} \quad (112a)$$

and

$$dA_{10} = A_{10} - 2h\tau\bar{\omega}s^2A_{01} \pm 2i\tau s \left[h\bar{\omega}(\beta A_{10} - h\bar{\omega}s^2A_{01}^2) \right]^{1/2}, \quad (112b)$$

where

$$A_{01} = \epsilon\bar{\psi} + \beta\bar{\kappa}\tau. \quad (112c)$$

The DOTEs will be stable, provided

$$|d_k| \leq 1 \text{ for } k = 0, 1, 2. \quad (113)$$

Under the strict inequality of Equation 113, the three eigenvalues d_0, d_1 , and d_2 define three decaying eigenwaves represented by Equations 109. Since d_0 is real, the corresponding eigenwave is a standing wave with no phase shift if $d_0 \geq 0$ (see Eq. 119). The other two eigenvalues d_1 and d_2 define a pair of eigenwaves progressing in opposite directions with the same decay and dispersion rates, provided

$$\beta A_{10} \geq h\bar{\omega}s^2A_{01}^2. \quad (114)$$

This condition holds true for all $0 \leq s \leq 1$ (Eq. 111b); i.e., for all wave vectors (γ_1, γ_2) if and only if

$$\beta A_{10} \geq h\bar{\omega}A_{01}^2. \quad (115)$$

If this condition fails, then there exist some short waves with large wave numbers, γ_1 and γ_2 , which become standing waves of different decay rates. However, all sufficiently long waves remain dispersively progressing and decaying at the same rates.

It seems physically plausible to treat all long and short waves equally and, hence, to impose the conditions of Equations 113 and 115 on the free parameters, ϵ, τ, κ , and $\bar{\kappa}$. Using Equations 112, 113, and 115, one finds

$$|d_1|^2 = |d_2|^2 = 1 - 4h\tau\bar{\omega}s^2 [\epsilon\bar{\psi} - (1 - \bar{\kappa})\beta\tau] / A_{10} \quad (116)$$

with

$$|d_1|^2 = |d_2|^2 = d_0 \text{ for } \bar{\kappa} = 1. \quad (117)$$

For $\bar{\kappa} < 1$, the stability condition requires

$$\epsilon \bar{\psi} \geq (1 - \bar{\kappa}) \beta \tau; \quad (118)$$

i.e., a minimum of eddy viscosity is necessary for stability. However, for $\bar{\kappa} = 1$, no minimum eddy viscosity is required, which explains the choice made here (Eq. 72) and by Hansen (1966), Zahel (1970, 1973, 1975), and Estes (1975, 1977).

For the chosen value $\bar{\kappa} = 1$, the stability condition is satisfied for all s and all eigenvalues d_0 , d_1 , and d_2 when

$$4h\epsilon\tau\bar{\psi}\bar{\omega} \leq A_{10}; \quad (119)$$

i.e., when

$$\tau = \frac{\Delta t}{\Delta t_r} \leq 1/2 (2 - \kappa) \epsilon h \bar{\psi} \bar{\omega}, \quad (120)$$

provided (Eq. 115 in explicit form) also

$$\frac{\beta}{h\bar{\omega}} \geq \beta^2 \tau^2 + 2\beta\epsilon\tau\bar{\psi} (1 - \kappa) + \epsilon^2 \bar{\psi}^2. \quad (121)$$

The obviously increased stability limits imposed by both Equations 120 and 121 explain the choice of $\kappa = 1$ made here for the present tide model (Eq. 72) in deviation from the value $\kappa = 0$ used by Hansen, Zahel, and Estes. It may also be recalled that as an important by-product, $\kappa = 1$ facilitated the simple hydrodynamical interpolation of empirical tidal data into the model described in Section 5.F.

With $\beta = 0.90$ (Eq's. 17) and the possible extreme values of $h = 1$ and, simultaneously, $\bar{\psi} = \bar{\omega} = 1$ (Eq's. 106 and 107), one finds from Equations 120 and 121 for $\kappa = 1$ and $\tau = 1$ the allowable range for the dimensionless eddy coefficient, ϵ :

$$0 \leq \epsilon \leq 0.3 \quad (\Delta t = \Delta t_r). \quad (122)$$

The same range holds also for the southern three colatitude lines $n = 166, 167, 168$, which violate the condition of Equation 49, but for which the relative depth, h , falls sufficiently below unity. The upper limit on ϵ could be raised somewhat by considering the simultaneous values of $\bar{\psi}$, $\bar{\omega}$, and h on each colatitude $n = 4, 5, \dots, 168$ separately. In order to obtain the best possible tidal field, extensive trial-and-error computations led to the choice

$$\Delta t = \Delta t_r = 186.309 \text{ sec and } \epsilon = 0.075. \quad (123)$$

This final choice completes the detailed parameter specifications of the present tide model.

At this point, it may be noticed that the stability requirement for the DOTEs restricts the possible amount of eddy dissipation. As is physically plausible, the finite-differencing parameters, κ and $\bar{\kappa}$, the mesh size, L , the depth, H , the time step, Δt , and the dimensionless eddy coefficient, ϵ , are intimately related to each other. Trial-and-error computations are needed to select those parameters for best results. It is particularly important to observe that (especially for $\bar{\kappa} = 1$) the rate of decay (Eq's. 112a, 116, and 117) of all eigenwaves depends directly on the product $h\epsilon$. Accordingly, for fixed ϵ , waves in deep ($h \approx 1$) ocean basins decay faster than in shallow ($h \ll 1$) regions if bottom friction is negligible.

It is obviously this physically realistic phenomenon that led to the introduction of the novel depth-dependent eddy viscosity, A , defined by Equations 6 or 103. For a depth-independent eddy viscosity, one has $h\epsilon = \text{constant}$, in which case waves would decay at the same rate in deep or shallow (see Sect. 6.A) oceans, even though no bottom friction is present. Following Hansen (1966), Zahel (1970, 1973, 1975), and Estes (1975, 1977), the present tide model also used at first a constant eddy viscosity with rather disappointing results caused by the strongly varying bathymetry.

It is interesting to note that for the limiting case of Equation 115, i.e., for

$$\beta A_{10} = h\bar{\omega} A_{01}^2, \quad (124)$$

Equation 112 assumes the simple form

$$dA_{01} = A_{01} - 2\beta\tau s^2 \pm 2i\beta\tau s(1 - s^2)^{1/2}. \quad (125)$$

Hence, for the northeast waves under 45° with wave numbers (Eq. 111b)

$$\gamma_1 = \gamma_2 = \gamma, \quad s^2 = \sin^2 \gamma \Delta \theta, \quad (126)$$

and ($\kappa = \bar{\kappa} = 1$)

$$d = \frac{\epsilon \bar{\psi} + \beta \tau e^{\pm 2i\gamma \Delta \theta}}{\epsilon \bar{\psi} + \beta \tau} = d_c + d_r e^{\pm 2i\gamma \Delta \theta} \quad (127)$$

Hence, in this case, the eigenvalues d_1 and d_2 lie on the circle

$$|d - d_c| = d_r, \quad d_c + d_r = 1 \quad (128)$$

as illustrated in Figure 5.

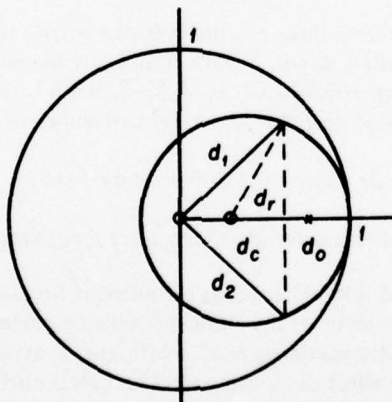


Figure 5. Illustration of Eigenvalues d_0 , d_1 , and $d_2 = \bar{d}_1$, in Circle $|d - d_c| \leq d_r$

6. DISCUSSION OF THE TIDE MODEL

A. DISCRETE VERSUS CONTINUOUS OCEAN-TIDE EQUATIONS

In Section 2(g), it was contended that discrete ocean-tide equations (DOTEs, Eq's. 67 and 68) reflect the physical reality of ocean tidal currents more perfectly and perceptibly than the corresponding continuous equations (COTEs, Eq's. 29 and 30). Although the latter follow from the former by a "formal" limit process, it is neither technically feasible nor theoretically desirable to seek convergence of the discrete solution to the continuous integral. In fact, in fluid-flow problems of global dimensions, it is not possible to approximate the conditions of the continuous case to any reasonable degree. Even with future computer technology, it will not be meaningful to refine significantly, for instance, the 1° by 1° grid system defined in Sect. 5.A, which, with its 100-km mesh size, is far from being anywhere near a continuous description. Any attempt to refine the grid system would have to be matched by an improved bathymetry (Sect. 5.B), which requires worldwide in situ measurements.

From the theoretical point of view, it is equally superfluous to seek an ϵ -approximation of the continuous situation, which in fact is only vaguely defined (Sect. 3.A). In laminar viscous-flow theory, such notions as particle (point) velocity and pressure, as well as the Navier-Stokes equations, are all derived from physically sound discrete (finite-difference) definitions by a formal limit procedure; i.e., by simply assuming the existence of the limit values (see, e.g., Schlichting, 1968; and Whitaker, 1968). While this assumption is well justified in most laminar-flow problems, it is well known today (see, e.g., Ladyzhenskaya, 1969) that, in general, even laminar motions must be sought in the class of generalized (distribution) functions. Hence, velocities, pressure, and their derivatives do not exist in the ordinary sense (pointwise); only their "functionals" (effects such as mass fluxes, forces, momenta) are physically defined.

The ambiguity of continuous-flow models becomes much more apparent in the critical laminar regime. Experiments (e.g., Busse and Whitehead, 1971) and theory (e.g., Schwiderski, 1972) have clearly established that, when given characteristic flow parameters (dimensions, velocities, etc.) exceed certain critical values, the corresponding, uniquely existent laminar motions become unstable and bifurcate into laminar flows of infinitely many different shapes. The classical laminar boundary and initial conditions (see, e.g., Sect's. 3.B and 5.E) are no longer sufficient to specify a unique motion. The situation seems to be governed by hysteresis and pure chance rather than rigorous physical selection principles.

Critical laminar motions become still more microscopically undefinable when the corresponding characteristic flow parameters (as the global dimensions of ocean currents) exceed further supercritical points and the motions go turbulent. The statistical approach underlying the "time-averaging" process to derive the so-called Navier-Stokes equations of mean turbulent flow (Eq's. 1 and 2) is entirely formal and vague (see, e.g., Schlichting, 1968). For example, what velocity (particle, point, etc.) is averaged over what time interval? In this respect, the present periodic tidal motions are clearly most illuminating of the problems at hand. If one averages (as usually meaningful) over a "sufficiently" long time span (say, longer than the tidal periods), then the averaged velocity should approach zero, which is obviously not of interest.

Evidently, turbulent particle velocities manifest themselves statistically through their integrated (macroscopic) physical effects, such as mass fluxes. Hence, the proper mathematical representation of turbulent motions should be sought in the class of generalized functions. Since the product of generalized functions has no mathematical meaning (see, e.g., Shilov, 1968), it appears understandable that there is no way to define the Reynolds stress tensor of turbulent motion (Sect. 3.C) by a meaningful ordinary or generalized function, because it contains quadratic products of the so-called fluctuating velocity residuals (see, e.g., Schlichting, 1968). However, its energy-dissipating (stress-like) effect is physically quite apparent and must be modeled in some macroscopic sense.

To avoid all conceptual difficulties of microscopic turbulent motions, it seems natural to fall back to the discrete (macroscopic) description of laminar flows that leads formally to the Navier-Stokes equations (see, e.g., Schlichting, 1968; and Whitaker, 1968). In fact, by proper "generalized" interpretation, virtually every notion used in the laminar regime retains its physical meaning in the discrete turbulent domain. For example, the "mean" x-velocity, u , of a "flow parcel" contained in a rectangular test (grid) cell of mesh lengths Δx , Δy , and Δz (Figure 6a) at some time, t , of a time interval, Δt , is defined as the mass flux (ΔM^x) crossing, say, the central ($x = x_1$) surface element (Δy , Δz) of the cell during the time span Δt divided by the fluid density, ρ , the area, $\Delta y \cdot \Delta z$, and the time, Δt , so that

$$u = \Delta M^x / \rho \Delta y \Delta x \Delta t. \quad (129)$$

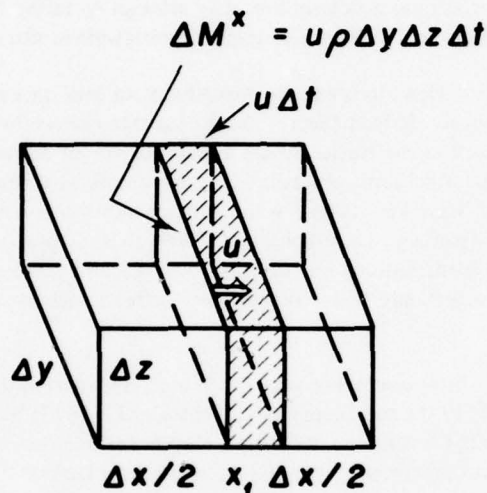


Figure 6a. Illustration of Average Velocity:

ΔM^x = Mass Flux in x-Direction,
 u = Mean Velocity in x-Direction,
and ρ = Fluid Density

This (generalized) definition of the mean-flow velocity, u , is uniformly valid for laminar and turbulent motions, since ΔM^x is a physically realistic (measurable) quantity for any $\rho > 0$, $\Delta x > 0$, $\Delta y > 0$, $\Delta z > 0$, and $\Delta t > 0$. If u exists in the limit $\Delta x \rightarrow 0$, $\Delta y \rightarrow 0$, $\Delta z \rightarrow 0$, and $\Delta t \rightarrow 0$, then u becomes the ordinary particle (or point) velocity. This assumption is well-justified in most (see above) laminar motions, where neighboring particles flow on smooth neighboring pathlines. In contrast to laminar flow, the limit assumption is certainly not justified in turbulent flow, where the fluid particles move in an indeterministically "turbulent," "fluctuating," or "eddy" way. In the sense of generalized functions, u could be defined in the limit by prescribing its mass flux (ΔM^x) for every nonvanishing ρ , Δx , Δy , Δz , and Δt .

Using similarly generalized definitions of all mean velocity components and pressure, and retaining their finite differences in place of (generally non-existent) ordinary derivatives, one arrives as usually at the discrete Navier-Stokes equations (analog of Eq's. 1 and 2) without requiring the existence of any limit values (see, e.g., Schlichting, 1968;

and Whitaker, 1968). They express simply the physical laws of conservation of momentum and mass for every test (mesh) cell. This is particularly tangible for the DOTE (Eq. 68), which conserves mass by balancing the excess of mass flux into a mesh cell with a corresponding increment in tidal height.

In the discrete form, the Navier-Stokes equations look formally the same for laminar and turbulent motions. Yet, when in the laminar case velocity and pressure exist pointwise in the limit, one has a unique microscopic (continuous) description of the flow subject only to specified boundary and initial conditions. Hence, the quality of a solution of the discrete model can be measured against the so-called exact integral of the continuous equations. In sharp contrast to the laminar case, no unique microscopic description of turbulent flow exists against which the quality of the discrete model could be measured. Therefore, the numerical analyst must seek an optimum size of the mesh cell (Δx , Δy , Δz) and the time span (Δt) in order to model the undetermined microscopic turbulent motion so that their macroscopic effects match the expected or observed features.

The strong dependence of a discrete turbulent-flow model on the size of the mesh cell (Δx , Δy , Δz) and the time span (Δt) can be assessed, for instance, from the definition of the average velocity, u , by Equation 129. With increasing mesh area ($\Delta y \cdot \Delta z$), more and more as well as larger and larger fluctuating or eddying motions are filtered out and remain unaccounted for in the average value of u . Hence, the maximum mesh lengths Δx , Δy , and Δz must be sufficiently smaller than the smallest wave length one wishes to resolve. On the other side, if the area ($\Delta y \cdot \Delta z$) in Equation 129 is chosen smaller and smaller, then u becomes more and more undetermined (fluctuating).

Similar arguments determine an optimum time step, Δt . In the present discrete tide model, the cell size was reasonably limited by the available bathymetric tables. The time step Δt (Eq. 123) was determined by trial-and-error computations so that 60 time points represent one-quarter of the M_2 -tide period.

Another significant distinction between the discrete Navier-Stokes equations of laminar and turbulent flow becomes apparent in the average-stress tensor. As is well known, the turbulent fluctuations neglected in the mean velocity and pressure manifest themselves as stress-like (energy-dissipating) forces that affect the mean motion. Unfortunately, no exact and unique constitutive equation is known today that relates those turbulent Reynolds stresses to the mean rate of strain (deformation of the flow parcel) determined by the average velocity (see, e.g., Schlichting, 1968; and Whitaker, 1968). In the Boussinesq (1877) substitution used in the present tide model, the mean turbulent-stress tensor is directly related to the average rate of strain (analog of Eq's. 5). Hence, the macroscopic stress effects of the turbulent fluctuations on the mean velocity are assumed to follow a similar simple law as the viscous laminar stresses in Newtonian fluids. Only the coefficient of viscosity is replaced by the so-called eddy viscosity which remains to be modeled to account for the otherwise neglected eddying motions in some best sense.

In the absence of better approximations, it seems idle to argue endlessly about the physical justification of the Boussinesq substitution; the fact remains that it represents the simplest possible constitutive equation, including zero used by some researchers. Moreover, it provides for considerable flexibility to model the microscopically undetermined but macroscopically apparent eddy dissipation by choosing suitable velocity-dependent or velocity-independent eddy viscosities either uniformly or separately for all three stress directions. Evidently, if the velocity field were known, a priori, then one could determine exact eddy viscosities, a posteriori, in many ways. In this connection, it is of interest to know that the mean flow is quite insensitive to fairly large variations (say 25 percent) of the eddy viscosity. This observation by Munk and Palmén (1951) was confirmed for oceanic tidal motions by the author's extensive computer experiments. It is probably related to the well-known fact that potential motions satisfy the complete Navier-Stokes equations of laminar flow with any constant viscosity. Above all, as with any other physical law, the Boussinesq substitution has successfully passed its crucial test in many practical applications in hydrodynamics, oceanography, and meteorology. The present ocean-tide model is no exception (see Sect. 6.B).

In order to illustrate the Boussinesq substitution in the discrete case, one may consider, for example, the average normal stress τ_1^{xx} produced by the filtered out (see the remarks to Eq. 129) fluctuating motions on the surface ($\Delta y, \Delta z$) at $x = x_1$ shown in Figure 6b. Following Boussinesq, one has (see the analogous Eq. 5c)

$$\tau_1^{xx} = 2A\rho \frac{u_2 - u_0}{2\Delta x}, \quad (130a)$$

where u_0 and u_2 are the corresponding mean velocities at $x = x_0 = x_1 - \Delta x$ and $x = x_2 = x_1 + \Delta x$. Hence, the turbulent stress τ_1^{xx} grows linearly with the rate of change of average velocity. Analogous to the corresponding laminar stress, this linear law appears physically acceptable, since the expected mean tidal velocities are small. One concludes from Equation 130a that a large change of mean flow produces a large turbulent stress which plausibly must be due to strong fluctuating motions.

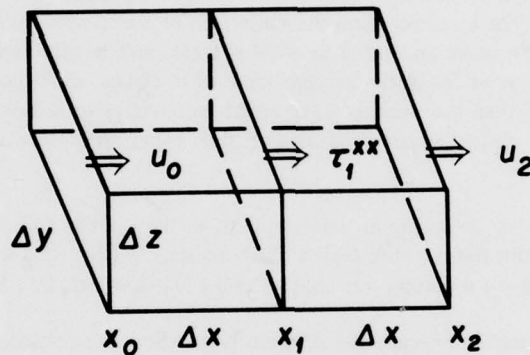


Figure 6b. Illustration of Mean Normal Stress:

u_0, u_2 = Average x-Velocities at $x = x_0, x_2$,
and τ_1^{xx} = Average Normal Stress

If one assumes a constant eddy viscosity, A , in Equation 130a, then the analogy between turbulent and laminar stress becomes complete. However, as was pointed out above, the strength of the fluctuating motions under consideration depends on the size of the surface area ($\Delta y \cdot \Delta z$), which justifies the assumption

$$A = a\Delta y\Delta z \quad (130b)$$

in Equation 130a, where a may be held constant or used for further modeling. Similar arguments can be developed for all six turbulent stress components (see Eq's. 5) with eddy viscosities equivalent to Equation 130b.

The novel eddy-viscosity law expressed by Equation 130b is obviously equivalent to the eddy viscosity introduced in the present tide model by Equation 6a. It also explains Equation 4a, which specifies the bottom-friction coefficient, B , of the discrete tide model. The need for a mesh-area-dependent eddy viscosity became apparent when initial tidal computations with a constant value failed to yield realistic results (see Sect's. 2(a) and 5.G). It must be emphasized that the microscopically indeterministic nature of turbulent motions is not completely removed in the discrete flow model. Its specific macroscopic effects on the mean flow are apparent in the required optimum choice of the grid system, time step, differencing parameters, and, most of all, the eddy-viscosity law and scaling coefficient. No information on the fine structure of the turbulence can be expected from such a model.

B. QUALITY OF THE OCEAN-TIDE MODEL

Because of the absence of an exact (continuous) ocean-tide model, the degree of reality achieved by any approximate (discrete) model must be measured against empirically known features of ocean tides. In contrast to other turbulent-flow problems, for instance in general ocean currents, a large number of tidal observations (Sect. 5.C) around the world are available for comparison. Since the present tide model incorporates essentially all known empirical data by hydrodynamical interpolation (Sect. 5.F), no direct comparison of observed and computed data is feasible.

Nevertheless, a rather vivid and comprehensive appraisal of the reality of the present tide model is possible by inspecting the quality of hydrodynamical interpolation; i.e., by evaluating the "smoothness" with which the computed tide "accepts or rejects" (Figure 7) the empirical tidal data. In fact, the smoothness characteristics of the novel hydrodynamical interpolation technique are distinctly different from those of other direct interpolation procedures using power or trigonometric polynomials. In the latter case, smoothness of the interpolation can be carried up to any desired degree by simple intend. The adjustment of hydrodynamical parameters (Sect. 5.F) in the former method does not imply any smoothness of the interpolation, unless both the empirical input data and the hydrodynamical tide model are compatible with each other. As is well known (see Sect's. 5.B and 5.C), local tidal distortions, caused by an isolated roughness (seamount or small island) in the bottom relief, affect the surrounding ocean tide very little. The major level of ocean tides is shaped by continental shorelines and large (in area and/or length) islands and ridges. In contrast to ordinary polynomial interpolations, an important feature of the new hydrodynamical interpolation method is that it preserves those significant properties of ocean tidal currents without any essential alterations.

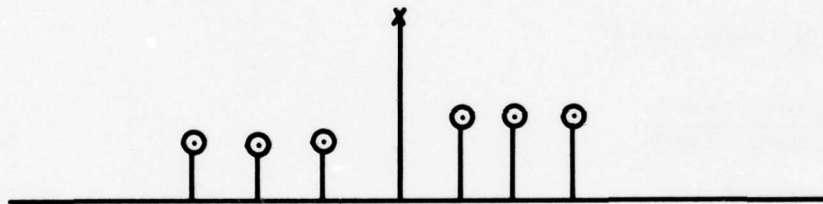


Figure 7. Illustration of "Rejected" (Protruding) Empirical Tidal Amplitude or Phase Value: x = Rejected Input Tide Values, and \circ = Computed Tide Values

Extensive computer experiments were conducted to test the important smoothness characteristics of the hydrodynamical interpolation procedure. Faulty input data were deliberately inserted and quickly recognized as rejected by (protruding out of; Figure 7) the computed surrounding tide. Indeed, the first computations, which included empirical tidal data, revealed immediately several input errors in the data. Vice versa, smoothly accepted empirical tidal data were randomly deleted to test their backlash reaction on the computed tide. As anticipated, no significant modifications were detected. Consequently, the hydrodynamical interpolation technique permits a check of the reality of both the tide model and the empirical tidal input data. If an input value is rejected by the computed tide, then one or the other or both are defective. Fortunately, only very few discrepancies between the different sources of observed M_2 -tide data (see Sect. 5.C) have been discovered that way.

The present discrete tide model has been applied to compute the global M_2 ocean tide. A complete discussion and tabulation of all amplitudes and phases will be presented in Part II of this report. In order to display the quality of the tidal model, the computed amplitudes (in cm) and phases (in degrees) along with their adjacent empirical values have been tabulated in "30° by 50° map form" for four typical ocean areas (Tables 5-8). All empirically supported input data along continental shores and at island stations are underlined in the tables. All near-shore deep-sea measurements included in the model are labeled by subbrackets. As was explained in Section 5.F, all distant offshore deep-sea measurements are not included in the tide model. However, their approximate locations are marked by wavy underlines and their corresponding observed data are listed in Table 4. Land points are left blank.

In the evaluation of the tidal accuracy, one must remember that the ocean tide at any fixed location is determined by two harmonic constants. If (ξ_0, δ_0) and (ξ, δ) denote the respective local amplitudes and phases of the "true" and "computed" tides

$$\zeta_0 = \xi_0 \cos(\sigma t - \delta_0), \quad \zeta = \xi \cos(\sigma t - \delta), \quad (131)$$

then their time-dependent error is

$$\tilde{\zeta} = \zeta_0 - \zeta = \tilde{\xi} \cos(\sigma t - \tilde{\delta}) \quad (132a)$$

with the standard deviation

$$\text{rms}(\tilde{\zeta}) = \frac{1}{2}\sqrt{2}\tilde{\xi}, \quad (132b)$$

where

$$\tilde{\xi}^2 = \xi_0^2 - 2\xi_0\xi \cos(\delta_0 - \delta) + \xi^2 \quad (132c)$$

and

$$\tan \tilde{\delta} = \frac{\xi_0 \sin \delta_0 - \xi \sin \delta}{\xi_0 \cos \delta_0 - \xi \cos \delta}. \quad (132d)$$

Some maximum errors are

$$\tilde{\xi}_M = \tilde{\xi}_M = \xi_0 + \xi \quad \text{for} \quad \delta_0 - \delta = 180^\circ, \quad (133a)$$

$$\tilde{\xi}_M = \tilde{\xi}_M = \xi_0 - \xi \quad \text{for} \quad \delta_0 - \delta = 0^\circ, \quad (133b)$$

$$\tilde{\xi}_M = \tilde{\xi}_M = 2\xi \sin \frac{1}{2}(\delta_0 - \delta) \quad \text{for} \quad \xi = \xi_0, \quad (134a)$$

and

$$\tilde{\xi}_M = \tilde{\xi}_M = \xi \quad \text{for} \quad \xi = \xi_0 \quad \text{and} \quad \delta_0 - \delta = 60^\circ. \quad (134b)$$

Equation 134b expresses the important fact that a 60° phase error results in an amplitude error equal to the tidal amplitude and, hence, renders the computed tidal prediction completely useless. Of course, in regions of sufficiently small amplitudes, any phase error is acceptable.

Tables 5a and 5b depict the tidal amplitudes and phases, respectively, of the northwestern Atlantic Ocean including the eastern Caribbean Sea. As can be verified by earlier tide models, this entire area was very difficult to model, because its rough bottom topography has a strong effect on the tidal currents that sweep over or across various barriers with rapidly changing water levels. There is the broad and shallow continental shelf along the whole North American shoreline with Cape Hatteras, Long Island, Cape Cod, Nova Scotia, and Newfoundland all protruding into the ocean basin. Furthermore, there are the Grand Banks, the Bahama Banks, and the long and narrow

Caribbean Ridge. Obviously, all of the corresponding local tidal features could not be realistically captured by the tide model without a proper representation of the bathymetry (Sect. 5.B) and without the hydrodynamical interpolation (Sect. 5.F) of the locally collected tidal observations.

Now, if one scans the tidal amplitudes and phases (Tables 5a and 5b) from the north to the south, one gathers the vivid impression that the whole computed ocean tide is completely locked into the array of empirical (underlined) tidal data everywhere along the continental coast and along the many aligned islands separating the Atlantic Ocean from the Gulf of Mexico and the Caribbean Sea. It is particularly impressive to see the observed tide data at the offshore islands (Sable—SI, Barbados—BB, and even as far as Bermuda—BI) and at the included near-shore (sub-brackets), deep-sea stations all realistically well-accepted by the computed surrounding tide. Moreover, one finds the excluded offshore deep-sea measurements (locations marked by wavy underlines) in the Atlantic and Caribbean Sea fully verified by the independent tide model.

As can be seen in the special listing of Table 4, the measured and computed amplitudes and phases at the Atlantic stations agree within 2 cm and 6° , respectively. The remaining discrepancy is probably within the experimental error due to short observation times and the use of the distant reference station Bermuda (Zettler et al., 1975), which exhibits even larger gaps between the various tidal observations listed in Table 3.

Attention may be drawn to the existence of considerable slopes between the empirical boundary data and the computed ocean-tide values in the high-amplitude ranges from Nova Scotia to Cape Cod and from Cape Hatteras to Florida's coast. Yet, these rapid tidal variations can be considered as realistic because throughout the same sections the empirical data, amongst themselves, display exactly the same roughness. This only substantiates clearly the fundamental difference between polynomial and hydrodynamical interpolation techniques pointed out above.

In Part II of this report, the same tidal roughness will be recognized in several similar coastal places around the world. From this typical phenomenon, one can draw the fortunate conclusion that, while some empirical data may be lacking high accuracy (see Table 2 and the British Admiralty Tide Tables, 1977), the computed adjacent ocean tide may retain its high quality.

In order to gain a deeper insight into the detailed tidal phenomena from the enclosed table charts (say, Tables 5a and 5b), it is helpful to recall the physical meaning of the tabulated tidal constants. The local tidal amplitude, ξ , is defined as half the tidal "range," which measures the total variation of the water level from high to low. Lines of constant amplitudes are called "corange lines." As can be seen from Equations 12 through 15, with $\lambda = 0$, the local phase, δ , specifies the tidal cresting time (in degrees) after the moon's (or sun's) passage over the Greenwich meridian ($\lambda = 0$). For the present M_2 tide (see Table 1), one has the following time conversions:

$$\left. \begin{aligned} 360^\circ &= 12.421 \text{ hours (period)} \\ 30^\circ &= 1.035 \text{ hours} \\ 1^\circ &= 2.070 \text{ minutes} \end{aligned} \right\} (135)$$

Lines of constant phases (simultaneous cresting times) are called "cotidal lines." In particular, at the $0^\circ = 360^\circ$ cotidal lines, which are conspicuously visible in the phase charts (Tables 5b to 8b), the tide crests simultaneously with the moon's passage over the Greenwich meridian. The tidal crest advances with time normal to the cotidal lines toward larger phases. A point of zero amplitude ($\xi = 0$) around which the tidal crest rotates from 0° to 360° is called an "amphidromic point;" it is marked in the tables by a circled star \otimes .

In the area of Tables 5a and 5b, a major amphidromic point is visible in the Caribbean Sea southeast of the island of Puerto Rico (PRI) near the marked deep-sea gauge station. The loosely connected Caribbean and Atlantic tides rotate counterclockwise around this point with the $0^\circ = 360^\circ$ cotidal line running northeastward. As a result

Table 5a. M₂ Tidal Amplitudes, ξ (cm), of the Northwestern Atlantic Ocean

260	281	282	283	284	285	286	287	288	289	290	291	292	293	294	295	296	297	298	299	300	301	302	303	304	305	306	307	308	309	310	311	312	313	314	315	316	317	318	319	320	321	322	323	324	325	326	327	328	329	330	331	332	333	334	335	336	337	338	339	340	341	342	343	344	345	346	347	348	349	350	351	352	353	354	355	356	357	358	359	360	361	362	363	364	365	366	367	368	369	370	371	372	373	374	375	376	377	378	379	380	381	382	383	384	385	386	387	388	389	390	391	392	393	394	395	396	397	398	399	400	401	402	403	404	405	406	407	408	409	410	411	412	413	414	415	416	417	418	419	420	421	422	423	424	425	426	427	428	429	430	431	432	433	434	435	436	437	438	439	440	441	442	443	444	445	446	447	448	449	450	451	452	453	454	455	456	457	458	459	460	461	462	463	464	465	466	467	468	469	470	471	472	473	474	475	476	477	478	479	480	481	482	483	484	485	486	487	488	489	490	491	492	493	494	495	496	497	498	499	500	501	502	503	504	505	506	507	508	509	510	511	512	513	514	515	516	517	518	519	520	521	522	523	524	525	526	527	528	529	530	531	532	533	534	535	536	537	538	539	540	541	542	543	544	545	546	547	548	549	550	551	552	553	554	555	556	557	558	559	560	561	562	563	564	565	566	567	568	569	570	571	572	573	574	575	576	577	578	579	580	581	582	583	584	585	586	587	588	589	590	591	592	593	594	595	596	597	598	599	600	601	602	603	604	605	606	607	608	609	610	611	612	613	614	615	616	617	618	619	620	621	622	623	624	625	626	627	628	629	630	631	632	633	634	635	636	637	638	639	640	641	642	643	644	645	646	647	648	649	650	651	652	653	654	655	656	657	658	659	660	661	662	663	664	665	666	667	668	669	670	671	672	673	674	675	676	677	678	679	680	681	682	683	684	685	686	687	688	689	690	691	692	693	694	695	696	697	698	699	700	701	702	703	704	705	706	707	708	709	710	711	712	713	714	715	716	717	718	719	720	721	722	723	724	725	726	727	728	729	730	731	732	733	734	735	736	737	738	739	740	741	742	743	744	745	746	747	748	749	750	751	752	753	754	755	756	757	758	759	760	761	762	763	764	765	766	767	768	769	770	771	772	773	774	775	776	777	778	779	780	781	782	783	784	785	786	787	788	789	790	791	792	793	794	795	796	797	798	799	800	801	802	803	804	805	806	807	808	809	810	811	812	813	814	815	816	817	818	819	820	821	822	823	824	825	826	827	828	829	830	831	832	833	834	835	836	837	838	839	840	841	842	843	844	845	846	847	848	849	850	851	852	853	854	855	856	857	858	859	860	861	862	863	864	865	866	867	868	869	870	871	872	873	874	875	876	877	878	879	880	881	882	883	884	885	886	887	888	889	890	891	892	893	894	895	896	897	898	899	900	901	902	903	904	905	906	907	908	909	910	911	912	913	914	915	916	917	918	919	920	921	922	923	924	925	926	927	928	929	930	931	932	933	934	935	936	937	938	939	940	941	942	943	944	945	946	947	948	949	950	951	952	953	954	955	956	957	958	959	960	961	962	963	964	965	966	967	968	969	970	971	972	973	974	975	976	977	978	979	980	981	982	983	984	985	986	987	988	989	990	991	992	993	994	995	996	997	998	999	1000	1001	1002	1003	1004	1005	1006	1007	1008	1009	1010	1011	1012	1013	1014	1015	1016	1017	1018	1019	1020	1021	1022	1023	1024	1025	1026	1027	1028	1029	1030	1031	1032	1033	1034	1035	1036	1037	1038	1039	1040	1041	1042	1043	1044	1045	1046	1047	1048	1049	1050	1051	1052	1053	1054	1055	1056	1057	1058	1059	1060	1061	1062	1063	1064	1065	1066	1067	1068	1069	1070	1071	1072	1073	1074	1075	1076	1077	1078	1079	1080	1081	1082	1083	1084	1085	1086	1087	1088	1089	1090	1091	1092	1093	1094	1095	1096	1097	1098	1099	1100	1101	1102	1103	1104	1105	1106	1107	1108	1109	1110	1111	1112	1113	1114	1115	1116	1117	1118	1119	1120	1121	1122	1123	1124	1125	1126	1127	1128	1129	1130	1131	1132	1133	1134	1135	1136	1137	1138	1139	1140	1141	1142	1143	1144	1145	1146	1147	1148	1149	1150	1151	1152	1153	1154	1155	1156	1157	1158	1159	1160	1161	1162	1163	1164	1165	1166	1167	1168	1169	1170	1171	1172	1173	1174	1175	1176	1177	1178	1179	1180	1181	1182	1183	1184	1185	1186	1187	1188	1189	1190	1191	1192	1193	1194	1195	1196	1197	1198	1199	1200	1201	1202	1203	1204	1205	1206	1207	1208	1209	1210	1211	1212	1213	1214	1215	1216	1217	1218	1219	1220	1221	1222	1223	1224	1225	1226	1227	1228	1229	1230	1231	1232	1233	1234	1235	1236	1237	1238	1239	1240	1241	1242	1243	1244	1245	1246	1247	1248	1249	1250	1251	1252	1253	1254	1255	1256	1257	1258	1259	1260	1261	1262	1263	1264	1265	1266	1267	1268	1269	1270	1271	1272	1273	1274	1275	1276	1277	1278	1279	1280	1281	1282	1283	1284	1285	1286	1287	1288	1289	1290	1291	1292	1293	1294	1295	1296	1297	1298	1299	1300	1301	1302	1303	1304	1305	1306	1307	1308	1309	1310	1311	1312	1313	1314	1315	1316	1317	1318	1319	1320	1321	1322	1323	1324	1325	1326	1327	1328	1329	1330	1331	1332	1333	1334	1335	1336	1337	1338	1339	1340	1341	1342	1343	1344	1345	1346	1347	1348	1349	1350	1351	1352	1353	1354	1355	1356	1357	1358	1359	1360	1361	1362	1363	1364	1365	1366	1367	1368	1369	1370	1371	1372	1373	1374	1375	1376	1377	1378	1379	1380	1381	1382	1383	1384	1385	1386	1387	1388	1389	1390	1391	1392	1393	1394	1395	1396	1397	1398	1399	1400	1401	1402	1403	1404	1405	1406	1407	1408	1409	1410	1411	1412	1413	1414	1415	1416	1417	1418	1419	1420	1421	1422	1423	1424	1425	1426	1427	1428	1429	1430	1431	1432	1433	1434	1435	1436	1437	1438	1439	1440	1441	1442	1443	1444	1445	1446	1447	1448	1449	1450	1451	1452	1453	1454	1455	1456	1457	1458	1459	1460	1461	1462	1463	1464	1465	1466	1467	1468	1469	1470	1471	1472	1473	1474	1475	1476	1477	1478	1479	1480	1481	1482	1483	1484	1485	1486	1487	1488	1489	1490	1491	1492	1493	1494	1495	1496	1497	1498	1499	1500	1501	1502	1503	1504	1505	1506	1507	1508	1509	1510	1511	1512	1513	1514	1515	1516	1517	1518	1519	1520	1521	1522	1523	1524	1525	1526	1527	1528	1529	1530	1531	1532	1533	1534	1535	1536	1537	1538	1539	1540	1541	1542	1543	1544	1545	1546	1547	1548	1549	1550	1551	1552	1553	1554	1555	1556	1557	1558	1559	1560	1561	1562	1563	1564	1565	1566	1567	1568	1569	1570	1571	1572	1573	1574	1575	1576	1577	1578	1579	1580	1581	1582	1583	1584	1585	1586	1587	1588	1589	1590	1591	1592	1593	1594	1595	1596	1597	1598	1599	1600	1601	1602	1603	1604	1605	1606	1607	1608	1609	1610	1611	1612	1613	1614	1615	1616	1617	1618	1619	1620	1621	1622	1623	1624	1625	1626	1627	1628	1629	1630	1631	1632	1633	1634	1635	1636	1637	1638	1639	1640	1641	1642	1643	1644	1645	1646	1647	1648	1649	1650	1651	1652	1653	1654	1655	1656	1657	1658	1659	1660	1661	1662	1663	1664	1665	1666	1667	1668	1669	1670	1671	1672	1673	1674	1675	1676	1677	1678	1679	1680	1681	1682	1683	1684	1685	1686	1687	1688	1689	1690	1691	1692	1693	1694	1695	1696	1697	1698	1699	1700	1701	1702	1703	1704	1705	1706	1707	1708	1709	1710	1711	1712	1713	1714	1715	1716	1717	1718	1719	1720	1721	1722	1723	1724
-----	-----	-----	-----	-----	-----	-----	-----	-----	-----	-----	-----	-----	-----	-----	-----	-----	-----	-----	-----	-----	-----	-----	-----	-----	-----	-----	-----	-----	-----	-----	-----	-----	-----	-----	-----	-----	-----	-----	-----	-----	-----	-----	-----	-----	-----	-----	-----	-----	-----	-----	-----	-----	-----	-----	-----	-----	-----	-----	-----	-----	-----	-----	-----	-----	-----	-----	-----	-----	-----	-----	-----	-----	-----	-----	-----	-----	-----	-----	-----	-----	-----	-----	-----	-----	-----	-----	-----	-----	-----	-----	-----	-----	-----	-----	-----	-----	-----	-----	-----	-----	-----	-----	-----	-----	-----	-----	-----	-----	-----	-----	-----	-----	-----	-----	-----	-----	-----	-----	-----	-----	-----	-----	-----	-----	-----	-----	-----	-----	-----	-----	-----	-----	-----	-----	-----	-----	-----	-----	-----	-----	-----	-----	-----	-----	-----	-----	-----	-----	-----	-----	-----	-----	-----	-----	-----	-----	-----	-----	-----	-----	-----	-----	-----	-----	-----	-----	-----	-----	-----	-----	-----	-----	-----	-----	-----	-----	-----	-----	-----	-----	-----	-----	-----	-----	-----	-----	-----	-----	-----	-----	-----	-----	-----	-----	-----	-----	-----	-----	-----	-----	-----	-----	-----	-----	-----	-----	-----	-----	-----	-----	-----	-----	-----	-----	-----	-----	-----	-----	-----	-----	-----	-----	-----	-----	-----	-----	-----	-----	-----	-----	-----	-----	-----	-----	-----	-----	-----	-----	-----	-----	-----	-----	-----	-----	-----	-----	-----	-----	-----	-----	-----	-----	-----	-----	-----	-----	-----	-----	-----	-----	-----	-----	-----	-----	-----	-----	-----	-----	-----	-----	-----	-----	-----	-----	-----	-----	-----	-----	-----	-----	-----	-----	-----	-----	-----	-----	-----	-----	-----	-----	-----	-----	-----	-----	-----	-----	-----	-----	-----	-----	-----	-----	-----	-----	-----	-----	-----	-----	-----	-----	-----	-----	-----	-----	-----	-----	-----	-----	-----	-----	-----	-----	-----	-----	-----	-----	-----	-----	-----	-----	-----	-----	-----	-----	-----	-----	-----	-----	-----	-----	-----	-----	-----	-----	-----	-----	-----	-----	-----	-----	-----	-----	-----	-----	-----	-----	-----	-----	-----	-----	-----	-----	-----	-----	-----	-----	-----	-----	-----	-----	-----	-----	-----	-----	-----	-----	-----	-----	-----	-----	-----	-----	-----	-----	-----	-----	-----	-----	-----	-----	-----	-----	-----	-----	-----	-----	-----	-----	-----	-----	-----	-----	-----	-----	-----	-----	-----	-----	-----	-----	-----	-----	-----	-----	-----	-----	-----	-----	-----	-----	-----	-----	-----	-----	-----	-----	-----	-----	-----	-----	-----	-----	-----	-----	-----	-----	-----	-----	-----	-----	-----	-----	-----	-----	-----	-----	-----	-----	-----	-----	-----	-----	-----	-----	-----	-----	-----	-----	-----	-----	-----	-----	-----	-----	-----	-----	-----	-----	-----	-----	-----	-----	-----	-----	-----	-----	-----	-----	-----	-----	-----	-----	-----	-----	-----	-----	-----	-----	-----	-----	-----	-----	-----	-----	-----	-----	-----	-----	-----	-----	-----	-----	-----	-----	-----	-----	-----	-----	-----	-----	-----	-----	-----	-----	-----	-----	-----	-----	-----	-----	-----	-----	-----	-----	-----	-----	-----	-----	-----	-----	-----	-----	-----	-----	-----	-----	-----	-----	-----	-----	-----	-----	-----	-----	-----	-----	-----	-----	-----	-----	-----	-----	-----	-----	-----	-----	-----	-----	-----	-----	-----	-----	-----	-----	-----	-----	-----	-----	-----	-----	-----	-----	-----	-----	-----	-----	-----	-----	-----	-----	-----	-----	-----	-----	-----	-----	-----	-----	-----	-----	-----	-----	-----	-----	-----	-----	-----	-----	-----	-----	-----	-----	-----	-----	-----	-----	-----	-----	-----	-----	-----	-----	-----	-----	-----	-----	-----	-----	-----	-----	-----	-----	-----	-----	-----	-----	-----	-----	-----	-----	-----	-----	-----	-----	-----	-----	-----	-----	-----	-----	-----	-----	-----	-----	-----	-----	-----	-----	-----	-----	-----	-----	-----	-----	-----	-----	-----	-----	-----	-----	-----	-----	-----	-----	-----	-----	-----	-----	-----	-----	-----	-----	-----	-----	-----	-----	-----	-----	-----	-----	-----	-----	-----	-----	-----	-----	-----	-----	-----	-----	-----	-----	-----	-----	-----	-----	-----	-----	-----	-----	-----	-----	-----	-----	-----	-----	-----	-----	-----	-----	-----	-----	-----	-----	-----	-----	-----	-----	-----	------	------	------	------	------	------	------	------	------	------	------	------	------	------	------	------	------	------	------	------	------	------	------	------	------	------	------	------	------	------	------	------	------	------	------	------	------	------	------	------	------	------	------	------	------	------	------	------	------	------	------	------	------	------	------	------	------	------	------	------	------	------	------	------	------	------	------	------	------	------	------	------	------	------	------	------	------	------	------	------	------	------	------	------	------	------	------	------	------	------	------	------	------	------	------	------	------	------	------	------	------	------	------	------	------	------	------	------	------	------	------	------	------	------	------	------	------	------	------	------	------	------	------	------	------	------	------	------	------	------	------	------	------	------	------	------	------	------	------	------	------	------	------	------	------	------	------	------	------	------	------	------	------	------	------	------	------	------	------	------	------	------	------	------	------	------	------	------	------	------	------	------	------	------	------	------	------	------	------	------	------	------	------	------	------	------	------	------	------	------	------	------	------	------	------	------	------	------	------	------	------	------	------	------	------	------	------	------	------	------	------	------	------	------	------	------	------	------	------	------	------	------	------	------	------	------	------	------	------	------	------	------	------	------	------	------	------	------	------	------	------	------	------	------	------	------	------	------	------	------	------	------	------	------	------	------	------	------	------	------	------	------	------	------	------	------	------	------	------	------	------	------	------	------	------	------	------	------	------	------	------	------	------	------	------	------	------	------	------	------	------	------	------	------	------	------	------	------	------	------	------	------	------	------	------	------	------	------	------	------	------	------	------	------	------	------	------	------	------	------	------	------	------	------	------	------	------	------	------	------	------	------	------	------	------	------	------	------	------	------	------	------	------	------	------	------	------	------	------	------	------	------	------	------	------	------	------	------	------	------	------	------	------	------	------	------	------	------	------	------	------	------	------	------	------	------	------	------	------	------	------	------	------	------	------	------	------	------	------	------	------	------	------	------	------	------	------	------	------	------	------	------	------	------	------	------	------	------	------	------	------	------	------	------	------	------	------	------	------	------	------	------	------	------	------	------	------	------	------	------	------	------	------	------	------	------	------	------	------	------	------	------	------	------	------	------	------	------	------	------	------	------	------	------	------	------	------	------	------	------	------	------	------	------	------	------	------	------	------	------	------	------	------	------	------	------	------	------	------	------	------	------	------	------	------	------	------	------	------	------	------	------	------	------	------	------	------	------	------	------	------	------	------	------	------	------	------	------	------	------	------	------	------	------	------	------	------	------	------	------	------	------	------	------	------	------	------	------	------	------	------	------	------	------	------	------	------	------	------	------	------	------	------	------	------	------	------	------	------	------	------	------	------	------	------	------	------	------	------	------	------	------	------	------	------	------	------	------	------	------	------	------	------	------	------	------	------	------	------	------	------	------	------	------	------	------	------	------	------	------	------	------	------	------	------	------	------	------	------	------	------	------	------	------	------	------	------	------	------	------	------	------	------	------	------	------	------	------	------	------	------	------	------	------	------	------	------	------	------	------	------	------	------	------	------	------	------	------	------	------	------	------	------	------	------	------	------	------	------	------	------	------	------	------	------	------	------	------	------	------	------	------	------	------	------	------	------	------	------	------	------	------	------	------	------	------	------	------	------	------	------	------	------	------	------	------	------	------	------	------	------	------	------	------	------	------	------	------	------	------	------	------	------	------	------	------	------	------	------	------	------	------	------	------	------	------	------	------	------	------	------	------	------	------	------

1	2	3	4	5	6	7	8	9	10	11	12	13	14	15	16	17	18	19	20	21	22	23	24	25	26	27	28	29	30	31	32	33	34	35	36	37	38	39	40	41	42	43	44	45	46	47	48	49	50	51	52	53	54	55	56	57	58	59	60	61	62	63	64	65	66	67	68	69	70	71	72	73	74	75	76	77	78	79	80	81	82	83	84	85	86	87	88	89	90	91	92	93	94	95	96	97	98	99	100	101	102	103	104	105	106	107	108	109	110	111	112	113	114	115	116	117	118	119	120	121	122	123	124	125	126	127	128	129	130	131	132	133	134	135	136	137	138	139	140	141	142	143	144	145	146	147	148	149	150	151	152	153	154	155	156	157	158	159	160	161	162	163	164	165	166	167	168	169	170	171	172	173	174	175	176	177	178	179	180	181	182	183	184	185	186	187	188	189	190	191	192	193	194	195	196	197	198	199	200	201	202	203	204	205	206	207	208	209	210	211	212	213	214	215	216	217	218	219	220	221	222	223	224	225	226	227	228	229	230	231	232	233	234	235	236	237	238	239	240	241	242	243	244	245	246	247	248	249	250	251	252	253	254	255	256	257	258	259	260	261	262	263	264	265	266	267	268	269	270	271	272	273	274	275	276	277	278	279	280	281	282	283	284	285	286	287	288	289	290	291	292	293	294	295	296	297	298	299	300	301	302	303	304	305	306	307	308	309	310	311	312	313	314	315	316	317	318	319	320	321	322	323	324	325	326	327	328	329	330	331	332	333	334	335	336	337	338	339	340	341	342	343	344	345	346	347	348	349	350	351	352	353	354	355	356	357	358	359	360	361	362	363	364	365	366	367	368	369	370	371	372	373	374	375	376	377	378	379	380	381	382	383	384	385	386	387	388	389	390	391	392	393	394	395	396	397	398	399	400	401	402	403	404	405	406	407	408	409	410	411	412	413	414	415	416	417	418	419	420	421	422	423	424	425	426	427	428	429	430	431	432	433	434	435	436	437	438	439	440	441	442	443	444	445	446	447	448	449	450	451	452	453	454	455	456	457	458	459	460	461	462	463	464	465	466	467	468	469	470	471	472	473	474	475	476	477	478	479	480	481	482	483	484	485	486	487	488	489	490	491	492	493	494	495	496	497	498	499	500	501	502	503	504	505	506	507	508	509	510	511	512	513	514	515	516	517	518	519	520	521	522	523	524	5
---	---	---	---	---	---	---	---	---	----	----	----	----	----	----	----	----	----	----	----	----	----	----	----	----	----	----	----	----	----	----	----	----	----	----	----	----	----	----	----	----	----	----	----	----	----	----	----	----	----	----	----	----	----	----	----	----	----	----	----	----	----	----	----	----	----	----	----	----	----	----	----	----	----	----	----	----	----	----	----	----	----	----	----	----	----	----	----	----	----	----	----	----	----	----	----	----	----	----	-----	-----	-----	-----	-----	-----	-----	-----	-----	-----	-----	-----	-----	-----	-----	-----	-----	-----	-----	-----	-----	-----	-----	-----	-----	-----	-----	-----	-----	-----	-----	-----	-----	-----	-----	-----	-----	-----	-----	-----	-----	-----	-----	-----	-----	-----	-----	-----	-----	-----	-----	-----	-----	-----	-----	-----	-----	-----	-----	-----	-----	-----	-----	-----	-----	-----	-----	-----	-----	-----	-----	-----	-----	-----	-----	-----	-----	-----	-----	-----	-----	-----	-----	-----	-----	-----	-----	-----	-----	-----	-----	-----	-----	-----	-----	-----	-----	-----	-----	-----	-----	-----	-----	-----	-----	-----	-----	-----	-----	-----	-----	-----	-----	-----	-----	-----	-----	-----	-----	-----	-----	-----	-----	-----	-----	-----	-----	-----	-----	-----	-----	-----	-----	-----	-----	-----	-----	-----	-----	-----	-----	-----	-----	-----	-----	-----	-----	-----	-----	-----	-----	-----	-----	-----	-----	-----	-----	-----	-----	-----	-----	-----	-----	-----	-----	-----	-----	-----	-----	-----	-----	-----	-----	-----	-----	-----	-----	-----	-----	-----	-----	-----	-----	-----	-----	-----	-----	-----	-----	-----	-----	-----	-----	-----	-----	-----	-----	-----	-----	-----	-----	-----	-----	-----	-----	-----	-----	-----	-----	-----	-----	-----	-----	-----	-----	-----	-----	-----	-----	-----	-----	-----	-----	-----	-----	-----	-----	-----	-----	-----	-----	-----	-----	-----	-----	-----	-----	-----	-----	-----	-----	-----	-----	-----	-----	-----	-----	-----	-----	-----	-----	-----	-----	-----	-----	-----	-----	-----	-----	-----	-----	-----	-----	-----	-----	-----	-----	-----	-----	-----	-----	-----	-----	-----	-----	-----	-----	-----	-----	-----	-----	-----	-----	-----	-----	-----	-----	-----	-----	-----	-----	-----	-----	-----	-----	-----	-----	-----	-----	-----	-----	-----	-----	-----	-----	-----	-----	-----	-----	-----	-----	-----	-----	-----	-----	-----	-----	-----	-----	-----	-----	-----	-----	-----	-----	-----	-----	-----	-----	-----	-----	-----	-----	-----	-----	-----	-----	-----	-----	-----	-----	-----	-----	-----	-----	-----	-----	-----	-----	-----	-----	-----	-----	-----	-----	-----	-----	-----	-----	-----	-----	-----	-----	-----	-----	-----	-----	-----	-----	-----	-----	-----	-----	-----	-----	-----	-----	-----	-----	-----	-----	-----	-----	-----	-----	-----	-----	-----	-----	-----	-----	-----	-----	-----	-----	-----	-----	-----	-----	-----	-----	-----	-----	-----	-----	-----	-----	-----	-----	-----	-----	-----	-----	-----	-----	-----	-----	-----	-----	-----	-----	-----	-----	-----	-----	---

of this rotation, the whole Caribbean Sea appears to be trapped and unable to develop any significant M_2 tide. In agreement with the observations, the M_2 tidal crest sweeps across the Caribbean Sea essentially from north to south with very little variation in water level.

If one follows the tidal crest around the amphidromic point from the Atlantic Ocean to the Caribbean Sea and back to the Atlantic, one recognizes a major tidal distortion caused by ocean ridges, which has long been discovered by practical tidalists (see, e.g., Harris, 1904; Bogdanov, 1961; Defant, 1961; and Luther and Wunsch, 1974). As the tide crosses the ridge between the islands, it suffers a distinct amplitude jump and a significant phase shift. For example, north of Puerto Rico (PRI) and Hispaniola and in the southeast around Barbados (BB), the computed and empirical Atlantic tide data display a higher water level and an earlier or, respectively, a delayed cresting time than the adjacent tide data on the Caribbean side. In particular, in full agreement with the observations, the tidal retardation time can easily exceed 30° (≈ 1 hr). The distortion seems to depend on the angle with which the tidal crest spills over the ridge. Maximum distortion appears to be associated with a normal crossing. It may be pointed out that the realistic resolution of tidal distortions by ocean ridges (see below and Part II) constitutes probably the most significant improvement of the present model over all earlier hydrodynamical models.

The Atlantic portion of the Caribbean-Atlantic amphidromic rotation is opposed by a southward advancing tide from about Newfoundland in the north and by an eastward progressing tide from about Cape Cod to Cape Hatteras in the west. As a result of this interaction of three opposing tidal waves, the middle latitudes (around $n = 60^\circ$) of the Atlantic display very few variations in tidal amplitudes and phases. In the high-amplitude sections between Nova Scotia and Cape Cod and between Cape Hatteras and Florida's coast, the Caribbean-Atlantic rotation system seems to be less affected by the opposing tidal waves. The extreme tidal amplitudes occurring at the former shore section are probably caused by the frontally advancing tidal crest splashing against the shallow coastal corner.

Although the computed tide in the Gulf of St. Lawrence displays the well-known amphidromic point (Defant, 1961), the grid system is much too crude to attach a high accuracy to the tidal constants in this border sea. For the same reason, the tidal data listed between Florida, Cuba, and the Bahamas are naturally less accurate than those in the open oceans.

Tables 6a and 6b illustrate the smoothness with which the computed tide of the northeastern Pacific Ocean attaches itself to the empirical tide data along the North American west coast. The tidal constants observed at the islands of Guadalupe (GI) and Farallon (FI), at the Cobb Seamount (CS), and at the included near-shore deep-sea stations fit realistically well into the computed surrounding tide. The amplitudes and phases of the excluded off-shore deep-sea measurements in the Pacific agree within 2 cm and 6° , respectively, with the computed data (Table 4), which is just the same accuracy as in the Atlantic.

Perhaps the most prominent feature of this area is the amphidromic point \otimes , around which the M_2 tide rotates counterclockwise. This amphidromic system was predicted by Munk et al. (1970) and Irish et al. (1971) in almost identical geographical position. Earlier hydrodynamical tide models failed to resolve this system on proper location, although several models matched the empirical data along the coast quite well. Since the northeastern Pacific falls short in major bottom and coastal irregularities when compared to the northwestern Atlantic, the indicated rapid loss of quality in westerly direction seemed disappointing. Yet, as will be demonstrated below, this shortcoming could have been concluded from the obvious failure of those models to reasonably reproduce the tide over most of the north and central Pacific Ocean.

As was mentioned before, the author's preliminary tide model (Schwiderski, 1976) used a bathymetry that failed to represent the hydrodynamical barrier effects of the Marianas, Nampo, Kuril, Aleutian, and Hawaiian Ridges, as well as of other seamount chains. Consequently, the M_2 tide of almost the whole central, western, and northern Pacific area was modeled as a single huge amphidromic system, as pictured by the similar maps of other

numerical tidalists such as Zahel (1971) and Estes (1975, 1977). The clockwise-rotating Pacific tide was free to sweep undisturbed into the Philippine, Okhotsk, and Bering Seas. By the time the computed tidal crest reached the Aleutian Islands, it was just about 180° out of phase. When the original bathymetry was replaced by hydrodynamically defined depth data (Sect. 5.B), the entire Pacific Ocean resembled a whirlpool after some continued computations over several quarter periods. The amphidromic system weakened and its center slipped slowly southward, but drastically improved phases appeared gradually along the Aleutian Ridge confirming the anticipated effect of ocean ridges.

The complete turnaround of the Pacific M_2 tide near the Aleutian Islands was speeded up when the empirical tidal constants were introduced into the model. In fact, a repeat of the same computations settled the Pacific Ocean tide into its final position in a rather dramatic fashion. Striking improvements were registered over the whole Pacific and, of course, also over the Atlantic and Indian Oceans.

As is depicted in Tables 7a and 7b for the north-central Pacific, the amphidromic system is replaced by a low-amplitude tide. It appears to be locked in between the Aleutian and Hawaiian Ridges in the north and south and also between the Emperor Seamount chain in the west and the high-amplitude tide in the east, which progresses in a westerly direction from the west coast of North America (Tables 6a and 6b). The amplitude topography of this area resembles the low-amplitude tide in the Caribbean Sea (Table 5a). When the westward-advancing tidal wave enters the region between the Aleutian and Hawaiian Ridges, it suffers a remarkable, almost symmetric retardation at both ridges. In fact, as the visible ($0^\circ = 360^\circ$) cotidal line in Table 7b reveals, the crest front of the tidal wave assumes the shape of an almost symmetric wedge. If one traces the 0° phase line westward beginning at both ridges, one can infer a definite idea about the realistic reproduction of the tide in this region. At both ends, the 0° phase is in full agreement with the empirical data. As the observed phases grow westward along both ridges, so grow proportionally the distances of the 0° phase line from the ridges.

The present computed M_2 -tide model indicates no longer any symptoms of the original phase problems (see above) at the Aleutian and Hawaiian Ridges. The computed amplitudes and phases approach the empirical tidal constants from both sides of the ridges as smoothly as could be desired. As the tidal wave spills over both ridges in northwestward or southwestward directions, respectively, it suffers a tidal distortion similar to that found before at the Caribbean Ridge. Amplitude jumps and major phase shifts are again in complete agreement with observations (see the remarks of Luther and Wunsch, 1974). It is particularly gratifying to find the phase shift well developed along the whole length of the Hawaiian Ridge from the Island of Hawaii to Midway, even though only few empirical data were used at both ends. Also, it may be noticed that the observed tidal constants at the distant and isolated island stations of Pribilof (PF), Midway (MW), and Johnston (JI) are all realistically well integrated by the surrounding computed tide.

Ironically, the old and new M_2 -tide maps constructed by Bogdanov (1961) and Luther and Wunsch (1974) by pure intuition and simple rules of thumb from empirical data came closest to the present charts. Indeed, both maps display no amphidromic system in the north-central Pacific. As will be verified in Part II, the computed amphidromic points between the Cook and Society Islands and near the southern edge of the Solomon Islands are both in almost identical positions with those charted by the same authors. Nevertheless, their detailed distribution of amplitudes and phases is still significantly different from the present one.

Perhaps the most spectacular display of the high quality of both the computed and the observed tidal data is brought out by Tables 8a and 8b depicting the high-amplitude tide of the central Pacific. Indeed, unlike any other open ocean area, the tabulated region is dotted with numerous tide gauge stations at island groups and at scattered isolated islands. In addition to the fully listed island chains, there are the isolated islands: Johnston (JI), Wake (WI), Kusaie (KI), Ocean (OI), Funafuti (FI), Wallis (IW), Niue (NI), and Norfolk (NF). The corresponding observed

WM 216 217 218 219 220 221 222 223 224 225 226 227 228 229 230 231 232 233 234 235 236 237 238 239 240 241 242 243 244 245

74

WM 216 217 218 219 220 221 222 223 224 225 226 227 228 229 230 231 232 233 234 235 236 237 238 239 240 241 242 243 244 245

75

Table 7a. M₂ Tidal Amplitudes, ξ (cm), of the North-Central Pacific Ocean

NM	177	178	179	180	181	182	183	184	185	186	187	188	189	190	191	192	193	194	195	196	197	198	199	200	201	202	203	204	205	206	
AN	30	31	32	33	34	35	36	37	38	39	40	41	42	43	44	45	46	47	48	49	50	51	52	53	54	55	56	57	58	59	60
29	28	28	27	27	27	27	27	27	27	27	27	27	27	27	27	27	27	27	27	27	27	27	27	27	27	27	27	27	27	27	27
31	30	28	27	26	26	26	26	26	26	26	26	26	26	26	26	26	26	26	26	26	26	26	26	26	26	26	26	26	26	26	26
33	32	27	26	26	25	25	25	25	25	25	25	25	25	25	25	25	25	25	25	25	25	25	25	25	25	25	25	25	25	25	25
35	34	25	24	24	24	24	24	24	24	24	24	24	24	24	24	24	24	24	24	24	24	24	24	24	24	24	24	24	24	24	24
37	36	24	23	23	23	23	23	23	23	23	23	23	23	23	23	23	23	23	23	23	23	23	23	23	23	23	23	23	23	23	23
39	38	23	22	22	22	22	22	22	22	22	22	22	22	22	22	22	22	22	22	22	22	22	22	22	22	22	22	22	22	22	22
41	40	22	21	21	21	21	21	21	21	21	21	21	21	21	21	21	21	21	21	21	21	21	21	21	21	21	21	21	21	21	21
43	42	21	20	20	20	20	20	20	20	20	20	20	20	20	20	20	20	20	20	20	20	20	20	20	20	20	20	20	20	20	20
45	44	20	19	19	19	19	19	19	19	19	19	19	19	19	19	19	19	19	19	19	19	19	19	19	19	19	19	19	19	19	19
47	46	19	18	18	18	18	18	18	18	18	18	18	18	18	18	18	18	18	18	18	18	18	18	18	18	18	18	18	18	18	18
49	48	18	17	17	17	17	17	17	17	17	17	17	17	17	17	17	17	17	17	17	17	17	17	17	17	17	17	17	17	17	17
51	50	17	16	16	16	16	16	16	16	16	16	16	16	16	16	16	16	16	16	16	16	16	16	16	16	16	16	16	16	16	16
53	52	16	15	15	15	15	15	15	15	15	15	15	15	15	15	15	15	15	15	15	15	15	15	15	15	15	15	15	15	15	15
55	54	15	14	14	14	14	14	14	14	14	14	14	14	14	14	14	14	14	14	14	14	14	14	14	14	14	14	14	14	14	14
57	56	14	13	13	13	13	13	13	13	13	13	13	13	13	13	13	13	13	13	13	13	13	13	13	13	13	13	13	13	13	13
59	58	13	12	12	12	12	12	12	12	12	12	12	12	12	12	12	12	12	12	12	12	12	12	12	12	12	12	12	12	12	12
61	60	12	11	11	11	11	11	11	11	11	11	11	11	11	11	11	11	11	11	11	11	11	11	11	11	11	11	11	11	11	11
63	62	11	10	10	10	10	10	10	10	10	10	10	10	10	10	10	10	10	10	10	10	10	10	10	10	10	10	10	10	10	10
65	64	10	9	9	9	9	9	9	9	9	9	9	9	9	9	9	9	9	9	9	9	9	9	9	9	9	9	9	9	9	9
67	66	9	8	8	8	8	8	8	8	8	8	8	8	8	8	8	8	8	8	8	8	8	8	8	8	8	8	8	8	8	8
69	68	8	7	7	7	7	7	7	7	7	7	7	7	7	7	7	7	7	7	7	7	7	7	7	7	7	7	7	7	7	7
71	70	7	6	6	6	6	6	6	6	6	6	6	6	6	6	6	6	6	6	6	6	6	6	6	6	6	6	6	6	6	6
73	72	6	5	5	5	5	5	5	5	5	5	5	5	5	5	5	5	5	5	5	5	5	5	5	5	5	5	5	5	5	5
75	74	5	4	4	4	4	4	4	4	4	4	4	4	4	4	4	4	4	4	4	4	4	4	4	4	4	4	4	4	4	4
77	76	4	3	3	3	3	3	3	3	3	3	3	3	3	3	3	3	3	3	3	3	3	3	3	3	3	3	3	3	3	3
79	78	3	2	2	2	2	2	2	2	2	2	2	2	2	2	2	2	2	2	2	2	2	2	2	2	2	2	2	2	2	2
81	80	2	1	1	1	1	1	1	1	1	1	1	1	1	1	1	1	1	1	1	1	1	1	1	1	1	1	1	1	1	1
83	82	1	0	0	0	0	0	0	0	0	0	0	0	0	0	0	0	0	0	0	0	0	0	0	0	0	0	0	0	0	0
85	84	0	0	0	0	0	0	0	0	0	0	0	0	0	0	0	0	0	0	0	0	0	0	0	0	0	0	0	0	0	0
87	86	0	0	0	0	0	0	0	0	0	0	0	0	0	0	0	0	0	0	0	0	0	0	0	0	0	0	0	0	0	0
89	88	0	0	0	0	0	0	0	0	0	0	0	0	0	0	0	0	0	0	0	0	0	0	0	0	0	0	0	0	0	0
91	90	0	0	0	0	0	0	0	0	0	0	0	0	0	0	0	0	0	0	0	0	0	0	0	0	0	0	0	0	0	0
93	92	0	0	0	0	0	0	0	0	0	0	0	0	0	0	0	0	0	0	0	0	0	0	0	0	0	0	0	0	0	0
95	94	0	0	0	0	0	0	0	0	0	0	0	0	0	0	0	0	0	0	0	0	0	0	0	0	0	0	0	0	0	0
97	96	0	0	0	0	0	0	0	0	0	0	0	0	0	0	0	0	0	0	0	0	0	0	0	0	0	0	0	0	0	0
99	98	0	0	0	0	0	0	0	0	0	0	0	0	0	0	0	0	0	0	0	0	0	0	0	0	0	0	0	0	0	0
101	100	0	0	0	0	0	0	0	0	0	0	0	0	0	0	0	0	0	0	0	0	0	0	0	0	0	0	0	0	0	0
103	102	0	0	0	0	0	0	0	0	0	0	0	0	0	0	0	0	0	0	0	0	0	0	0	0	0	0	0	0	0	0
105	104	0	0	0	0	0	0	0	0	0	0	0	0	0	0	0	0	0	0	0	0	0	0	0	0	0	0	0	0	0	0
107	106	0	0	0	0	0	0	0	0	0	0	0	0	0	0	0	0	0	0	0	0	0	0	0	0	0	0	0	0	0	0
109	108	0	0	0	0	0	0	0	0	0	0	0	0	0	0	0	0	0	0	0	0	0	0	0	0	0	0	0	0	0	0
111	110	0	0	0	0	0	0	0	0	0	0	0	0	0	0	0	0	0	0	0	0	0	0	0	0	0	0	0	0	0	0
113	112	0	0	0	0	0	0	0	0	0	0	0	0	0	0	0	0	0	0	0	0	0	0	0	0	0	0	0	0	0	0
115	114	0	0	0	0	0	0	0	0	0	0	0	0	0	0	0	0	0	0	0	0	0	0	0	0	0	0	0	0	0	0
117	116	0	0	0	0	0	0	0	0	0	0	0	0	0	0	0	0	0	0	0	0	0	0	0	0	0	0	0	0	0	0
119	118	0	0	0	0	0	0	0	0	0	0	0	0	0	0	0	0	0	0	0	0	0	0	0	0	0	0	0	0	0	0
121	120	0	0	0	0	0	0	0	0	0	0	0	0	0	0	0	0	0	0	0	0	0	0	0	0	0	0	0	0	0	0
123	122	0	0	0	0	0	0	0	0	0	0	0	0	0	0	0	0	0	0	0	0	0	0	0	0	0	0	0	0	0	0
125	124	0	0	0	0	0	0	0	0	0	0	0	0	0	0	0	0	0	0	0	0	0	0	0	0	0	0	0	0	0	0
127	126	0	0	0	0	0	0	0	0	0	0	0	0	0	0	0	0	0	0	0	0	0	0	0	0	0	0	0	0	0	0
129	128	0	0	0	0	0	0	0	0	0	0	0	0	0	0	0	0	0	0	0	0	0	0	0	0	0	0	0	0	0	0
131	130	0	0	0	0	0	0	0	0	0	0	0	0	0	0	0	0	0	0	0	0	0	0	0	0	0	0	0	0	0	0
133	132	0	0	0	0	0	0	0	0	0	0	0	0	0	0	0	0	0	0	0	0	0	0	0	0	0	0	0	0	0	0
135	134	0	0	0	0	0	0	0	0	0	0	0	0	0	0	0	0	0	0	0	0	0	0	0	0	0	0	0	0	0	0
137	136	0	0	0	0	0	0	0	0	0	0	0	0	0	0	0	0	0	0	0	0	0	0	0	0	0	0	0	0	0	0
139	138	0	0	0	0	0	0	0	0	0	0	0	0	0	0	0	0	0	0	0	0	0	0	0	0	0	0	0	0	0	0
141	140	0	0	0	0	0	0	0	0	0	0	0	0	0	0	0	0	0	0	0	0	0	0	0	0	0	0	0	0	0	0
143	142	0	0	0																											

Table 7b. M_2 Tidal Phases, δ ($^\circ$), of the North-Central Pacific Ocean[illegible]

Table 8a. M_2 Tidal Amplitudes, ξ (cm), of the Central Pacific Ocean

1	2	3	4	5	6	7	8	9	10	11	12	13	14	15	16	17	18	19	20	21	22	23	24	25	26	27	28	29	30	31	32	33	34	35	36	37	38	39	40	41	42	43	44	45	46	47	48	49	50	51	52	53	54	55	56	57	58	59	60	61	62	63	64	65	66	67	68	69	70	71	72	73	74	75	76	77	78	79	80	81	82	83	84	85	86	87	88	89	90	91	92	93	94	95	96	97	98	99	100
1	2	3	4	5	6	7	8	9	10	11	12	13	14	15	16	17	18	19	20	21	22	23	24	25	26	27	28	29	30	31	32	33	34	35	36	37	38	39	40	41	42	43	44	45	46	47	48	49	50	51	52	53	54	55	56	57	58	59	60	61	62	63	64	65	66	67	68	69	70	71	72	73	74	75	76	77	78	79	80	81	82	83	84	85	86	87	88	89	90	91	92	93	94	95	96	97	98	99	100
1	2	3	4	5	6	7	8	9	10	11	12	13	14	15	16	17	18	19	20	21	22	23	24	25	26	27	28	29	30	31	32	33	34	35	36	37	38	39	40	41	42	43	44	45	46	47	48	49	50	51	52	53	54	55	56	57	58	59	60	61	62	63	64	65	66	67	68	69	70	71	72	73	74	75	76	77	78	79	80	81	82	83	84	85	86	87	88	89	90	91	92	93	94	95	96	97	98	99	100
1	2	3	4	5	6	7	8	9	10	11	12	13	14	15	16	17	18	19	20	21	22	23	24	25	26	27	28	29	30	31	32	33	34	35	36	37	38	39	40	41	42	43	44	45	46	47	48	49	50	51	52	53	54	55	56	57	58	59	60	61	62	63	64	65	66	67	68	69	70	71	72	73	74	75	76	77	78	79	80	81	82	83	84	85	86	87	88	89	90	91	92	93	94	95	96	97	98	99	100
1	2	3	4	5	6	7	8	9	10	11	12	13	14	15	16	17	18	19	20	21	22	23	24	25	26	27	28	29	30	31	32	33	34	35	36	37	38	39	40	41	42	43	44	45	46	47	48	49	50	51	52	53	54	55	56	57	58	59	60	61	62	63	64	65	66	67	68	69	70	71	72	73	74	75	76	77	78	79	80	81	82	83	84	85	86	87	88	89	90	91	92	93	94	95	96	97	98	99	100
1	2	3	4	5	6	7	8	9	10	11	12	13	14	15	16	17	18	19	20	21	22	23	24	25	26	27	28	29	30	31	32	33	34	35	36	37	38	39	40	41	42	43	44	45	46	47	48	49	50	51	52	53	54	55	56	57	58	59	60	61	62	63	64	65	66	67	68	69	70	71	72	73	74	75	76	77	78	79	80	81	82	83	84	85	86	87	88	89	90	91	92	93	94	95	96	97	98	99	100
1	2	3	4	5	6	7	8	9	10	11	12	13	14	15	16	17	18	19	20	21	22	23	24	25	26	27	28	29	30	31	32	33	34	35	36	37	38	39	40	41	42	43	44	45	46	47	48	49	50	51	52	53	54	55	56	57	58	59	60	61	62	63	64	65	66	67	68	69	70	71	72	73	74	75	76	77	78	79	80	81	82	83	84	85	86	87	88	89	90	91	92	93	94	95	96	97	98	99	100
1	2	3	4	5	6	7	8	9	10	11	12	13	14	15	16	17	18	19	20	21	22	23	24	25	26	27	28	29	30	31	32	33	34	35	36	37	38	39	40	41	42	43	44	45	46	47	48	49	50	51	52	53	54	55	56	57	58	59	60	61	62	63	64	65	66	67	68	69	70	71	72	73	74	75	76	77	78	79	80	81	82	83	84	85	86	87	88	89	90	91	92	93	94	95	96	97	98	99	100
1	2	3	4	5	6	7	8	9	10	11	12	13	14	15	16	17	18	19	20	21	22	23	24	25	26	27	28	29	30	31	32	33	34	35	36	37	38	39	40	41	42	43	44	45	46	47	48	49	50	51	52	53	54	55	56	57	58	59	60	61	62	63	64	65	66	67	68	69	70	71	72	73	74	75	76	77	78	79	80	81	82	83	84	85	86	87	88	89	90	91	92	93	94	95	96	97	98	99	100
1	2	3	4	5	6	7	8	9	10	11	12	13	14	15	16	17	18	19	20	21	22	23	24	25	26	27	28	29	30	31	32	33	34	35	36	37	38	39	40	41	42	43	44	45	46	47	48	49	50	51	52	53	54	55	56	57	58	59	60	61	62	63	64	65	66	67	68	69	70	71	72	73	74	75	76	77	78	79	80	81	82	83	84	85	86	87	88	89	90	91	92	93	94	95	96	97	98	99	100
1	2	3	4	5	6	7	8	9	10	11	12	13	14	15	16	17	18	19	20	21	22	23	24	25	26	27	28	29	30	31	32	33	34	35	36	37	38	39	40	41	42	43	44	45	46	47	48	49	50	51	52	53	54	55	56	57	58	59	60	61	62	63	64	65	66	67	68	69	70	71	72	73	74	75	76	77	78	79	80	81	82	83	84	85	86	87	88	89	90	91	92	93	94	95	96	97	98	99	100
1	2	3	4	5	6	7	8	9	10	11	12	13	14	15	16	17	18	19	20	21	22	23	24	25	26	27	28	29	30	31	32	33	34	35	36	37	38	39	40	41	42	43	44	45	46	47	48	49	50	51	52	53	54	55	56	57	58	59	60	61	62	63	64	65	66	67	68	69	70	71	72	73	74	75	76	77	78	79	80	81	82	83	84	85	86	87	88	89	90	91	92	93	94	95	96	97	98	99	100
1	2	3	4	5	6	7	8	9	10	11	12	13	14	15	16	17	18	19	20	21	22	23	24	25	26	27	28	29	30	31	32	33	34	35	36	37	38	39	40	41	42	43	44	45	46	47	48	49	50	51	52	53	54	55	56	57	58	59	60	61	62	63	64	65	66	67	68	69	70	71	72	73	74	75	76	77	78	79	80	81	82	83	84	85	86	87	88	89	90	91	92	93	94	95	96	97	98	99	100
1	2	3	4	5	6	7	8	9	10	11	12	13	14	15	16	17	18	19	20	21	22	23	24	25	26	27	28	29	30	31	32	33	34	35	36	37	38	39	40	41	42	43	44	45	46	47	48	49	50	51	52	53	54	55	56	57	58	59	60	61	62	63	64	65	66	67	68	69	70	71	72	73	74	75	76	77	78	79	80	81	82	83	84	85	86	87	88	89	90	91	92	93	94	95	96	97	98	99	100
1	2	3	4	5	6	7	8	9	10	11	12	13	14	15	16	17	18	19	20	21	22	23	24	25	26	27	28	29	30	31	32	33	34	35	36	37	38	39	40	41	42	43	44	45	46	47	48	49	50	51	52	53	54	55	56	57	58	59	60	61	62	63	64	65	66	67	68	69	70	71	72	73	74	75	76	77	78	79	80	81	82	83	84	85	86	87	88	89	90	91	92	93	94	95	96	97	98	99	100
1	2	3	4	5	6	7	8	9	10	11	12	13	14	15	16	17	18	19	20	21	22	23	24	25	26	27	28	29	30	31	32	33	34	35	36	37	38	39	40	41	42	43	44	45	46	47	48	49	50	51	52	53	54	55	56	57	58	59	60	61	62	63	64	65	66	67	68	69	70	71	72	73	74	75	76	77	78	79	80	81	82	83	84	85	86	87	88	89	90	91	92	93	94	95	96	97	98	99	100
1	2	3	4	5	6	7	8	9	10	11	12	13	14	15	16	17	18	19	20	21	22	23	24	25	26	27	28	29	30	31	32	33	34	35	36	37	38	39	40	41	42	43	44	45	46	47	48	49	50	51	52	53	54	55	56	57	58	59	60	61	62	63	64	65	66	67	68	69	70	71	72	73	74	75	76	77	78	79	80	81	82	83	84	85	86	87	88	89	90	91	92	93	94	95	96	97	98	99	100
1	2	3	4	5	6	7	8	9	10	11	12	13	14	15	16	17	18	19	20	21	22	23	24	25	26	27	28	29	30	31	32	33	34	35	36	37	38	39	40	41	42	43	44	45	46	47	48	49	50	51	52	53	54	55	56	57	58	59	60	61	62	63	64	65	66	67	68	69	70	71	72	73	74	75	76	77	78	79	80																				

Table 8b. M_2 Tidal Phases, δ ($^\circ$), of the Central Pacific Ocean

101	102	103	104	105	106	107	108	109	110	111	112	113	114	115	116	117	118	119	120	121	122	123	124	125	126	127	128	129	130	131	132	133	134	135	136	137	138	139	140	141	142	143	144	145	146	147	148	149	150	151	152	153	154	155	156	157	158	159	160	161	162	163	164	165	166	167	168	169	170	171	172	173	174	175	176	177	178	179	180	181	182	183	184	185	186	187	188	189	190	191																														
71	72	73	74	75	76	77	78	79	80	81	82	83	84	85	86	87	88	89	90	91	92	93	94	95	96	97	98	99	100	101	102	103	104	105	106	107	108	109	110	111	112	113	114	115	116	117	118	119	120	121	122	123	124	125	126	127	128	129	130	131	132	133	134	135	136	137	138	139	140	141	142	143	144	145	146	147	148	149	150	151	152	153	154	155	156	157	158	159	160	161	162	163	164	165	166	167	168	169	170	171	172	173	174	175	176	177	178	179	180	181	182	183	184	185	186	187	188	189	190	191
120	119	118	117	116	115	114	113	112	111	110	109	108	107	106	105	104	103	102	101	100	99	98	97	96	95	94	93	92	91	90	89	88	87	86	85	84	83	82	81	80	79	78	77	76	75	74	73	72	71	70	69	68	67	66	65	64	63	62	61	60	59	58	57	56	55	54	53	52	51	50	49	48	47	46	45	44	43	42	41	40	39	38	37	36	35	34	33	32	31	30	29	28	27	26	25	24	23	22	21	20	19	18	17	16	15	14	13	12	11	10	9	8	7	6	5	4	3	2	1	0
120	119	118	117	116	115	114	113	112	111	110	109	108	107	106	105	104	103	102	101	100	99	98	97	96	95	94	93	92	91	90	89	88	87	86	85	84	83	82	81	80	79	78	77	76	75	74	73	72	71	70	69	68	67	66	65	64	63	62	61	60	59	58	57	56	55	54	53	52	51	50	49	48	47	46	45	44	43	42	41	40	39	38	37	36	35	34	33	32	31	30	29	28	27	26	25	24	23	22	21	20	19	18	17	16	15	14	13	12	11	10	9	8	7	6	5	4	3	2	1	0
120	119	118	117	116	115	114	113	112	111	110	109	108	107	106	105	104	103	102	101	100	99	98	97	96	95	94	93	92	91	90	89	88	87	86	85	84	83	82	81	80	79	78	77	76	75	74	73	72	71	70	69	68	67	66	65	64	63	62	61	60	59	58	57	56	55	54	53	52	51	50	49	48	47	46	45	44	43	42	41	40	39	38	37	36	35	34	33	32	31	30	29	28	27	26	25	24	23	22	21	20	19	18	17	16	15	14	13	12	11	10	9	8	7	6	5	4	3	2	1	0
120	119	118	117	116	115	114	113	112	111	110	109	108	107	106	105	104	103	102	101	100	99	98	97	96	95	94	93	92	91	90	89	88	87	86	85	84	83	82	81	80	79	78	77	76	75	74	73	72	71	70	69	68	67	66	65	64	63	62	61	60	59	58	57	56	55	54	53	52	51	50	49	48	47	46	45	44	43	42	41	40	39	38	37	36	35	34	33	32	31	30	29	28	27	26	25	24	23	22	21	20	19	18	17	16	15	14	13	12	11	10	9	8	7	6	5	4	3	2	1	0
120	119	118	117	116	115	114	113	112	111	110	109	108	107	106	105	104	103	102	101	100	99	98	97	96	95	94	93	92	91	90	89	88	87	86	85	84	83	82	81	80	79	78	77	76	75	74	73	72	71	70	69	68	67	66	65	64	63	62	61	60	59	58	57	56	55	54	53	52	51	50	49	48	47	46	45	44	43	42	41	40	39	38	37	36	35	34	33	32	31	30	29	28	27	26	25	24	23	22	21	20	19	18	17	16	15	14	13	12	11	10	9	8	7	6	5	4	3	2	1	0
120	119	118	117	116	115	114	113	112	111	110	109	108	107	106	105	104	103	102	101	100	99	98	97	96	95	94	93	92	91	90	89	88	87	86	85	84	83	82	81	80	79	78	77	76	75	74	73	72	71	70	69	68	67	66	65	64	63	62	61	60	59	58	57	56	55	54	53	52	51	50	49	48	47	46	45	44	43	42	41	40	39	38	37	36	35	34	33	32	31	30	29	28	27	26	25	24	23	22	21	20	19	18	17	16	15	14	13	12	11	10	9	8	7	6	5	4	3	2	1	0
120	119	118	117	116	115	114	113	112	111	110	109	108	107	106	105	104	103	102	101	100	99	98	97	96	95	94	93	92	91	90	89	88	87	86	85	84	83	82	81	80	79	78	77	76	75	74	73	72	71	70	69	68	67	66	65	64	63	62	61	60	59	58	57	56	55	54	53	52	51	50	49	48	47	46	45	44	43	42	41	40	39	38	37	36	35	34	33	32	31	30	29	28	27	26	25	24	23	22	21	20	19	18	17	16	15	14	13	12	11	10	9	8	7	6	5	4	3	2	1	0
120	119	118	117	116	115	114	113	112	111	110	109	108	107	106	105	104	103	102	101	100	99	98	97	96	95	94	93	92	91	90	89	88	87	86	85	84	83	82	81	80	79	78	77	76	75	74	73	72	71	70	69	68	67	66	65	64	63	62	61	60	59	58	57	56	55	54	53	52	51	50	49	48	47	46	45	44	43	42	41	40	39	38	37	36	35	34	33	32	31	30	29	28	27	26	25	24	23	22	21	20	19	18	17	16	15	14	13	12	11	10	9	8	7	6	5	4	3	2	1	0
120	119	118	117	116	115	114	113	112	111	110	109	108	107	106	105	104	103	102	101	100	99	98	97	96	95	94	93	92	91	90	89	88	87	86	85	84	83	82	81	80	79	78	77	76	75	74	73	72	71	70	69	68	67	66	65	64	63	62	61	60	59	58	57	56	55	54	53	52	51	50	49	48	47	46	45	44	43	42	41	40	39	38	37	36	35	34	33	32	31	30	29	28	27	26	25	24	23	22	21	20	19	18	17	16	15	14	13	12	11	10	9	8	7	6	5	4	3	2	1	0
120	119	118	117	116	115	114	113	112	111	110	109	108	107	106	105	104	103	102	101	100	99	98	97	96	95	94	93	92	91	90	89	88	87	86	85	84	83	82	81	80	79	78	77	76	75	74	73	72	71	70	69	68	67	66	65	64	63	62	61	60	59	58	57	56	55	54	53	52	51	50	49	48	47	46	45	44	43	42	41	40	39	38	37	36	35	34	33	32	31	30	29	28	27	26	25	24	23	22	21	20	19	18	17	16	15	14	13	12	11	10	9	8	7	6	5	4	3	2	1	0
120	119	118	117	116	115	114	113	112	111	110	109	108	107	106	105	104	103	102	101	100	99	98	97	96	95	94	93	92	91	90	89	88	87	86	85	84	83	82	81	80	79	78	77	76	75	74	73	72	71	70	69	68	67	66	65	64	63	62	61	60	59	58	57	56	55	54	53	52	51	50	49	48	47	46	45	44	43	42	41	40	39	38	37	36	35	34	33	32	31	30	29	28	27	26	25	24	23	22	21	20	19	18	17	16	15	14	13	12	11	10	9	8	7	6	5	4	3	2	1	0
120	119	118	117	116	115	114	113	112	111	110	109	108	107	106	105	104	103	102	101	100	99	98	97	96	95	94	93	92	91	90	89	88	87	86	85	84	83	82	81	80	79	78	77	76	75	74	73	72	71	70	69	68	67	66	65	64	63	62	61	60	59	58	57	56	55	54	53	52	51	50	49	48	47	46	45	44	43	42	41	40	39	38	37	36	35	34	33	32	31	30	29	28	27	26	25	24	23	22	21	20	19	18	17	16	15	14	13	12	11	10	9	8	7	6	5	4	3	2	1	0
120	119	118	117	116	115	114	113	112	111	110	109	108	107	106	105	104	103	102	101	100	99	98	97	96	95	94	93	92	91	90	89	88	87	86	85	84	83	82	81	80	79	78	77	76	75	74	73	72																																																																								

tidal constants listed in nongeographical arrangement appeared incoherent and, hence, uncorrelated, giving rise to doubt their true value. Yet, the computed tidal wave sweeps across the whole area in a southwesterly direction with little variation of its high amplitude. As the wave crest passes through the many checkpoints, it integrates and correlates without a single exception all the empirical data into one coherent unity.

C. CONCLUSIONS

The hydrodynamical modeling of global ocean tides, described and tested above, shows that the original question posed by contemporary researchers (Section 1) can be successfully answered. In fact, one infers from the evaluation of the constructed M_2 tide (Sect. 6.B) that it is now possible to predict the M_2 -tide elevation of the ocean surface over the geoid anywhere in the open oceans with an accuracy of better than 5 cm. This accuracy goes considerably beyond the originally desired error bounds. It leaves ample room for superposable errors due to the additional tidal constituents listed in Table 1, which must be constructed with equivalent relative accuracy. The computation of the leading three components, S_2 , K_1 , and O_1 , is presently in progress.

Naturally, the achieved high accuracy of the M_2 tide in the open oceans drops off somewhat near continental or island stations where empirical data are missing or are less accurate themselves (see the introduction to the British Admiralty Tide Tables, 1977). Also, less accurate predictions must be anticipated in small border seas, bays, estuaries, and channels where the 1° by 1° grid system precludes a sufficient resolution. To improve the present tide model in those areas, significantly improved observations will be needed along with a locally refined network and corresponding bathymetric data.

REFERENCES

1. Accad, Y. and Pekeris, C. L., 1963. "The K_2 Tide in Oceans Bounded by Meridians and Parallels," *Proc. Roy. Soc. London, A*, 278, p. 110.
2. Airy, G. B., 1842. "Tides and Waves," *Encyclo. Metropol. London*.
3. Bartels, J., 1957. "Gezeitenkräfte," *Handbuch der Physik XLVIII, Geophysik II*, Springer, Berlin.
4. Berghaus, H., 1845. "Phys. Handatlas," *Gotha*.
5. Bogdanov, C. T., 1961a. "New Charts of the Cotidal Lines of Semidiurnal Tidal Waves (M_2 and S_2) for the Pacific Ocean," *Sov. Oceanography*, I, p. 28.
6. Bogdanov, C. T., 1961b. "New Charts of the Diurnal Tide (K_1 and O_1) for the Pacific Ocean," *Sov. Oceanography*, I, p. 46.
7. Bogdanov, C. T., Kim, K. V., and Magarik, V. A., 1964. "A Numerical Solution of the Hydrodynamical Equations of Tides on the BESM-2 Computer for the World Ocean Area," *Trans. Inst. Oceanography, Acad. Sci.*, 75, p. 73 (in Russian).
8. Bogdanov, C. T. and Magarik, V. A., 1967. "A Numerical Solution of the Problem of Semidiurnal Tidal Wave Distribution (M_2 and S_2) in the Ocean," *Dokl. Akad. Nauk. USSR*, 172, p. 1315 (in Russian).
9. Bogdanov, C. T. and Magarik, V. A., 1969. "A Numerical Solution of the Problem of Tidal Wave Propagation in the World Ocean," *Izv. Atmos. Oceanic Phys.*, 5, p. 1309 (in Russian).
10. Boussinesq, J., 1877. "Théorie de L'écoulement Tourbillant," *Mem. Pres. Acad. Sci. XXIII*, 46, Paris.
11. Boussinesq, J., 1896. "Expression du Frottement Extérieur des L'écoulement Tumultueux d'une Fluide," *Comptes Rend. Acad. Sci.*, 122, p. 1445.
12. Brettschneider, G., 1967. "Anwendung des Hydrodynamisch-Numerischen Verfahrens zur Ermittlung der M_2 -Mitschwingungszeit der Nordsee," *Mitteilungen des Inst. f. Meereskunde der Univ. Hamburg*, VII.
13. *British Admiralty Tide Tables*, 1977, Vols. 1, 2, and 3.
14. Bryan, K., 1963. "A Numerical Investigation of a Nonlinear Model of a Wind-Driven Ocean," *J. Atmos. Sci.*, 20, p. 594.
15. Bryan, K. and Cox, M. D., 1967. "A Numerical Investigation of the Oceanic General Circulation," *Tellus*, 19, p. 54.
16. Busse, F. H. and Whitehead, J. A., 1971. "Instabilities of Convection Rolls in a High Prandtl Number Fluid," *J. Fluid Mech.*, 47, p. 305.
17. Cantor, G., 1901. "Vorlesungen über Geschichte der Mathematik," Vol. 3, *Leipzig*.
18. Cartwright, D. E., 1968. "A Unified Analysis of Tides and Surges Around North and East Britain," *Phil. Trans. Roy. Soc., London, Ser. A*, 263, p. 1.

19. Cartwright, D. E., 1969. "Extraordinary Tidal Currents Near St. Kilda," *Nature*, 223, p. 938.
20. Cartwright, D. E., 1971. "Tides and Waves in the Vicinity of St. Helena," *Phil. Trans. Roy. Soc., London, Ser. A*, 270, p. 603.
21. Cartwright, D. E., Munk, W. H., and Zetler, B. D., 1969. "Pelagic Tidal Measurements," *EOS*, 50 p. 472.
22. Cartwright, D. E., and Taylor, R. J., 1971. "New Computations of the Tide-Generating Potential," *Geophys. J. Roy. Astr. Soc.*, 23, p. 45.
23. Cox, M. D., 1970. "A Mathematical Model of the Indian Ocean," *Deep-Sea Res.*, 17, p. 45.
24. Crowley, W. P., 1968. "A Global Numerical Model: Part 1," *J. Comp. Phys.*, 3, p. 111.
25. Crowley, W. P., 1970. "A Numerical Model for Viscous, Free-Surface, Barotropic Wind-Driven Ocean Circulations," *J. Comp. Phys.*, 5, p. 139.
26. Darwin, G. H., 1883. "Report on the Harmonic Analysis of Tidal Observations," *Brit. Ass. for adv. Sci. Rep.*; see also *Sci. Pap.* 1; Cambridge, 1907.
27. Defant, A., 1957. "Flutwellen und Gezeiten des Wassers," *Handbuch der Physik XLVIII, Geophysik II*, Springer, Berlin.
28. Defant, A., 1961. *Physical Oceanography, Vol. II*, Pergamon Press, New York.
29. Dietrich, G., 1944a. "Die Gezeiten des Weltmeeres als Geographische Erscheinung," *Z. d. ges. Erdkunde*, p. 69.
30. Dietrich, G., 1944b. "Die Schwingungssysteme der Halb-und Eintägigen Tiden in den Ozeanen," *Veröff. Inst. Meereskunde, Univ. Berlin, N. F. A.*, No. 41.
31. Dietrich, G., 1963. *General Oceanography*, Interscience Publishers, John Wiley & Sons, New York.
32. Dishon, M., 1964. "Determination of the Average Ocean Depths from Bathymetric Data," *Int. Hydro. Rev.*, 41, p. 77.
33. Dishon, M. and Heezen, B. C., 1968. "Digital Deep-Sea Sounding Library," *Int. Hydro. Rev.*, 45, p. 23.
34. Döös, B. R., et al., 1974. *Modeling for the First GARP Global Experiment*, GARP Publication Series No. 14.
35. Doodson, A. T., 1921. "The Harmonic Development of the Tide-Generating Potential," *Proc. Roy. Soc., London, Ser. A*, 100.
36. Ekman, V. W., 1902. "Om Jordrotationens Inverkan på Vindströmmar i Hafvet," *Nyt. Mag. f. Naturvid.*, Vol. 20, *Kristiania*.
37. Estes, R., 1975. *A Computer Software System for the Generation of Global Numerical Solutions of Diurnal and Semidiurnal Ocean Tides*, Contract NAS5-20045, Business and Technol. Syst. TR-75-27.
38. Estes, R., 1977. *A Computer Software System for the Generation of Global Ocean Tides Including Crustal Loading Effects*, Contract NAS5-20045, Business and Technol. Syst. TR-77-41.
39. Eyrie, M., 1968. "Maregraphs de Grandes Profondeurs," *Cahiers Oceanographiques*, 20, p. 355.

40. Farrell, W. E., 1972a. "Deformation of the Earth by Surface Loads," *Rev. Geophys. Space Phys.*, 10, p. 261.
41. Farrell, W. E., 1972b. "Global Calculations of Tidal Loading," *Nature*, 238, p. 43.
42. Farrell, W. E., 1973. "Earth Tides, Ocean Tides, and Tidal Loading," *Phil. Trans. Roy. Soc., London, Ser. A*, 274, p. 253.
43. Ferrel, W., 1874. "Tidal Researches," *U.S. Coast and Geod. Surv. Rep.*, pp. 154, 239, 245.
44. Filloux, J. H., 1969. "Bourbon Tube Deep-Sea Tide Gages," *Proc. Symp. on Tsunamis and Tsunami Research*, Honolulu.
45. Fomin, L. M., 1964. *The Dynamic Method in Oceanography*, Elsevier Publishing Co., Amsterdam.
46. Friedrich, H. J., 1966. "Numerische Berechnung der Allgemeinen Zirkulation im Meere nach einem Differenzen Verfahren, Vornehmlich für den Atlantischen Ozean," *Mitteilungen des Inst. f. Meereskunde der Univ. Hamburg*, III.
47. Friedrich, H. J., 1970. "Preliminary Results from a Numerical Multilayer Model for the Circulation in the North Atlantic," *Deutsche Hydr. Zeit.*, 23, p. 145.
48. Gallagher, B. S., Shimada, K. M., Gonzales, F. L., Jr., and Stroup, E. D., 1971. "Tides and Currents in Fanning Atoll Lagoon," *Pacific Sci.*, 25, p. 191.
49. Gates, L. R. and Nelson, A. B., 1975. "A New (Revised) Tabulation of the Scripps Topography on a 1° Global Grid," *Part II: Ocean Depths*, Rand Corp. Rep. 1277, Santa Monica, California.
50. Gohin, F., 1961. "Determination des Denivellations et des Courants de Maree," *Proc. Seventh Conf. Coastal Eng.*, The Hague, Netherlands, Aug. 1960, Vol. 2, p. 485.
51. Gordeyev, R. G., Kagan, B. A., and Rivkind, V. Y., 1973. "Numerical Solution of the Dynamic Tidal Equations in the Global Ocean," *Dokl. Akad. Nauk USSR*, 209, p. 340 (in Russian).
52. Grace, S. F., 1931. "The Semidiurnal Lunar Tidal Motion of the Red Sea," *Mon. Not. Roy. Astr. Soc., Geophys. Suppl.*, 2, p. 316.
53. Hansen, W., 1948. "Die Ermittlung der Gezeiten Beliebiger Gestalteter Meeresgebiete mit Hilfe des Randwertverfahrens," *Deutsche Hydr. Zeit.*, 1, p. 157.
54. Hansen, W., 1949. "Die halbtägigen Gezeiten im Nordatlantischen Ozean," *Deutsche Hydr. Zeit.*, 2, p. 44.
55. Hansen, W., 1962. "Hydrodynamical Methods Applied to Oceanographic Problems," *Mitteilungen des Inst. f. Meereskunde der Univ. Hamburg*, I.
56. Hansen, W., 1966. "Die Reproduktion der Bewegungsvorgänge im Meere mit Hilfe Hydrodynamisch-Numerischer Verfahren," *Mitteilungen des Inst. f. Meereskunde der Univ. Hamburg*, V.
57. Harris, R. A., 1904. "Manual of Tides," *Part IVb: Report of the Superintendent, U.S. Coast and Geodetic Survey*, p. 313.
58. Hendershott, M. C., 1972. "The Effects of Solid-Earth Deformation on Global Ocean Tides," *Geophys. J. Roy. Astr. Soc.*, 29, p. 380.

59. Hendershott, M. C., 1973. "Ocean Tides," *EOS*, 54, p. 76.
60. Hendershott, M. C., 1975. "Global Numerical Tide Solutions with Inclusion of Ocean Self-Gravitation and of Solid Earth Tidal Loading," *XVI General Assembly of IUGG*, Grenoble, France.
61. Hendershott, M. C., 1977. "Numerical Models of Ocean Tides," *The Sea*, Vol. 6, p. 47.
62. Hendershott, M. C. and Munk, W. H., 1970. "Tides," *Ann. Rev. Fluid Mech.*, 2, p. 205.
63. Holland, W. R. and Hirschman, A. D., 1972. "A Numerical Calculation of the Circulation in the North Atlantic Ocean," *J. Phys. Oceanogr.*, 2, p. 336.
64. Hopfner, F., 1931. "Die Gezeiten der Meere," *Handbuch der Experimental-physik, Geophysik, 2. Teil, Akademische Verlagsgesellschaft*, M. B. H., Leipzig.
65. Hough, S., 1897. "On the Application of Harmonic Analysis to the Dynamical Theory of the Tides," *Phil. Trans.*, A, 189, p. 201.
66. International Hydrographic Bureau, 1966. *Tides, Harmonic Constants*, Spec. Publ., No. 26, Monaco.
67. Irish, J., Munk, W. H., and Snodgrass, F., 1971. " M_2 Amphidrome in the Northeast Pacific," *Geophys. Fluid. Dyn.*, 2, p. 355.
68. Jachens, R. C. and Kuo, J. T., 1973. "The O_1 Tide in the North Atlantic Ocean as Derived from Land-Based Tidal Gravity Measurements," *Proc. of the Seventh Symp. on Earth Tides, Sopron, Hungary*, Akad. Kiado, Budapest.
69. Johns, B., 1966. "Vertical Structure of Tidal Flows in River Estuaries," *Geophys. J. Res., Astr. Soc.*, 12, p. 103.
70. Kagan, B. A., 1971. "Bottom Friction in a One-Dimensional Tidal Flow," *Izv. Acad. Sci. USSR, Atm. and Oce. Phys.*, 7, No. 11 (in Russian).
71. Kagan, B. A., 1972. "Resistance Law of Tidal Flow," *Izv. Acad. Sci. USSR, Atm. and Oce. Phys.*, 8, No. 5.
72. Kuo, J. T., Jachens, R. C., White, G., and Ewing, M., 1970a. "Tidal Gravity Measurements Along a Transcontinental Profile Across the United States," *6^e Symp. Int. Sur les Marées Terrestres, Strasbourg, 1969*, Comm. Obs. Roy. Belg., No. 9, p. 96.
73. Kuo, J. T., Jachens, R. C., Ewing, M., and White, G., 1970b. "Transcontinental Tidal Gravity Profile Across the United States," *Sci.*, 168, p. 968.
74. Kuo, J. T., Jachens, R. C., and Lee, S. S., 1977. "The Northeastern Pacific O_1 and the North Atlantic M_2 Ocean Tides as Derived from Inversion," *Eighth Int. Symp. on Earth Tides*, Bonn, Fed. Rep. Germany.
75. Ladyzhenskaya, O. A., 1969. *The Mathematical Theory of Viscous Incompressible Flow*, Science Publishers, Gordon and Breach, New York.
76. Lamb, H., and Swain, L., 1915. "A Tidal Problem," *Phil. Mag.*, 29, p. 737.
77. Lamb, H., 1932. *Hydrodynamics*, Dover Publications, New York.

78. Laplace, P. S., 1775. "Recherches sur Quelques Points de Système du Monde," *Mem. Acad., Roy. Sci.*, 88.
79. Leith, C. E., 1968. "Two-Dimensional Eddy Viscosity Coefficients," *Proc. WMO/IUGG Symp. on Numerical Weather Prediction*, Tokyo, p. 140.
80. Luther, D. S. and Wunsch, C., 1975. "Tidal Charts of the Central Pacific Ocean," *J. Phys. Oce.*, 5, p. 227.
81. Marchuk, G. I., Kagan, B. A., and Tamsalu, R. E., 1969. "A Numerical Method of Calculating Tidal Motion in Border Seas," *Izv. Atmos. Oce. Phys.*, 5, p. 694.
82. Marchuk, G. I., Gordeyev, R. G., Rivkind, V. Y., and Kagan, B. A., 1973. "A Numerical Method for the Solution of Tidal Dynamics Equations and the Results of Its Application," *J. Comp. Phys.*, 13, p. 15.
83. McGregor, R. C., 1972. "The Influence of Eddy Viscosity on the Vertical Distribution of Velocity in the Tidal Estuary," *Geophys. J. Res., Astr. Soc.*, 29, p. 103.
84. Miyazaki, M., Kuronuma, S., and Inoue, T., 1967. "Tidal Constants Along the Coast of Japan," *Oceanogr. Mag.*, 19, p. 13.
85. Miles, J., 1974. "On Laplace's Tidal Equations," *J. Fluid Mech.*, 66, p. 241.
86. Mofjeld, H. O., 1975. "Empirical Model for Tides in the Western North Atlantic Ocean," *NOAA, TR ERL 340-AOML19, Boulder, Colorado*.
87. Munk, W. H., 1950. "On the Wind-Driven Ocean Circulation," *Wind-Driven Ocean Circulation*, Blaisdell Publishing Co., New York, 1963.
88. Munk, W. H., 1966. "Abyssal Recipes," *Deep-Sea Res.*, 13, p. 707.
89. Munk, W. H., and Palmén, E., 1951. "Note on the Dynamics of the Antarctic Circumpolar Current," *Tellus*, 3, p. 53.
90. Munk, W. H., and Cartwright, D. E., 1966. "Tidal Spectroscopy and Prediction," *Phil. Trans., Roy. Soc., London, Ser. A*, 259, p. 533.
91. Munk, W. H., Snodgrass, F., and Wimbush, M., 1970. "Tides Offshore: Transition from California Coastal to Deep-Sea Waters," *Geophys. Fluid Dyn.*, 1, p. 161.
92. National Ocean Survey, 1942. "Tidal Harmonic Constants," *U.S. Coast and Geodetic Survey*, Washington, D.C.
93. Neumann, G., and Pierson, W. J. Jr., 1966. *Principles of Physical Oceanography*, Prentice-Hall, Inc., Englewood Cliffs, New Jersey.
94. Newton, I., 1687. *Philosophiae Naturalis Principia Mathematica*, London.
95. Nowroozi, A. A., 1972. "Long-Term Measurements of Pelagic Tidal Height Off the Coast of Northern California," *J. Geophys. Res.*, 77, p. 434.
96. O'Brian, J. J., 1971. "A Two-Dimensional Model of the Wind-Driven North Pacific," *Investig. Pesquera*, 35, p. 331.

97. Pearson, C. A., 1975a. *Deep-Sea Tide and Current Observations in the Gulf of Alaska and Northeast Pacific*, NOAA T. Memo. NOS 16, Rockville, Maryland.
98. Pearson, C. A., 1975b. *Deep-Sea Tide Observations Off the Southeastern United States*, NOAA T. Memo. NOS 17, Rockville, Maryland.
99. Pekeris, C. L. and Accad, Y., 1969. "Solution of Laplace's Equation for the M_2 Tide in the World Oceans," *Phil. Trans. Roy. Soc., London, Ser. A*, 265, p. 413.
100. Platzman, G. W., 1971. "Ocean Tides and Related Waves," *Lect. Appl. Math., Vol. 14*, A.M.S., Providence, Rhode Island.
101. Platzman, G. W., 1972a. "Two-Dimensional Free Oscillations in Natural Basins," *J. Phys. Oceanogr.*, 2, p. 117.
102. Platzman, G. W., 1972b. "North Atlantic Ocean: Preliminary Description of Normal Modes," *Science*, 178, p. 156.
103. Platzman, G. W., 1975. "Normal Modes of the Atlantic and Indian Oceans," *J. Phys. Oceanogr.*, 5, p. 201.
104. Poincaré, H., 1910. "Lecons de Méchanique Céleste," Vol. 3, *Theorie des Marées*, Gauthier-Villars, Paris.
105. Prandtl, L., 1925. "Über die Ausgebildete Turbulenz," *ZAMM*, 5, p. 136.
106. Proudman, J., 1915. "Free and Forced Longitudinal Tidal Motion in a Lake," *Proc. London Math. Soc.*, 14.
107. Proudman, J., 1952. *Dynamical Oceanography*, Dover Publications, Inc., New York.
108. Proudman, J. and Doodson, A. T., 1927. "On the Tides in an Ocean Bounded by Two Meridians on a Non-Rotating Earth," *Mon. Not. Roy. Astr. Soc., Geophys. Suppl.*, 1, p. 468.
109. Prüfer, G., 1936. "Die Gezeiten des Indischen Ozeans," *Veröff. Inst. f. Meereskunde, Berlin*, N.A.F. No. 37.
110. Reid, R. O., Robinson, A. R., and Bryan, K., 1975. *Numerical Models of Ocean Circulation*, Nat. Acad. of Sciences, Washington, D.C.
111. Richardson, L. F., 1922. *Weather Prediction by Numerical Methods*, Cambridge University Press, London.
112. Richtmyer, R. D., 1957. *Difference Methods for Initial-Value Problems*, Interscience Publishers, Inc., New York.
113. Schlichting, H., 1968. *Boundary-Layer Theory*, McGraw-Hill Book Co., New York.
114. Schwiderski, E. W., 1972. "Bifurcation of Convection in Internally Heated Fluid Layers," *The Phys. of Fluids*, 15, p. 1882.
115. Schwiderski, E. W., 1976. "Preliminary M_2 Tide," Computer Tape, NSWC/DL, Dahlgren, Virginia.
116. Schwiderski, E. W., 1978a. *Hydrodynamically Defined Ocean Bathymetry*, NSWC/DL-TR, in press.
117. Schwiderski, E. W., 1978b. *Global Ocean Tides, Part II: The Semidiurnal Principal Lunar Tide (M_2)*, NSWC/DL-TR, in press.
118. Shilov, G. E., 1968. *Generalized Functions and Partial Differential Equations*, Gordon and Breach, New York.

119. Smagorinsky, J., 1963. "General Circulation Experiments With the Primitive Equations. I. The Basic Experiment," *Mon. Weather Rev.*, 91, p. 99.
120. Smith, S. M., Menard, H. M., and Sharman, G., 1966. "Worldwide Ocean Depths and Continental Elevations Averaged for Areas Approximating One-Degree Squares of Latitude and Longitude," Ref. 65-8, Scripps Inst. of Oceanogr., La Jolla, California.
121. Snodgrass, F. E., 1968. "Deep-Sea Instrument Capsule," *Science*, 162, p. 78.
122. Stern, M. E., 1975. *Ocean Circulation Physics*, Academic Press, New York.
123. Sterneck, R. V., 1920, 1921. "Die Gezeiten der Ozeane, 1. und 2. Mitteilung," *Sitz. Ber. Akad. Wis., Wien*, 129, p. 131; 130, p. 363.
124. Stommel, H., 1960. *The Gulf Stream*, University of California Press, Berkeley.
125. Taylor, G. I., 1918. "Tidal Friction in the Irish Sea," *Phil. Trans. Roy. Soc., Ser. A*, 220, p. 1.
126. Thomson, W. (Lord Kelvin), 1868. "Report of Committee for the Purpose of Harmonic Analysis of Tidal Observations" *Brit. Ass. Adv. Sci. Rep., London*.
127. Thomson, W. (Lord Kelvin), 1879. "On Gravitational Oscillations of Rotating Water," *Proc. Roy. Soc., Edinburgh*, 10.
128. Tiron, K. D., Sergeev, Y. N., and Michurin, A. N., 1967. "Tidal Charts for the Pacific, Atlantic, and Indian Oceans," *Vestn., Leningrad University*, 24, p. 122.
129. Trepka, L. V., 1967. "Anwendung des Hydrodynamisch-Numerischen Verfahrens zur Ermittlung des Schelfeinflusses auf die Gezeiten in Modellkanälen und Modellozeanen," *Mitteilungen des Inst. f. Meereskunde der Univ. Hamburg*, IX.
130. Ueno, T., 1964a, b. "Theoretical Studies on Tidal Waves Traveling Over the Rotating Globe, I and II," *Oceanogr. Mag.*, 15, p. 99; 16, p. 47.
131. Villain, C., 1952. "Cartes des Lignes Cotidals dans les Océans," *Ann. Hydrog. (Paris)*, 3, p. 269.
132. Voit, S. S., 1967. "Tides in Seas and Oceans," *Fis. Atmos. Okeana*, 3, p. 579 (in Russian).
133. Whewell, W., 1833. "Essay Towards a First Approximation to a Map of Cotidal Lines," *Phil. Trans. Roy. Soc., London*, 1, p. 147.
134. Whewell, W., 1848. "On the Tides of the Pacific and On the Diurnal Inequality," *Phil. Trans. Roy. Soc., London*, 16, p. 1.
135. Whitaker, S., 1968. *Introduction to Fluid Mechanics*, Prentice-Hall, Inc., Englewood Cliffs, New Jersey.
136. Wunsch, C., 1972. "Bermuda Sea Level in Relation to Tides, Weather, and Baroclinic Fluctuations," *Rev. Geophys.*, 10, p. 1.
137. Zahel, W., 1970. "Die Reproduktion Gezeitenbedingter Bewegungsvorgänge im Weltozean Mittels des Hydrodynamisch-Numerischen Verfahrens," *Mitteilungen des Inst. f. Meereskunde der Univ. Hamburg*, XVII.

138. Zahel, W., 1973. "The Diurnal K_1 Tide in the World Ocean—A Numerical Investigation," *Pure Appl. Geophys.*, 109, p. 1819.
139. Zahel, W., 1975. "A Global Hydrodynamic-Numerical 1° -Model of the Ocean Tides. The Oscillation System of the M_2 -Tide and Its Distribution of Energy Dissipation," *XVI General Assembly of IUGG, Grenoble, France*.
140. Zetler, B., Munk, W., Mofjeld, H., Brown, W., and Dormer, F., 1975. "MODE Tides," *J. Phys. Oceanogr.*, 5, p. 430.

DISTRIBUTION

Library of Congress
Washington, DC 20540
ATTN: Gift and Exchange Division

(4)

Naval Oceanographic Office
Washington, DC 20390
ATTN: Dr. T. Davis

Defense Documentation Center
Cameron Station
Alexandria, VA 22314

(12)

Technical Director (SP-20)
Strategic Systems Project Office
Washington, DC 20390

Director
Defense Mapping Agency, HQ
Washington, DC 20360
ATTN: Dr. C. F. Martin
P. W. Schwimmer

Fleet Numerical Weather Central
Monterey, CA 93940
ATTN: CDR B. Schramm

Defense Mapping Agency
Hydrographic Center
Washington, DC 20360
ATTN: MAJ J. Jérôme

Director
Naval Research Laboratory
Washington, DC 20360
ATTN: V. E. Noble
B. S. Yaplee
A. Shapiro
D. T. Chen

Defense Mapping Agency
Topographic Center
Washington, DC 20315
ATTN: Randy Smith
Mrs. I. Fischer

Army Engineers Topographic Laboratory
Ft. Belvoir, VA 22060
ATTN: Dr. A. Mancini

Defense Mapping Agency
Aerospace Center
St. Louis, MO 63118
ATTN: Don McEntee

Air Force Geodetic Laboratory
L. G. Hanscom Field
Bedford, MA 01730
ATTN: Mr. G. Hadgigeorge

Office of Naval Research
800 N Quincy St.
Arlington, VA 22203
ATTN: G. R. Hamilton
Dr. W. S. Wilson
J. G. Heacock
R. S. Andrews
Dr. Leila D. Bram
R. D. Cooper
M. Cooper

NOAA/National Ocean Survey
National Geodetic Survey
Rockville, MD 20852
ATTN: B. Chovitz
B. C. Douglas
C. C. Goad
F. Morrison

Oceanographer of the Navy
Hoffman 2
200 Stova St.
Alexandria, VA 22332

NOAA/National Ocean Survey
Oceanographic Division
Rockville, MD 20852
ATTN: D. C. Simpson

NOAA/Atlantic Oceanographic and Meteorological Lab.
Physical Oceanography Laboratory
ATTN: G. A. Maul
H. M. Byrne

NOAA/Pacific Marine Environmental Lab.
Seattle, WA 98105
ATTN: Dr. J. R. Apel
H. O. Mofjeld
C. A. Pearson

NOAA/Geophysical Fluid Dynamics Laboratory
Princeton University
Princeton, NJ 08540
ATTN: Dr. J. Smagorinsky
Dr. K. Bryan
Dr. M. D. Cox

NOAA/National Center for Atmospheric Research
Boulder, CO 80303
ATTN: Dr. W. R. Holland

NASA/Goddard Space Flight Center
ATTN: Dr. J. W. Siry
Dr. P. Musen
D. E. Smith
J. G. Marsh

NASA/Wallops Station
Information Processing and Analysis Branch
Wallops Island, VA 23337
ATTN: C. D. Leita

Director
U.S. Army Ballistic Research Laboratory
Aberdeen Proving Ground, MD 21005
ATTN: DRDAR-TSB-S (STINFO)

Smithsonian Astrophysical Observatory
60 Garden St.
Cambridge, MA 02138
ATTN: Dr. E. M. Gaposchkin
Dr. G. C. Wiffenbach
Ms. Dianne Hills

National Science Foundation
1951 Constitution Ave., N.W.
Washington, DC 20550
ATTN: Mathematical Sciences Division

Scripps Institution of Oceanography
University of California, San Diego
La Jolla, CA 92037
ATTN: Dr. W. H. Munk
Dr. M. C. Hendershott
Prof. B. D. Zetler
Prof. S. M. Smith
Prof. H. W. Menard

MIT/Dept. Earth & Planetary Sciences
Cambridge, MA 02139
ATTN: Dr. C. Wunsch
Dr. D. S. Luther

Woods Hole Oceanographic Institute
Woods Hole, MA 02543
ATTN: Dr. H. M. Stommel
Dr. G. Veronis
Dr. N. P. Fofonoff

Battelle Columbus Laboratories
505 King Ave.
Columbus, OH 43201
ATTN: A. G. Mourad

Dr. J. W. Chamberlain
Editor, *Rev. Geophys. and Space Physics*
Rice University
Houston, TX 77001

Dr. R. H. Rapp
Ass. Editor, *JGR*
Ohio State University
Dept. of Geodetic Science
1958 Neil Ave.
Columbus, OH 43210

Dr. R. O. Reid
Texas A&M University
College Station, TX 77843

Florida State University
Dept. of Oceanography
Tallahassee, FL 32306
ATTN: Dr. J. J. O'Brien
Dr. W. Sturges

Prof. J. T. Kuo
Lamont-Doherty Geological Observatory
Columbia University
Palisades, NY 10964

Prof. W. J. Pierson, Jr.
1641 Rosalind Ave.
Elmont, NY 11003

Dr. R. H. Estes
Business and Technological Systems, Inc.
Aerospace Building, Suite 605
10210 Greenbelt Rd.
Seabrook, MD 20801

T. V. Martin
Sci. Res. and Appl. Group
Washington Analytical Services Center, Inc.
6801 Kenilworth Ave.
Riverdale, MD 20840

Dr. S. K. Jordan
The Analytic Sciences Corporation
6 Jacob Way
Reading, MA 01867

The Rand Corporation
Santa Monica, CA 90406
ATTN: Director, Climate Program

The Hydrographer of the Navy
Ministry of Defence
Hydrographic Department
Taunton, Somerset, England

Director
Bureau Hydrographique International
7, Ave. President J. F. Kennedy
Monte-Carlo, Monaco

G. C. Dohler, P. Eng.
Canadian Hydrographic Services
Ocean and Aquatic Affairs
615 Booth St.
Ottawa, Canada K1A0H3

Prof. D. E. Cartwright
Institute of Oceanographic Sciences
Bidston Observatory
Birkenhead, L437RA, U.K.

Institut für Meereskunde
Universität Hamburg
Heimhuder Str. 71
2 Hamburg 13, Germany
ATTN: Prof. Dr. W. Hansen
Dr. W. Zahel

Dr. G. Seeber
Tech. Universität Hannover
Nienburger Str. 6
D3 Hannover, Germany

Dr. J. Schmitt
Astron. Geodäsie & Satellitengeodäsie
Techn. Hochschule Darmstadt
Petersenstr. 13
D-61 Darmstadt, Germany

Prof. P. Melchior
Observatoire Royal de Belgique
Avenue Circulaire 3
1180 Brussels, Belgium

E. SMETS
The Laboratory of Hydraulic Research
Berchemlei 118
B-2200 Borgerhout, Belgium

Dr. C. LeProvost
Institut d. Mécanique
BP. 53
38041 Grenoble, France

Meteorological Res. Institute
4-35-8 Koenji-Kita
Suginami
Tokyo, Japan
ATTN: T. Ueno
M. Miyazaki

R. S. Chugh, Director
Geodetic Research Branch
Dehra Dun, India

Prof. G. Obenson
University of Lagos
Lagos, Nigeria

Local: D

K, K01, K02, K04, K05H, K05J
K10, K10I, K11, K12, K12H, K12S, K12W
K20, K30, K55, K60, K70, K73, K73B, K73S
R04
E41
X210 (2)
X210 (GIDEP) (2)
K05S (100)



END

DATE
FILMED

1-79

DDC

AD-A060 913

NAVAL SURFACE WEAPONS CENTER DAHLGREN LAB VA
GLOBAL OCEAN TIDES. PART I. A DETAILED HYDRODYNAMICAL INTERPOLA--ETC(U)
SEP 78 E W SCHWIDERSKI

F/G 8/3

UNCLASSIFIED

NSWC/DL-TR-3866

GIDEP-E125-1971

NL

2 OF 2
AD A
060913



SUPPLEMENTARY
INFORMATION



END
DATE
FILMED
6-81
DTIC

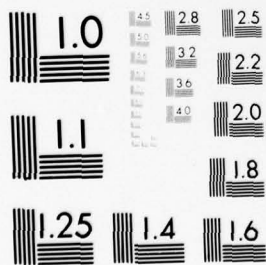
OF



SUPP

A

60913



MICROCOPY RESOLUTION TEST CHART
NATIONAL BUREAU OF STANDARDS-1963-A

IN

UPPLEMENTARY

INFORMATION

AD-A060913

LIST OF CORRECTIONS TO NSWC/DL TR-3866

Page 3: In Table 1, change amplitude K of S_2 to: $K(S_2) = 0.112841$
and D to: $D = d + 365(y - 1975) + \text{Int}[(y-1973)/4]$

Page 22: In Eq. 14 change η_0 to: $\eta_0 = \frac{1}{2}K(3\cos^2\theta - 2) \cos(\sigma t + \pi)$

Page 27: Top line change β to: $\beta = 0.90$

In first equation of Eq. 32 add: $\bar{H}_\lambda = H_\lambda/H$, $\bar{H}_{\lambda\lambda} = H_{\lambda\lambda}/H$.

Page 29: Change Eq. 37c to: $\frac{1}{2}K(3\sin^2\theta - 2)$.

Page 31: In V-equation of Eq. (43) change $\sin\theta$ to $\sin 2\theta$.

Page 32: Change Eq. 45 to:

$$\begin{aligned}\eta &= \frac{1}{2}K(3\sin^2\theta - 2) e^{i\sigma t} \\ &= \tilde{K}_1(3\sin^2\theta - 2) e^{i\sigma t} \\ U &= \frac{1}{2}\tilde{K}_2 \sin\theta e^{i\sigma t} \\ V &= \frac{-i\tilde{K}_1}{2}\sigma R \sin 2\theta e^{i\sigma t}\end{aligned}$$

In Equation 45a change \tilde{K}_2 and \tilde{K}_1 to:

$$\begin{aligned}\tilde{K}_2 &= -\tilde{K}_1/\tilde{K}_3 \\ \tilde{K}_1 &= -3\alpha_{GH_0} K [(6\beta_{GH_0} - \sigma^2 R^2 + \Omega R \tilde{K}_3) + i\sigma(6A_0 + B_0 R^2/H_0)].\end{aligned}$$

Note: A higher order approximation of improved accuracy is in preparation.

Page 33: Change \tilde{K}_1 to: $\tilde{K}_1 = -3\tilde{K}$.

Page 47: In $B_{m,n}$ change for $\nu = 0$:

$$-3 \sin 4n\Delta\theta \text{ to } +6\sin 4n\Delta\theta.$$

Page 52: In Eq. 84 change the left-side ξ to ζ .

Page 56: In Eq. 94 change k_1 and k_2 to: $k_1 = .06$, $k_2 = .03$.

ATE
LMED
-8